UNIVERSITY OF TWENTE.

Faculty of Engineering Technology

On the applicability of the mandrel peel test to characterize the fracture toughness of non-symmetric interfaces

Linda N. Grafen S1919431

Thesis

August 10, 2020

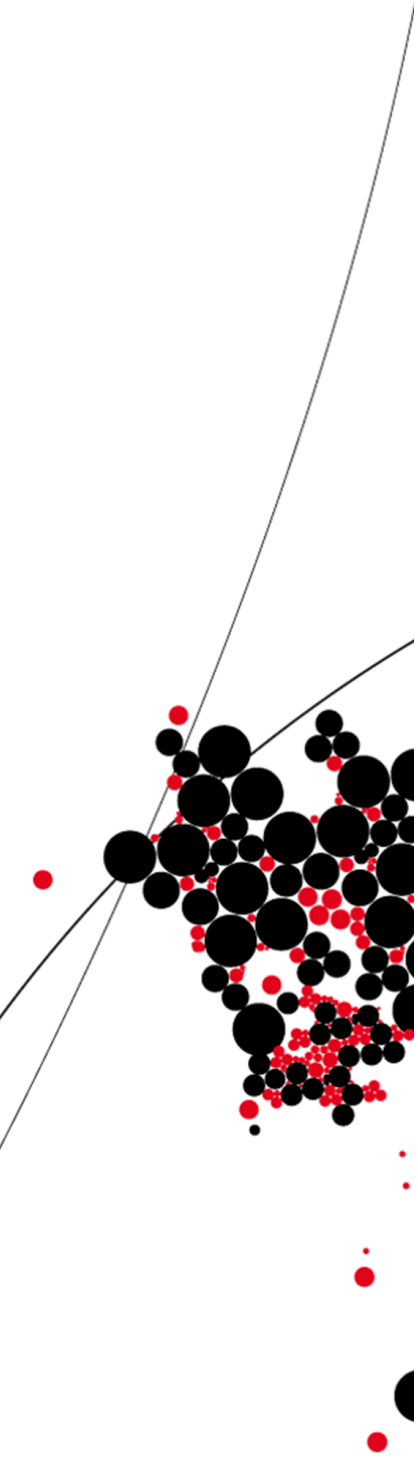

Supervisor
dr. ir. W.J.B. Grouve

Mechanical Engineering MS3 group
Faculty of Engineering Technology
University of Twente
P.O. Box 217
7500 AE Enschede
The Netherlands

Summary

Delamination is one of the most detrimental damage modes in fiber reinforced composites. The resistance to delamination is characterized by the interlaminar fracture toughness, which is an important parameter used in the design of load-bearing composites structures. Most of the methods found in literature are designed to determine the delamination propagation of laminates where the crack propagates parallel between a symmetric or 0°-0°interface. Since most structural composite products are multi-directional (MD), these methods arguably leave little practical value.

This research analyses the applicability of the mandrel peel test to measure the interlaminar fracture toughness of non-symmetric interfaces. For this purpose, carbon/PEEK specimen with a 0°-θ°interface were manufactured and tested. The applicability of the mandrel peel setup to measure non-symmetric interfaces is quite favorable over for example the Double Cantilever Beam (DCB) test, as the manufacturing of the specimen is relatively easy as symmetry of the interface is not required. Furthermore, the test procedure itself is rather simple and straightforward. It was found that the fracture toughness decreases with increasing fiber angle, but due to the high experimental scatter the significance of these findings are questionable. Furthermore, crack migration away from the intended interface and stick-slip behavior was encountered. The tendency of the crack to propagate away from the intended interface makes it difficult to relate the measured fracture toughness to the intended interlaminar fracture toughness. As such, this result means that the mandrel peel setup was not able to measure the delamination resistance of 0°-θ°carbon/PEEK interfaces.

The fracture behavior of carbon/PEEK material found in this study is similar to other studies and measurement methods, with crack propagation away from the intended interface is a common phenomenon. As the crack behavior is found the be similar among studies, it is recommended to test the method with a more brittle matrix material.

Nomenclature

The next list describes several symbols and abbreviations that will later be used within the body of this report.

Abbreviations

//	Crack propagation interface
CFRP	Carbon fiber-reinforced polymer
DCB	Double cantilever beam
ELS	End-loaded split
ENF	End notch flexure
F-B	Fast-Brittle
HM	Height of mandrel with respect to sample
I-B	Intermediate-brittle
MD	multi-directional
MP	Mandrel peel
PA	Peel-arm
PEEK	Polyether ether ketone
S-D	Slow-ductile
UD	Unidirectional

Greek symbols

Δ	Correction factor crack tip rotation and deflection
δ	Displacement mm
ϵ	Maximum bending strain peel-arm (mandrel peel)
ϵ_m	Elastic strain in peel-arm
ϵ_r	Pre-strain in the peel-arm
μ	Friction
σ_r	Residual stresses [N/m^2]
θ	Angle

Roman symbols

G_c	Critical energy release rate [kJ/m^2]

G_{Ic}	Critical energy release rate of mode I [kJ/m^2]
r_y	Radius of plastic yield zone [mm]
a	Crack length during crack propagation [mm]
B	Specimen width [mm]
C	Specimen compliance [mm/N]
D_c	Non-dimensional ratio
E	Young's modulus [N/m^2]
F	Correction factor for large displacement of test specimen arms
F_a	Alignment force [N]
F_p	Peeling force [N]
F_{ip}	Initial peak force over specimen width [F/mm]
F_{peak}	Peak force [N]
h	Thickness of peel-arm (mandrel peel)
N	Correction factor for stiffening of specimen by load blocks
P	Force [N]
R	Mandrel radius [mm]
t	Thickness of peel-arm [mm]
U_d	Energy dissipated during peeling [J]
U_s	Strain energy stored in peel arm
U_{ext}	External work [J]

Contents

Chapter 1

Introduction

The past decades the industry shows a shift away from the usage of heavy, homogeneous, and well understood metal structures to more lightweight, and versatile polymer matrix composites [1], due to their attractive characteristics like high stiffness-to-weight and strength-to-weight ratios [2]. Traditional metal beams and sheet metal structures are replaced with state of the art composite sandwich structures and laminates.

Composite materials offer limitless potential, in particular the carbon fiber-reinforced polymer (CFRP) material. This material has become a design favorite, often applied with high performance resins such as polyether ether ketone (PEEK) or high-end epoxy resins. Carbon fiber composites are by nature a highly directional material which exhibits favorable characteristics in the fiber direction and have a good strength-to-weight ratio [1]. CFRP composites have excellent corrosion resistance and strong in-plane strengths when compared to for example aluminum alloys [3]. However, the directional nature of CFRP material puts special burden on the engineers to properly design the components for its expected load and application. When loaded transversely to the fiber direction, unidirectional (UD) plies are particularly weak due to the relatively low strengths of the matrix material [1]. Based on the stacking sequence, material properties, and boundary conditions, the dominant failure mechanisms can vary significantly including matrix damage, fiber breakage, transverse cracks, delamination, and buckling, see figure 1.1.

For laminated CFRP composites, one of the most critical degradation modes is delamination. Delamination occurs when a crack propagates at the interface between two adjacent plies, this can be seen in the green squares of figure 1.1. This event can be caused by several factors, such as manufacturing defects, impact events [4] or buckling [5]. When a delamination is initiated, the crack propagation, and therefore the type of damage, depends on among others the dimensions of the delamination, the load, and the fracture energy [5]. Once delamination occurs, the residual strength under compressive loading could significantly decrease, leading to catastrophic failure [3] such as sudden loss of global stability [5].

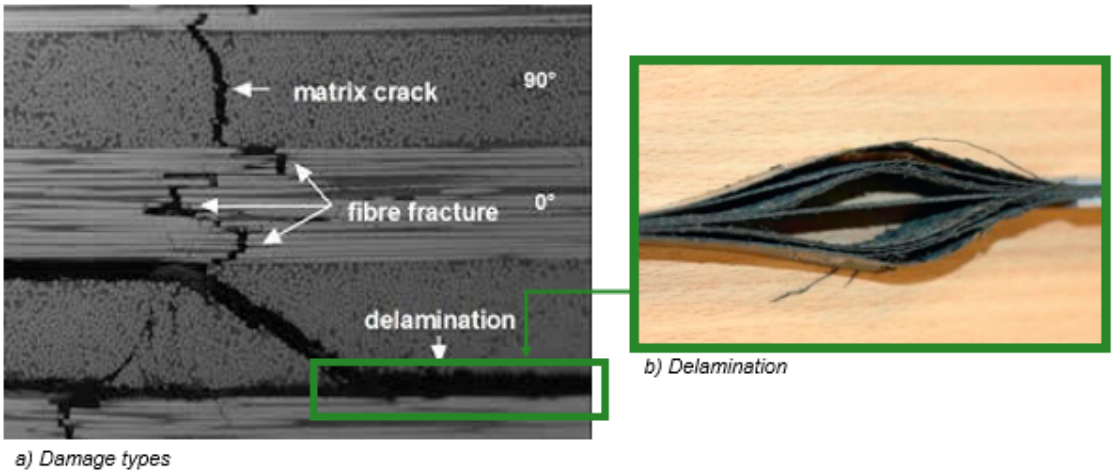

Figure 1.1: a) Different damage types [6]; b) Delamination [4]

1.1 Problem statement

Since the usage of light and high strengths materials in the aerospace industries deploy rapidly, the CFRP delamination failures and their relevant modeling approaches have been studied extensively [3]. One of the most widely accepted approaches to characterize the resistance of delamination is by means of fracture mechanics. By measuring the interlaminar fracture toughness of the composite laminate, the critical energy release rate (G_c) can be determined [7]. The most common testing methods found in the literature for the fracture toughness are the double cantilever beam (DCB) test [3, 7–12], standard peeling tests [13], end-notch flexure (ENF) [10–12], and end-loaded split (ELS) test [7–9]. More details on the different testing methods for the G_c will be discussed in section 2.2.

The previously mentioned experimental methods are mostly designed to determine the delamination propagation of laminates where the crack propagates parallel between a *0°-0°*interface. Since most structural composite products are multi-directional (MD) and delamination usually develops between plies of different orientations [7], these methods arguably leave little practical value. In addition, MD CFRP laminates typically exhibit multiple delamination cracks at several interfaces under low velocity impact or fatigue load and the different fiber orientations make the crack propagate in a non-parallel interface. Instead of propagating at its initial interface, the delamination can grow through the thickness of the laminate joining neighbouring damages or it can propagate into neighbouring interfaces on its own. Delamination migration in MD laminates involves complex interactions of the delamination front with the surrounding matrix and fiber materials, leaving the influence of interfacial fiber orientations on delamination migration a very limited studied topic [14]. The DCB method is available to analyse the effect of fiber orientation on the fracture toughness of UD laminates, but is not successful for laminates where the crack propagates through an interface where one ply orientation is parallel to the crack while the other ply is not (such as a *0°-θ°*interface) [15]. This is due to the fact that the global stiffness of the specimen arms plays a role [16] together with the required symmetry of the crack propagation interface during the DCB test [15]. MD laminates can be tested with the DCB test, as long as the interface is symmetric ($\theta°$-$\theta°$). This leaves the influence of the fiber orientation of a 0°-θ°interface on the fracture toughness an almost unstudied topic. A promising method to test *0°-θ°*interfaces is the mandrel peel (MP) test. The MP method is a modification of the *90°*peel test [9], where the peel-arm is bend around a mandrel which is able to rotate [13]. The advantage over the standard peel test is that the radius of the mandrel prevents the fiber fracture during the peeling [8]. Previous studies already showed that the mandrel peel test is able to characterize the fracture toughness of UD-UD, UD-woven, and UD-metal combinations [9]. More information on the mandrel peel test is given in chapter 3. A total of two studies used the MP method to analyse the fracture toughness of *0°-θ°*interfaces and both show deviating results. This study will examine the influence of the fiber direction on the fracture toughness of carbon/PEEK MD laminates with a *0-θ* interface.

1.2 Objective and outline

This study will describe the relevant theory and experiments to answer the following research question:

> *"Is the mandrel peel setup applicable to establish a relation between the interlaminar fracture toughness and an 0°-θ° interface of carbon/PEEK UD laminates?"*

To answer this question, this study will start with a literature review about the delamination resistance and the current most used testing methods, looking particularly at the influence of the fiber-direction interface on the interlaminar fracture toughness. Chapter 3 will discuss the mandrel peel method and its parameters. A preliminary study is done to examine the effect of the specimen dimensions and mandrel peel settings on the crack propagation before the actual experiments on the influence of fiber direction on the fracture toughness are studied. The research questions of the preliminary study can be found in section 3.5.1 of chapter 3. The methodology of the preliminary study can be found in appendix A, whereas the results in appendix B. The results of the preliminary study are the direct input for the methodology of this research. After the methodology is described in chapter 4, the results, conclusion, and recommendations of this study will be given in chapter 5, 6, and 7.

Chapter 2

Background information

By selecting the appropriate combination of matrix material, reinforcement material and stacking sequence, a laminated composite can be made to exactly meet the required properties. However, one of the greatest weaknesses of laminated composites is the risk of delamination [16]. Delamination is the separation failure between two adjacent laminae in a laminated structure and is one of the most predominant and life-limiting failure mechanism in composite structures. Delaminations can occur due to non-optimum consolidation during manufacturing, introduction of foreign bodies, impact damage, or internal stresses of the structure or due to any type of loading [17]. Delamination damages start with the initiation stage and is followed by the propagation stage. The propagation stage of delamination damage is characterized by the delamination toughness, or fracture toughness, which exists of the combined contribution of local and non-local dissipation. Examples of local and non-local dissipation are adhesive failures of the interface and fiber bridging, respectively [3]. Fiber bridging attributes to among others fiber nesting of adjacent plies, weak interfaces, extended crack tip yield zones, larger fiber volume fraction, and crack branching in angle laminates. Nesting is most common in UD laminates where the fibers from the adjacent plies migrate and intermingle with others during the consolidation cycle [18].

The delamination resistance is believed to be a material property of the composite material [11] that characterizes the resistance of the material to ply separation. Evaluating the delamination growth under various environmental conditions and loading is important for a critical and reliably estimation of the structural failure and service life. The criteria used to evaluate delamination propagation is usually established in terms of the strain energy release rate and fracture toughness [11]. The fracture toughness refers to the energy required to separate the interface of two adjacent surfaces. This energy should be independent of the joint geometry and only represent the fracture behavior of the intended interface [13]. The delamination resistance of composite materials is believed to depend on numerous factors, such as the direction of the crack propagation [12, 19], the mode ratio's of the loading [7, 10–12], the material properties [20, 21], and fiber bridging [2, 11]. In addition, many observations have been made on the effect of ply orientation and interlaminar fracture toughness, showing contradicting results [16], as already mentioned in chapter 1. As the delamination propagation in MD laminates involves complex interactions of the damage with the surrounding matrix and fibers [14], it is important to get a proper understanding on these complex interactions.This chapter will provide an overview of the properties interacting with the delamination resistance.

2.1 Fracture toughness

Determining the global description of the fracture process of composite materials can be done by the form of critical stress intensity factors, describing the local stress state close to a crack tip, and critical strain energy release rates. These properties need to be obtained for all three fracture modes to fully characterise a material [22], see figure 2.1a. The interaction of the three modes is not well established yet. Even for mode I, which is a pure tensile opening load and considered to be the most dangerous fracture mode, the determination of the fracture toughness is not easy to establish [15]. For UD laminates the fracture toughness modes I and II are safe to assume to be constant intrinsic parameters or material properties of composite material, independent on the delamination length and specimen size. However, this assumption is not valid for MD laminates, which are the laminates most used in practice. For MD laminates, the fracture toughness is frequently found to increase as the delamination propagates due to large-scale fiber bridging

across the delamination plane [11]. In addition, the fracture characteristics should be taken into account as well and can be categorized in three different fracture types: interlaminar fractures, intralaminar fractures, and translaminar fractures, see figure 2.1b. Translaminar fracture types include fiber breakage and result in the highest amount of energy dissipation within the laminate. This type of damage requires an energy to fail typically several orders of magnitude larger than that of the other two failure types. Intralaminar fractures propagate between the fibers through the thickness of the laminate, rather than between the plies as is the case for interlaminar fracture types [22].

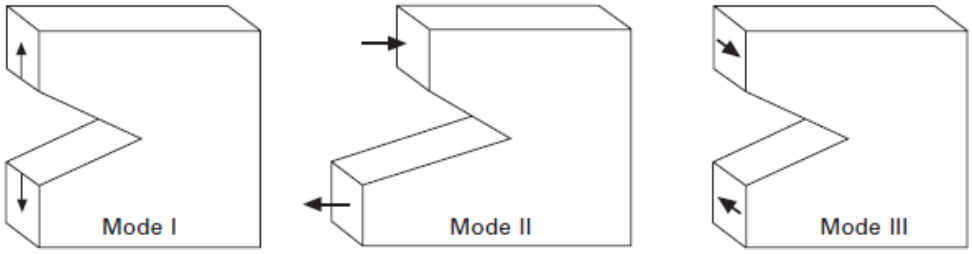

(a) Fracture modes. Mode I: tensile opening. Mode II: in-plane shear . Mode III: out-of-plane shear [22]

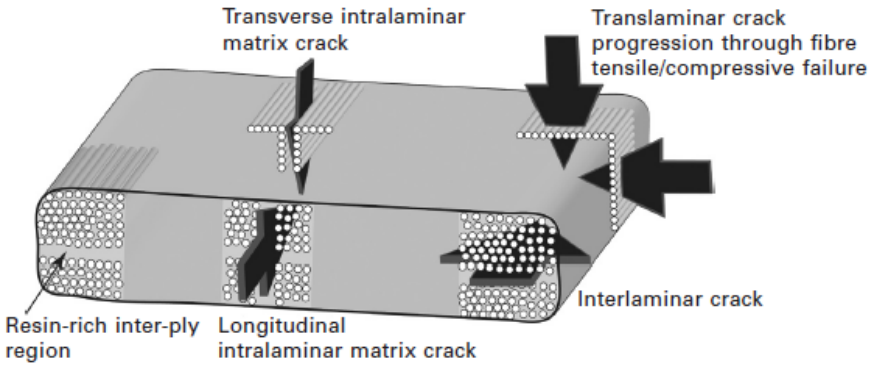

(b) Ply-level fracture mechanisms of continuous fiber-reinforced composites [22]

Figure 2.1: Fracture mechanics [22]

2.1.1 Crack initiation

Before the delamination can propagate, the delamination has to initiate. This initiation stage can occur due to for example impact events, manufacturing defects [4] or buckling [5]. External and internal damages around the failure event can appear and when this damage zone attains a critical volume, crack initiation occurs [15]. This critical volume is also referred to as the peak load. It is found that additional residual stress in the laminates generates higher values of the peak load and therefore influences the crack initiation [23]. Khan et al. [24] studied the damage development at mode I fatigue delamination tips in carbon/epoxy laminates and found that the delamination growth was sudden as the load level crossed the peak value. Micro-cracks around the crack tip were observed and crossed the matrix layer and touch both the upper and lower fibers of the adjacent plies just before the delamination starts to grow, as can be seen in figure 2.2a. The intact matrix can be seen as a ligament bridging the delamination plane plies.

In addition, it is assumed that the initiation value is affected by the ply-angle of both adjacent plies and sub-adjacent plies. This assumption is justified as damage around the crack tip is developed around the adjacent layers, as well as in the sub-adjacent layers [15]. As the fiber angle of plies near the crack tip increases, the intensity of micro-cracking in the resin within these plies also increases. This damage leads to a drop in delamination toughness as the loading of the crack tip zone is locally higher. For this it is known that the initiation toughness is predominantly governed by the micro-crack of the resin near the insert tip and can result in unstable crack initiation [16]. This can be seen in figure 2.2b, where a typical delamination tip is shown where cracks and disbondings are ahead of the delamination tip. These cracks are not in the same plane as the delamination interface, but change position alternatively above and below the intended delamination plane. This behavior makes it possible for the delamination to locally jump from

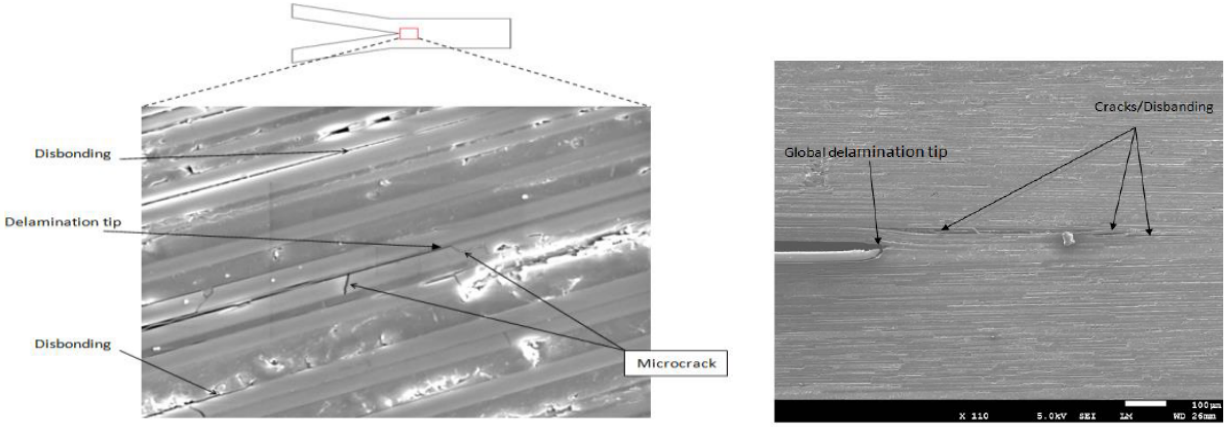

(a) Micro-cracks around the crack tip just before delamination growth [24] *(b)* Delamination tip front

Figure 2.2: Delamination tip behavior [22]

its intended propagating interface [24]. In an experimental setup as for example the double cantilever beam test, a pre-crack by means of a film between plies is required. When a crack is initiated from a film insert, the mechanisms of the plastic deformation around the crack tip differ than without a film insert [15]. This insinuates that the peak load is also affected by a film insert.

The plastic deformation of the matrix and cracking in the matrix around the crack tip show to be of influence on both the initiation as propagating value [15]. The micro-cracking and plastic yielding zone around the crack tip can already initiate the crack in the wrong interface as was discussed before, resulting that the delamination will not propagate through the intended interface. When the crack initiates in the intended interface, the change of delamination plane must be avoided at all times in order to generate valid interlaminar fracture toughness values. When the intended delamination interface does not coincide with the fiber direction, the delamination propagation interface often changes repeatedly for angle-ply, cross-ply, and UD interfaces. This is perhaps the greatest concern for measuring the G_c of MD laminates [7] and it is therefore important to understand the crack propagation behavior and factors, as this can influence the propagation plane.

2.1.2 Crack propagation

An important part of determining the fracture toughness of multi-directional CFRP material is the propagation and migration of the delamination. Delamination migration is the repeatedly changing of the crack propagation interface and is often observed for laminated interfaces when the intended crack growth direction does not coincide with the fiber orientation [7]. multi-directional laminates typically contain multiple random delamination cracks at several interfaces under low velocity impact or fatigue load and may be accompanied by transverse and general cracks. When the delaminations and cracks grow, delaminations in other interfaces may grow as well. Examples of random damages around the delamination interface can be found in figure 2.3. Furthermore, the delaminations of the neighbouring interfaces can join each other or the delamination can kink out of the initiation interface into neighboring interfaces on its own [14].

In addition, the fiber volume fraction of the laminates also plays a role in the crack propagation. Sacchetti et al. [25] found that the fracture toughness of carbon/PEEK increases with increasing thickness of a matrix rich bond line. Even when a matrix rich area is present near the crack tip but the crack does not propagate through it, the fracture toughness increases. This phenomenon is generally related to the radius of the plastic yield zone (r_y) in front of the crack tip. A matrix rich interface allows for a larger r_y, which relates to a higher energy dissipation that is reflected by a higher G_c. It is even argued that when the high plastic yielding zone is larger than the matrix rich region, the crack path migrates towards the weakest region, resulting in unstable crack growth. The r_y can be determined as follows:

$$r_y = \frac{1}{4\pi}(\frac{K_{IC}}{\sigma_y})^2(\frac{3}{2}(1-2\nu^2)) \tag{2.1}$$

where K_{IC} is the stress intensity factor related to the fracture toughness of the polymer, σ_y the tensile

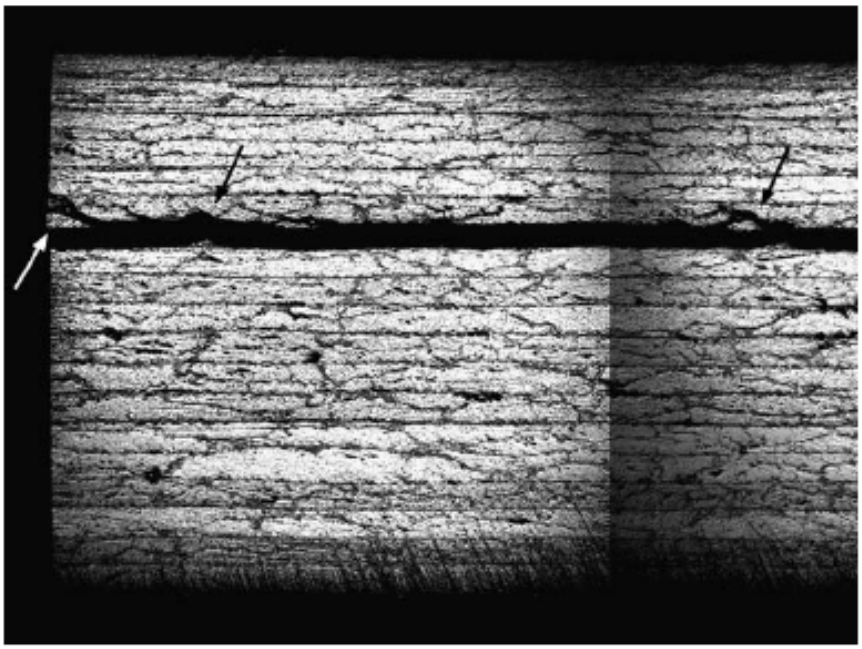

Figure 2.3: Random damages around the delamination interface, marked by the arrows [7]

yield stress of the polymer, and ν it Poisson's ratio. The energy release rate of the polymer can also be related to the K_{IC} factor:

$$G_{IC} = \frac{(1-\nu^2)K_{IC}^2}{E} \tag{2.2}$$

where *E* represents the modulus of the polymer [25]. For the polymer PEEK, Sacchetti et al. [25] determined the r_y to be 0.225 mm and the fracture toughness to be 4.8 kJ/m^2. When the matrix rich region increases further than the r_y, the crack will remain within the matrix rich region. It is suggested that the maximum theoretical G_c is reached when the matrix rich thickness is equal or larger than two time the plastic yield radius ($2r_y$), which is the toughness of the pure polymer. For the case of PEEK material, this would be 0.45 mm. However, another suggestion is that the G_c will keep on increasing with an increasing matrix rich bond line thickness. Figure 2.4 schematically shows the crack growth behavior and plastic zone development in a matrix rich bond line [25].

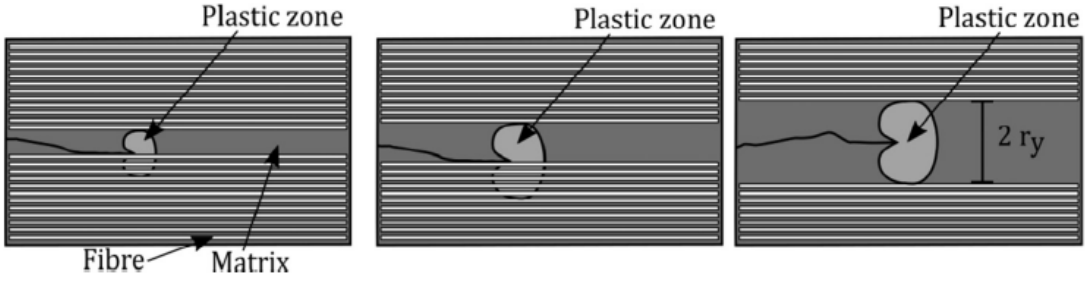

Figure 2.4: Crack growth behavior and plastic zone development related to the matrix rich bond line [25]

It can be observed that the fiber volume fraction deviates tremendously for a carbon/PEEK UD laminated sample, see figure 2.5. As matrix rich regions show to be tougher than fiber rich regions, these fiber volume deviations inside the laminate can change the crack propagation and fracture toughness value [25]. When the crack would propagate through or nearby these matrix rich zones, the material properties change and a sudden increase in toughness will be encountered, affecting the fracture toughness. In addition, the non-uniformity of the matrix rich zones contributes to unstable crack propagation. It is known that when a crack propagates from a region of higher toughness to a region of lower toughness, the elastic energy stored in

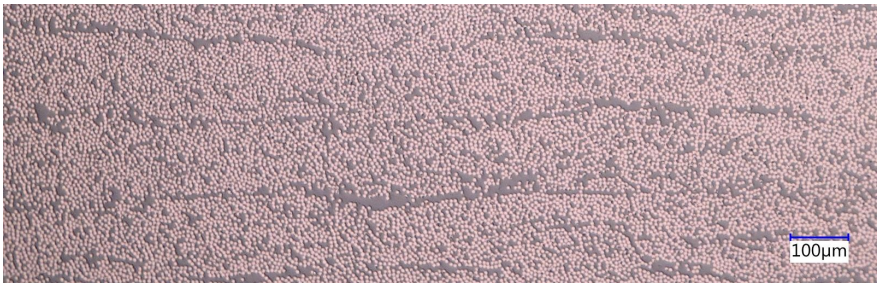

Figure 2.5: Variation in fiber volume of a carbon/PEEK UD laminate

the sample is more than required to make the crack propagate in a stable manner, causing the crack to propagate in an unstable manner [25].

The type of material where the crack propagates through determines for a great part the failure type. PEEK is a semi-crystalline polymer whose crystallinity varies with the cooling rate of the manufacturing technique. This variation indicates a change in matrix properties. Especially when full-scale structures are being manufactured, variations in cooling rate are sometimes inevitable which can result in variations of the material properties [20]. The variation in the matrix properties when present make it difficult to study the effect of the fiber direction on the interlaminar fracture toughness, as the matrix properties can vary within the intended interface. To eliminate the variation of the crystallinity as much as possible, it is important to cool the laminates according to the manufacturing guidelines and use as little variation in sample thickness as possible.

In 1987, Purslow [20] studied the fracture surface of DCB peeled carbon/PEEK specimen by means of fractographic research and found three types of failure: Slow ductile fractures, intermediate-brittle fractures, and fast-brittle fractures. The crack initiates as a slow ductile (S-D) fracture, this is the first type of failure. Due to massive plastic deformation in the initiation phase, shear stresses cannot develop and the crack propagates in a transverse mode. As the crack accelerates through the material, the failure becomes more brittle but remains transverse by nature. The crack front remains blunt and hairline cracks on several planes start to occur. This is the second type of failure, called the intermediate-brittle (I-B) fracture. I-B fractures show themselves as narrow bands with a wide variation in topography, as the crack velocity may vary considerably during this phase and failure occurs randomly between the planes before the hairline cracks fully develop. When the crack velocity becomes sufficiently rapid, shear stresses can now develop and plastic deformation is drastically reduced. Features such as rivers, scarps and cusps start to form on the fracture surface. This type of failure is the fast-brittle (F-B) fracture type and is the last type of fracture observed at room temperature. The different fracture types from are represented in the fractographic image of figure 2.6.

The F-B fractures occur preferentially between plies of different orientations, where one ply contains the direction of propagation. The unstable rapid crack propagation during the F-B phase often causes a reduction in the crack opening force at the tip and the failure will begin to decelerate, unless the crack opening displacement is very fast. As the crack is allowed to slow further, plastic deformation takes place and the energy absorption acts as positive feedback on the F-B crack propagation. When a significant amount of plastic deformation causes a much greater energy absorption of the ductile failure, the F-B crack will rapidly decelerate to a more stable S-D failure [20]. Another influence on the crack velocity are possible differences in Young's modulus of the composite laminate. It was found that the energy release rate increases when a crack approaches a soft inclusion, causing the crack to accelerate. When a stiff inclusion is being approached, the crack decelerates. The crack can sense such inclusions of different Young's modulus ahead at a distance approximately two times the inclusion size [26]. As the fibers within the crack propagation path can be observed as inclusions, the crack will naturally accelerate and decelerate according to the fiber volume of the interface which in turn affects the fracture type.

2.2 Testing methods

This study focuses on the suitability of the MP method to measure the interlaminar fracture toughness of mode I propagation (G_{Ic}) of a 0°-θ°interface. The MP setup measures a mode mixity, but the mode I is

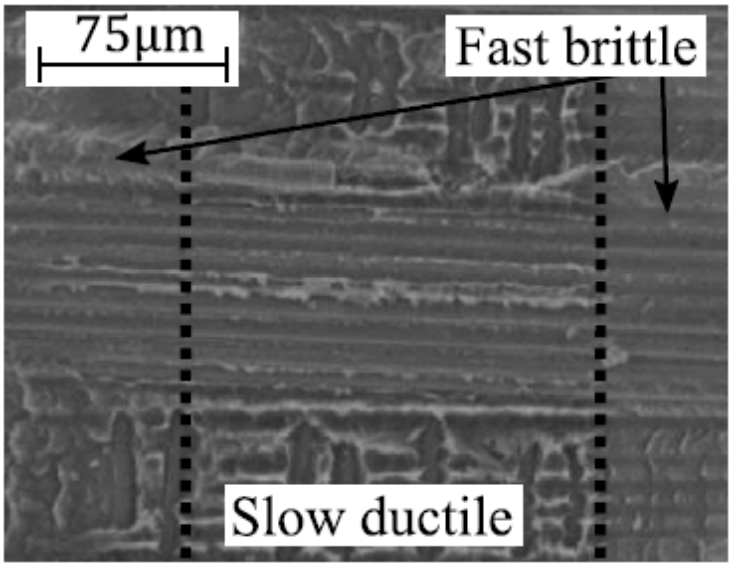

Figure 2.6: Fractographic image of carbon/PEEK with slow-ductile and fast-brittle failure types [21]

dominant [21]. A wide variety of testing methods to measure the fracture toughness are available and the most used testing methods are already well established. This section will give an overview on the methods that are suitable for this study with their most common advantages and disadvantages.

2.2.1 Double cantilever beam testing

The most widely used testing method for mode I interlaminar fracture toughness is the DCB test [22], see figure 2.7, which measures the longitudinal fracture toughness when the crack propagates parallel to the fiber direction between two plies [27]. The specimen has a pre-crack generated in the mid-plane and is loaded via the end-blocks, as can be seen in figure 2.7 [22]. This type of setup is open to a relatively simple analysis of the data, based on elementary beam mechanics [28]. The mode I fracture toughness is determined as follows:

$$G_{Ic} = \frac{P^2}{2B}\frac{dC}{da}1001[22] \tag{2.3}$$

with *B* as the width of the specimen, *P* the force, δ the displacement, *a* the crack length during crack propagation, and *C* the specimen compliance (ratio between displacement and applied load). As the arms of the specimen are not perfectly built in and rotations may occur at the crack tip, correction factors are required by using the modified beam theory method of data reduction. In this method, the DCB specimen is treated as if it had a longer crack length [22]. This expands equation 2.3 to:

$$G_{Ic} = \frac{3P\delta}{2B(a+\Delta)}\frac{F}{N}1001[21] \tag{2.4}$$

where Δ is a correction factor for the crack tip rotation and deflection. Factors *F* and *N* are correction factors for the large displacement of the test specimen arms and stiffening of the specimen by the load blocks, respectively [21].

The DCB test is standardized by for example the ISO Standard 15024-2001 [22, 27] or ASTM D5528-13 [27] and these standardizations are one of the main advantages of the DCB test. However, these standardizations concern only UD specimen and some difficulties arise when the DCB test method is used. For example, unstable crack propagation is mentioned for both woven fabric reinforced composites [9, 21] and UD laminated composites [3, 7, 11, 16, 27]. Secondly, it is reported that the G_{Ic} can vary widely with the DCB test as a function of the stacking sequence, adjacent fiber orientations and specimen geometry [15,16], making it more difficult to isolate the analysis of the intended interface and to compare results among different studies. Thirdly, the crack front of the DCB specimen may be curved and skewed, making the

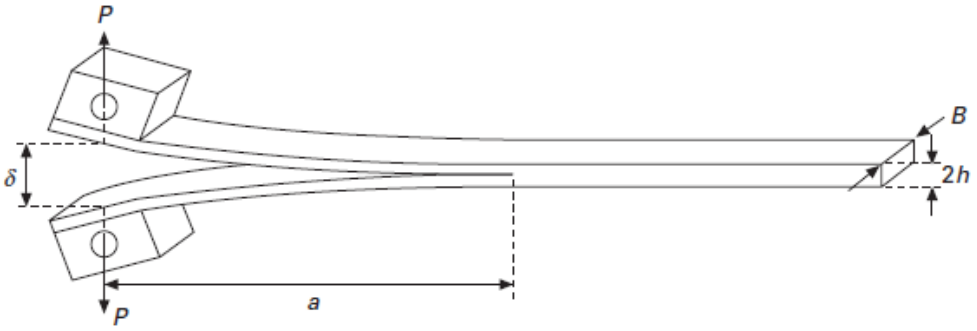

Figure 2.7: Schematic view of DCB test [22]

interpretation of the test data ambiguous. Ideally, the strain energy release rate should be uniform along the crack front in order to utilize the beam model to reduce the experimental data, but it is found to be non-uniform [29]. This non-uniformity is an effect of the DCB test, as during this test the mode I strain energy release rate is highest at the center and lowest at the edges. The non-uniformity is correlated to a non-dimensional ratio (D_c) and strongly depends on the stacking sequence of MD laminates. When the D_c value is sufficiently small, the current believe was that the non-uniformity could be neglected. However, it was found that even laminates with a small D_c the non-uniformity of the distribution of strain energy release rate across the delamination front is still of influence [16]. In addition, the specimen aspect ratios also play a roll in the non-uniformity, which are the crack length divided over the width and the thickness divided over the width [15]. The crack front curvature and skewness depend on the stacking sequence of the specimen and may contribute to the dependency of the fracture toughness on the lay-up. Consequently, the design of the DCB specimen should minimize the variation and skewness, which limits the design criteria [29]. Furthermore, the DCB test is not suitable to measure non-symmetrical interfaces, as otherwise the stiffness of the peel-arms are not equal which result in crack propagation away from the intended interface [15]. Finally, during the DCB test the position of the crack tip and crack length should be known at all times. A precise measurement of the crack tip position is not easy to achieve during the experiments, favoring methods that do not require to measure this [30].

2.2.2 Peeling tests

The peel tests measure the energy required to peel off a relatively flexible peel-arm from a rigid base. Peeling methods are an attractive application over the DCB test as the specimen can be designed quite economically and different material interfaces can be analysed [13]. Further advantages of the peeling tests are that the rate of delamination and the location of failure can be controlled quite precisely, simplifying the experimental process [28]. Peel tests can be classified by their different fixture configuration and commonly used peel test include the 90°peel test [13,28,31], 180°peel test [28,31], and climbing drum test [13,28,31], see figure 2.8. Each method will briefly be discussed.

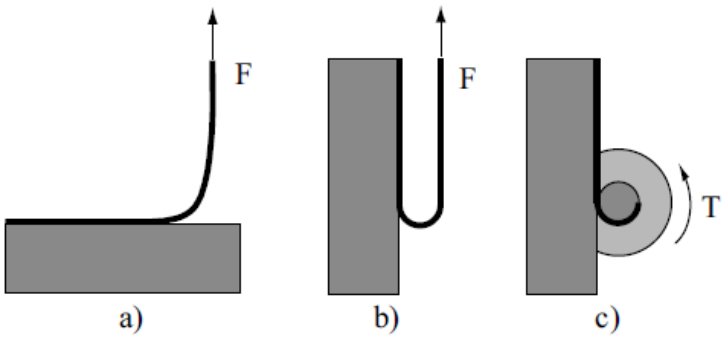

Figure 2.8: Standard peel test configurations: a) 90°peel test; b) 180°peel test; c) climbing drum test [28]

90°and 180°peeling tests

The 90°peel method (PN-EN 28510-1, EN 1939, ASTM D3330/D3330M-4) can be applied when one of the two adhesive joint adherends is flexible. The 180°peel method (PN-EN ISO 8510, ASTM D903) is applicable to test bonded joints of rigid and flexible adherends, as long as they can be bend to the required angle. When substrates exhibit lower flexibilities and whose peel strength cannot be determined at an angle of 180°for the risk of cracking or breaking, the 90°peel method shows itself to be particularly useful [31]. The major drawbacks of these methods are that the testing apparatus cannot guarantee to maintain a constant peel angle [31] and that the the location of failure at the peel front can become unstable, making the interpretation of the results ambiguous [28]. Furthermore, the peel-arm is inevitably bent with a certain curvature during the peeling, which can cause problems. When measuring a relatively tough interface with respect to the peel-arm, the curvature of the peel arm at the peel front could become too large, causing the fibers in the peel-arm to fracture [13].

Climbing drum test

The climbing drum method (ASTM D1781 [30]) is applicable when the peel-arm is flexible. The measurements are performed using a device equipped with a drum. The drum has two flanges, to which the peel-arm is attached. An external force applies a torque which causes the drum to roll on the specimen in the specified direction, detaching the peel-arm from the rigid body. During the climbing drum test, the bending angle of the peel-arm is maintained constant [31]. The advantage of the climbing drum test over the 90°and 180°peeling tests is that it can control the radius of curvature of the peel-arm [28]. However, peel-arm fracture prior to peel off can also occur in the climbing drum test as the conformation of the tape to the drum may not be achieved properly [13]. Other disadvantages of the climbing drum test are the combination of requirements, as it needs a large drum radius, flexible and thin peel arm and a large applied force during winding. As a thin peel arm cannot in all cases hold the required applied force, the requirements can sometimes be in contrast with each other. Furthermore, the weight of the drum is related to its diameter, which in turn is related to the peel-arm thickness. A large drum weight makes the handling of the test setup more difficult [30], leaving this method open for alternative testing methods.

2.2.3 Mandrel peel test

A promising method to examine the interlaminar fracture toughness between two adjacent plies is the mandrel peel (MP) test, where the peel-arm of a sample is bend around a mandrel and fixed in a universal testing machine, while the base is fixed on a sliding table [32]. Figure 2.9 shows a schematic overview of the MP test. There are many advantages of the MP method in comparison with the other tests. For example, the tested interface can be isolated from the rest of the specimen [21], the peel curvature can be maintained while the risk of fiber breakage decreases [13], and the peel angle does not fluctuate. From a practical viewpoint, the MP test is relatively simple to perform with straightforward sample preparation and data reduction procedure in comparison with the DCB test. In addition, the MP test requires less instrumentation as the crack length is not needed to be measured during testing. Moreover, the MP test generates more fracture toughness values for a single specimen in comparison with the DCB test, as the mandrel arrests unstable crack propagation. Consequently, the MP test generates more data points than the DCB test, resulting in a higher statistical relevance of the results [21]. Finally, Sacchetti et al. [21] found that the mandrel peel test limits the instability of unstable crack propagation in comparison with the DCB test.

The determination of the fracture toughness value by means of the MP setup is explained in the paper of W. Grouve et al. [8] and will be explained in the following section. The fracture toughness value is determined through the change in elastic strain energy per unit area of crack growth:

$$G = \frac{1}{b}\left(\frac{dU_{ext}}{da} - \frac{dU_d}{da} - \frac{dU_s}{da}\right) \tag{2.5}$$

where U_{ext} is the external work, U_d the energy dissipated during peeling, U_s the strain energy stored in the peel arm, *b* the width of the peel-arm, *da* the crack length increment, and *bda* the crack area change. The residual stresses due to the processing of thermoplastic composites should be included into the analysis of the external work, performed by the peel force F_p and alignment force F_a. The relation of the external

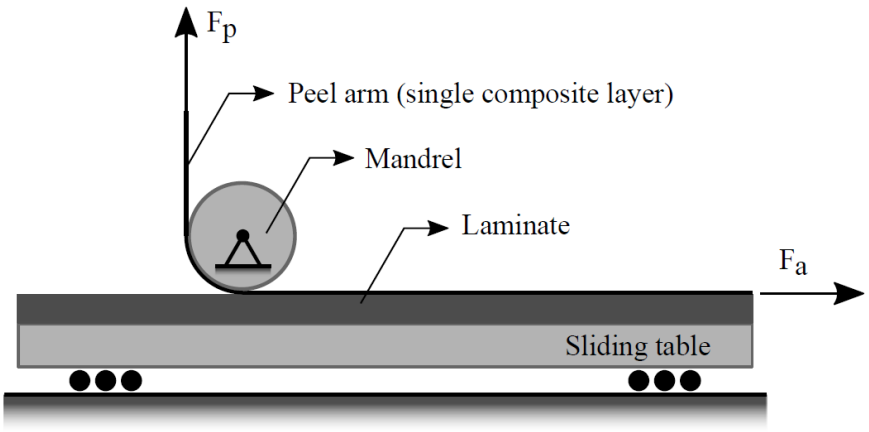

Figure 2.9: Mandrel peel setup [21]

work (dU_{ext}) is as follows:

$$dU_{ext} = -F_a da + F_p da + F_p da(\epsilon_m - \epsilon_r) = (F_p - F_a)da + \frac{F_p^2}{btE}da - \frac{F_p \sigma_r}{E}da \tag{2.6}$$

where *E* is the Young's modulus, *t* the thickness of the peel-arm ϵ_m the elastic strain in the peel-arm, and ϵ_r the pre-strain in the peel-arm caused by the residual stress σ_r in the bonded state. Furthermore, energy will be dissipated through friction (μ) in the setup and this should be taken into account. It is assumed that the friction is proportional to applied peel force, yielding an energy dissipation by friction of:

$$dU_d = \mu F_p da \tag{2.7}$$

The global strain energy (U_s) of the system consists of the tensile strain energy and residual strain energy that is stored in the peel-arm and bonded part of the peel-arm respectively. The change of the strain energy with respect to the crack growth is stated as:

$$dU_s = \frac{1}{2}\sigma_m \epsilon_m btda - \frac{1}{2}\sigma_r \epsilon_r btda = \frac{1}{2}\frac{F_p^2}{btE}da - \frac{1}{2}\frac{bt\sigma_r^2}{E}da \tag{2.8}$$

The energy release rate is found by combining the previously mentioned equations to:

$$G = \frac{1}{b}[F_p(1-\mu) - F_a + \frac{1}{2}\frac{F_p^2}{btE}da - \frac{1}{2}\frac{bt\sigma_r^2}{E}da] \tag{2.9}$$

However, as the energy dissipated through the plastic work together with the elastic strain of a UD peel-arm can be neglected, U_s and ϵ_m can be set to zero. This results in following equation for the energy release rate [8]:

$$G = \frac{1}{b}[F_p(1-\mu) - F_a] \tag{2.10}$$

2.2.4 Comparing DCB with MP

When measuring the interlaminar fracture toughness value, it is desirable that the crack will propagate in the slow-ductile (S-D) failure mode, as the fast-brittle (F-B) mode is more unstable. As both the DCB test and MP test are able to measure the fracture toughness value, it is important to understand the crack propagation during both methods in order to find the most suitable testing method. Both test methods measure the fracture toughness values by letting the crack propagate through an intended interface, but the means of arresting the unstable crack propagation differs. Sacchetti et al. [21] compared both methods by means of a fractographic analysis. It was found that for the DCB test the material itself has to stop the instable brittle propagation each time it occurs, meaning that the probability of crack arrests for the DCB test are therefore higher in tougher, matrix-rich regions. As for the MP test, the mandrel arrests the

unstable crack propagation, meaning that the crack arrest position will not necessarily be in a though region. This leaves that the interlaminar fracture toughness of the DCB is measured in tougher regions, resulting in an overestimation of the fracture toughness. As the MP test does measure the fracture toughness in more random positions, it is a more appealing method to measure the fracture toughness values. When Sacchetti et al. [21] analyzed the fracture surface of the peeled specimen, the two distinct S-D and F-B regions were observed, see figure 2.10. The F-B propagation is less common to find on the surface of MP specimen in comparison with DCB specimen, which again gains more favor to use the MP test over the DCB test when it comes to measuring the fracture toughness values. Nevertheless, it should be stated that unstable crack propagation is still predominantly observed on the fracture surface of MP specimen [21], so the experimental results should be analyzed with care.

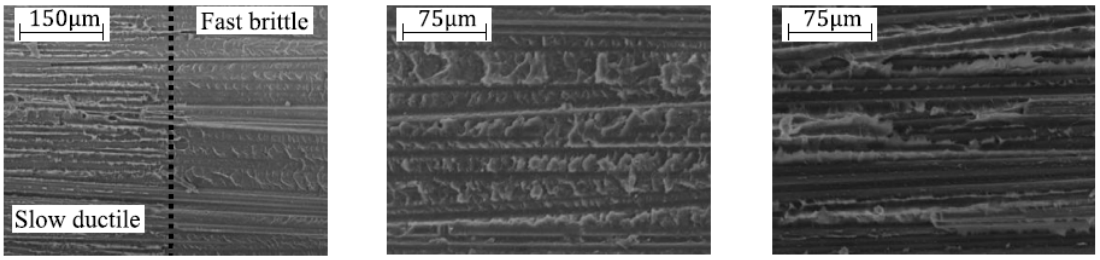

Figure 2.10: SEM fractography of MP surface from specimen of Sacchetti et al. [21]. Left: Combination of stable (slow-ductile) and unstable (fast-brittle) crack propagation. Center: Close-up of unstable crack propagation (fast-brittle). Right: Close-up of stable crack propagation (slow-ductile) [21]

The MP test is still in its early stages when it comes to measuring the fracture toughness values of laminated materials and several studies have been done to see if the test is suitable for this. Sacchetti et al. [9] compared the MP test with the DCB test and found promising results as more crack re-initiations after stick-slip were observed per unit length after unstable crack propagation (more information on the stick-slip behavior during the MP test will be discussed in chapter 3, section 3.1). In addition, Grouve et al. [8] found that the MP test was able to quantify the fracture toughness of a hybrid interface, which was not possible with the DCB test and end-loaded split (ELS) test. Su et al. [13] confirmed the findings of Grouve et al. [8], but added that the friction of the MP test influences the measurements of interfaces with lower fracture toughness significantly. It is not expected that the friction will affect the current study. Based on all the mentioned advantages of the MP test over the DCB and other peel tests, it is important to validate the MP method. One major blind spot of the MP test is when it comes to measuring the G_{Ic} of MD laminates, as it has not been established yet if the MP method is suitable for this. This research will aim to establish the suitability of the MP test on measuring the G_{Ic} of MD carbon/PEEK laminates. Chapter 3 will discuss the mandrel peel setup in detail, while the next section will discuss the relevant available theory on the effect of the fiber orientation on the measured fracture toughness value.

2.3 Fiber orientation interface

Over the past three decades, different observations have been reported regarding the effect of fiber orientation adjacent to the crack propagation on delamination behavior. For example, some studies find an effect of the fiber orientation and delamination resistance, where other studies claim to find no dependency when studying the same ply interface and material. Bin Mohamed Rehan et al. [16] examined these contradicting results of the fiber orientation dependency and found that different lay-ups used for the same delamination interface result in a significant difference in initiation delamination toughness, indicating that the effects due to the lay-up difference influences the delamination toughness. It is explained that the cause of this effect is the global stiffness of the laminate. It seems contradicting that the global stiffness is the cause of the different initiation toughness, as the stiffness of the samples is taken into account in the determination the fracture toughens. However, it has already been examined that the mode I fracture toughness values measured on specimens with different stiffness can be significantly different, even though the specimen have the same delamination interface. As the global stiffness depends mostly on the stacking sequence, it can

be concluded that the G_c of MD laminates does not only depend on the ply orientation interface, but also by the stacking sequence and testing method. In addition, the G_c values also seem to be influenced by the testing method. To observe the effect of the ply interface on the G_c values it is therefore important to use specimen with the same global stiffness and to avoid non-uniformity during testing [16].

As the results of the fiber orientation effect on the G_c value show contradicting results among different studies, the relation between the two is not still not fully understood. This makes it more challenging to establish whether the MP test is a suitable method to measure the effect of fiber orientation on the G_c. Therefore it is important to understand the already established literature on the fiber orientation. First, the results generated from the DCB test will be discussed, followed by the results of the MP test. Each section will end with an overview of the found results.

2.3.1 Fiber orientation and DCB test

A. Ramji et al. [14] studied the effect of interfacial fiber orientation on the delamination migration of CFRP laminates under mode I loading. The authors used carbon/epoxy with five different types of lay-up:

1. $[(0\ /\ 90)_7]_s$, with a *90°-90°*crack propagation interface
2. $[(0\ /\ 0)_7]_s$, with a *0°-0°*crack propagation interface
3. $[0\ /\ 90]_{14}$, with a *0°-90°*crack propagation interface
4. $[(0\ /\ 90)_6\ /\ -45\ /\ 90\ /\ 45\ /\ 0\ /(90\ /\ 0)_6]_s$, with a *90°-45°*crack propagation interface
5. $[(90\ /\ 0)_6, -45\ /\ 0\ /\ 45\ /\ 90\ /(0\ /\ 90)_6]_s$, with a *0°-45°*crack propagation interface

It was found that all orientations exhibit varying levels of crack migration away from the intended interface associated with the interfacial fiber orientation, except for the *0°-0°*interfaces. In addition, improved resistance to delamination growth is observed of the *90°-90°*, *0°-90°*, *90°-45°*interfaces with respect to the *0°-0°*interfaces. Furthermore it was found that delamination migration is closely linked to the distributions of the fiber and matrix materials around the crack front. It is suggested that the delamination path can be predicted based on the analysis of resin rich regions [14]. This is in line with the theory discussed in section 2.1.1 and 2.1.2. Finally, it was stated that the fracture toughness is most likely closely related to the delamination migration and interfacial fiber orientation. However, the results of the latter statement are not free of boundary effects and are delamination length dependent, requiring further research [14].

The specimen of the previous mentioned study measures symmetrical MD interfaces as the DCB test is not suitable to measure non-symmetrical interfaces, as the stiffness of the two peel-arms should be exactly the same to assure pure mode I fracture conditions. When the crack is not located at the exact mid-plane, mode II contributions can reach 37% of the total fracture energy release. Even if the specimen are managed to be symmetrical, the multiple cracking or crack shifting during the crack growth can destroy the specimen symmetry and measuring the G_{Ic} of the intended interface is not possible [15]. The fact that a *0°*- θ°angled interfaces cannot guarantee the required symmetry of the specimen makes the DCB test unsuited for measuring the G_{Ic} of those interfaces. Nonetheless, Gong et al. [15] tried to establish a relation between the fiber orientation and G_{Ic} for carbon/epoxy UD sheet by means of the DCB test, where symmetric angled interfaces were used. Three stacking sequence groups were made:

1. 16-ply: $[30$ / -30_2 / 03 / -30 /30_2 / -$30]_{sym}$
   The crack propagation plane is *30°- 30°*.
2. 16-ply: $[30$ / -30_2 / 30 / -30 /30_2 / -$30]_{anti-sym}$
   The crack propagation plane is *30°- -30°*.
3. 26-ply: $[0\ /\ \alpha\ /\ -\alpha\ /\ 0_2\ /\ -\alpha\ /\ 0\ /\ \alpha\ /\ 0_2\ /\ \alpha\ /\ -\alpha\ /\ 0]_{sym}$, with α = *0°*, *15°*, *30°*, *45°*.
   The crack propagation plane is *0°- 0°*. The goal of this lay-up is to isolate the effect of the stacking sequence on the G_{Ic} measurement.

Ideally, specimens that have a straight crack front have a quasi-uniform strain energy release rate (G_1) width-wise distribution, but the existence of the laminate coupling terms such as D_{12}, D_{16}, D_{26}, and B_{ij} complicate this distribution. With the DCB test, the G_1 value is highest at the center and lowest at the edges.

The degree of this non-uniformity increases with the material non-dimensional ratio D_c, which equals the coupling terms $D_{12}^2/D_{11}D_{22}$, and represents the relative difference in DCB deflexion between the cases of plane strain and plane stress. The skewness of G_1 depends on the non-dimensional material ratio B_t, which equals the coupling terms D_{16}/D_{11}. The non-uniformity of the strain energy release rate distribution along the crack front does not only depend on the laminate dimensionless parameters D_c and B_t, but also on the specimen aspect ratios crack length/width and thickness/width [15]. It was found that the 26-ply samples of the *0°*-*0°*interface show an increase in G_{Ic} with the sub-adjacent ply-angle α. The G_{Ic} value for specimen with sub-adjacent plies of *45°*show a 30% increase of the G_{Ic} with respect to *0°*angle. The same observation was found for the 16-ply specimen with the α-α interface. The G_{Ic} value increases as the adjacent ply-angle changes from *0°*to *45°*. The G_{Ic} value for specimen with a *90°*angle show a 13% higher G_{Ic} than that of specimen with an angle of *0°*. In addition, no difference in G_{Ic} values were found between the symmetrical and anti-symmetrical interfaces. These results indicate that the delamination resistance for mode I MD laminates are influenced by the adjacent ply orientations and even by the sub-adjacent ply-angles [15], making this study on the influence of the fiber orientation of the delamination interface inconclusive. The influence of the adjacent and sub-adjacent ply orientations can be explained as the damage around the crack tip is developed around the adjacent layers, as well as in the sub-adjacent layers. Only when the damage zone attains a critical volume, the crack can initiate to propagate [15]. The influence of the adjacent layers on the damage zone is an important statement as this effect should also be true for specimen tested with any type of testing method. The G_{Ic} values are not explicitly stated in this study and can therefore not be given. However, it can be stated that an increasing ply-angle was found to increase the fracture toughness.

As previously mentioned studies showed that the stiffness of the peel-arms are of great importance, Bin Mohamed Rehan et al. [16] aimed to isolate the influence of the ply orientation on the delamination behavior under mode I loading of carbon/epoxy material. The fully isotropic symmetric laminates were created by stacking 48 plies with the crack plane being placed symmetric about the mid-plane, resulting in six different symmetric delamination interfaces with sub-adjacent plies:

1. 0-0, with a *90°*sub-adjacent ply
2. 0-0, with a *45°*sub-adjacent ply
3. 45-45, with a *-45°*sub-adjacent ply
4. 45-45, with a *90°*sub-adjacent ply
5. 90-90, with a *0°*sub-adjacent ply
6. 90-90, with a *45°*sub-adjacent ply

The laminates were created in a way that the dimensionless parameters D_c and B_t, the in-plane stiffness and bending stiffness of each lay-up, are all equal to get equal global elastic properties, and to avoid non-uniformity. It was found that the bending elastic modulus of all specimen was independent of their stacking sequence, so the effect of the fiber orientation on the crack interface was isolated and analyzed correctly. However, many tested specimen showed unstable crack initiation and crack migration, reducing the measured quantities significantly. The available experimental data showed that the initiation toughness decreases slightly with the ply-angle for both adjacent and sub-adjacent plies, most likely due to the micro-cracking in the resin near the crack tip zone. In addition, it was found that the propagation resistance increases with the ply-angle and that the influence of the adjacent ply orientation seems dominant. These results are directly related to fiber bridging, as both bridging intensity and surface roughness appears to increase with the angle of interfacial plies [16].

2.3.2 Literature overview measured G_{Ic} DCB

Table 2.1 shows an overview of the results of the studies that were discussed in the previous section.

Table 2.1: Overview results literature research DCB test

Material	Interface	Lay-up	G_{Ic} [J/m^2]	Study
carbon/epoxy	90°-90°	$[(0\ /\ 90)_7]_s$	1164	[14]
carbon/epoxy	0°-0°	$[(0\ /\ 0)\_7]_s$	369	[14]
carbon/epoxy	90°-0°	$[0\ /\ 90]_{14}$	843	[14]
carbon/epoxy	90°-45°	$[(0\ /\ 90)_6\ /\ -45\ /\ 90\ /\ 45\ /\ 0\ /(90\ /\ 0)_6]_s$	801	[14]
carbon/epoxy	0°-45°	$[(90\ /\ 0)_6,\ -45\ /\ 0\ /\ 45\ /\ 90\ /(0\ /\ 90)_6]_s$	746	[14]
carbon/epoxy	30°-30°	$[30\ /\ \text{-}30_2\ /\ 03\ /\ \text{-}30\ /30_2\ /\ \text{-}30]_{sym}$	equal to 30°- -30°	[15]
carbon/epoxy	30°- -30°	$[30\ /\ \text{-}30_2\ /\ 30\ /\ \text{-}30\ /30_2\ /\ \text{-}30]_{anti-sym}$	equal to 30°-30°	[15]
carbon/epoxy	0°-0°	$[0\ /\ \alpha\ /\ \text{-}\alpha\ /\ 0_2\ /\ \text{-}\alpha\ /\ 0\ /\ \alpha\ /\ 0_2\ /\ \alpha\ /\ \text{-}\alpha\ /\ 0]_{sym}$, α = 0°	+- 390	[15]
carbon/epoxy	0°-0°	$[0\ /\ \alpha\ /\ \text{-}\alpha\ /\ 0_2\ /\ \text{-}\alpha\ /\ 0\ /\ \alpha\ /\ 0_2\ /\ \alpha\ /\ \text{-}\alpha\ /\ 0]_{sym}$, α=15°	+- 410	[15]
carbon/epoxy	0°-0°	$[0\ /\ \alpha\ /\ \text{-}\alpha\ /\ 0_2\ /\ \text{-}\alpha\ /\ 0\ /\ \alpha\ /\ 0_2\ /\ \alpha\ /\ \text{-}\alpha\ /\ 0]_{sym}$, α=30°	+- 430	[15]
carbon/epoxy	0°-0°	$[0\ /\ \alpha\ /\ \text{-}\alpha\ /\ 0_2\ /\ \text{-}\alpha\ /\ 0\ /\ \alpha\ /\ 0_2\ /\ \alpha\ /\ \text{-}\alpha\ /\ 0]_{sym}$, α=45°	+- 450	[15]
carbon/epoxy	0°-0°	48 plies, 90°sub-adjacent ply	478.86	[16]
carbon/epoxy	0°-0°	48 plies, 45°sub-adjacent ply	541.76	[16]
carbon/epoxy	45°-45°	48 plies, -45°sub-adjacent ply	502.96	[16]
carbon/epoxy	45°-45°	48 plies, 90°sub-adjacent ply	412.52	[16]
carbon/epoxy	90°-90°	48 plies, 0°sub-adjacent ply	428.43	[16]
carbon/epoxy	90°-90°	48 plies, 45°sub-adjacent ply	392.72	[16]
carbon/epoxy	0°-0°	48 plies UD	629.70	[16]

2.3.3 Fiber orientation and mandrel peel test

Grouve et al. [8] studied in 2013 the applicability of the MP test for the G_c of thermoplastic composites by comparing it with the DCB and ELS test for mode I and II respectively. As the current study focuses on the mode I, only the DCB results will be discussed. The MP setup has a mandrel radius of 5 mm, an alignment force of approximately 75 N and a peeling rate of 15 mm/min. Two type of laminates were produced:

1. carbon/PPS hybrid specimen with 5 Harness Satin weave and UD reinforcement, 3.44 mm in thickness.
   Pre-crack for DCB test is inserted between the 0°UD ply and a [90/0] weave ply.
2. carbon/PPS UD pre-preg, 2.93 mm in thickness.
   Pre-crack for DCB test inserted at the mid-plane.

The lay-up of the weave specimen was chosen such that for the DCB test the flexural rigidity of both arms was approximately the same and any influence of deformation due to residual thermal stresses was minimized. The pre-cracks for the MP specimen were inserted between the first and second ply. The specimen for the DCB test are 20 mm wide, while the MP test specimen are 8 mm in width. The results show that the UD specimen with the MP test show a decrease of 20% on the G_{Ic} factor in comparison with the DCB test. As the fiber bridging of the MP specimen shows to be smaller than with the DCB specimen it is suggested that this causes the decrease of the fracture toughness value. For the hybrid specimen the DCB test was unsuccessful, as the crack migrated into the adjacent UD plies. The G_{Ic} could however be obtained by means of the MP test and show a standard deviation of less than 5% of the average, suggesting that the repeatability is satisfactory [8]. The lower measured G_{Ic} of the UD specimen with respect to the DCB specimen could be related to the non-uniformity of the crack front [15] and the different stiffness of the specimen arms during the DCB test [16]. If this is the case, it is possible that the MP test is more suitable to measure the fracture toughness than the DCB test, as the MP test excludes those factors.

Sacchetti et al. [9] continued in 2016 to study the applicability of the MP test to quantify the G_{Ic} of carbon/PEEK 5 harness satin weave composite specimen, with a lay-up of $[(0/90)/(0/90)_r]_{4s}$. The DCB specimen are 20 mm in width while the MP specimen are 10 and 18 mm wide. The MP setup has a mandrel radius of 10 mm, an alignment force of approximately 60 N and 108 N for the 10 mm wide and

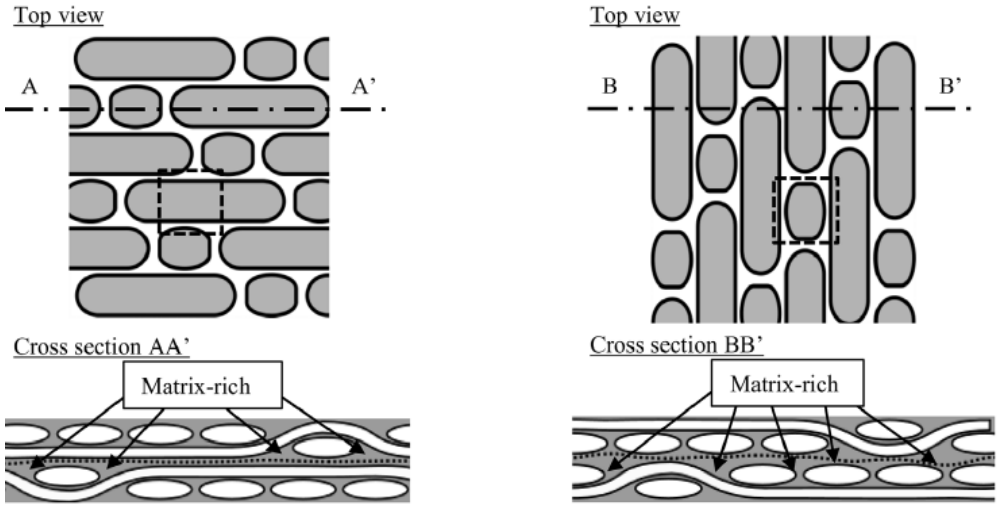

Figure 2.11: Crack propagation paths. Left) parallel specimen. Right) perpendicular specimen

18 mm wide specimen, respectively. The effect of the peeling rate was set to 3 mm/min and 30 mm/min to study the peeling rate effect on the measured G_{Ic}. It was found that the results are not affected by the peeling rate, but an increase in specimen width results in a decrease of the G_{Ic} and standard deviation. The authors suggest to implement further research to understand the effect of the specimen width on the results, as this result was not expected. For the 10 mm wide specimen, the measured G_{Ic} shows to be similar with the DCB samples. It was concluded that the MP test can be considered to be an easy and fast test compared to the DCB test, as both methods yield similar G_{Ic} values and similar crack propagation.

However, the MP test showed that the unstable crack growth is limited in comparison with the DCB test, resulting in 20 times more data points per unit crack length than the DCB test. However, the MP test shows a lightly higher standard deviation with respect to the DCB test [9].

A second study by the same authors in 2018 also focuses on the applicability of the MP test to quantify the G_{Ic} of carbon/PEEK 5 harness weave material, but this time the G_{Ic} was measured both parallel as perpendicular to the predominant fiber direction at the crack propagation interface and was compared with both the DCB and ELS test [21]. As this study focuses on the mode I, only the DCB results will be discussed. The used lay-up was $[(0/90)/(0/90)_r]_{4s}$. The MP setup has a mandrel radius of 10 mm, an alignment force of approximately 60 N and the peeling rate was set to be 30 mm/min. It was found again that the measured G_{Ic} of the DCB and MP specimen are similar and that the unstable crack propagation of the specimen is immediately arrested by the mandrel, limiting the instability of the crack propagation.

In addition, it was found that the perpendicular specimen showed a higher fracture toughness than the parallel ones with both the DCB as MP test. This is due to the division of matrix to fiber regions of both types of specimen. The parallel specimen show that the crack front is composed of both fiber bundles and matrix regions. This composition does not change with crack propagation, as the crack is wide compared to the unit cell size. For the perpendicular specimen, the composition at the crack tip caries along the crack length with matrix-rich zones between the fiber bundles exactly lining up with the crack front at regular intervals. This makes that the crack how to propagate through the tough matrix material, resulting in a higher measured G_c. Figure 2.11 shows the crack propagation path of both the parallel as the perpendicular specimen. In addition, it was stated that the G_c is also influenced by the tortuosity of the crack path, an increase in tortuosity leads to an increase of G_c. When looking at figure 2.11, it can be seen that the tortuosity of the crack propagation changes with the parallel and perpendicular specimen. The perpendicular specimen show to have a higher tortuosity than the parallel specimen [21]. The observation that the crack tortuosity and crack direction influence the G_c value for carbon/PEEK weave material is a strong indication that the fiber direction of MD carbon/PEEK laminates influence the G_{Ic}, as the crack does not propagate parallel to the fiber direction. It will therefore encounter more matrix-rich zones and the crack will show higher tortuosity as the fiber angle increases. The fractographic research performed during the study of Sacchetti et al. [21] is already discussed in section 2.2.4.

Non-symmetrical interfaces and the mandrel peel test

The previously mentioned studies analyzed weave and hybrid composite material, and did not look into the possibility of using the MP method to measure the fracture toughness of non-symmetrical interfaces. Forkink [33] tried to establish a relation between the fracture toughness and interface fiber direction of carbon/PEEK *0*°-θ°interface laminates by means of the MP test. An alignment force of 75 N with a peeling rate of 15 mm/min was used. The radius of the mandrel is not stated. The used lay-up is not symmetric and is [0//θ/0_{14}], where // indicates the location of the pre-crack. Due to the non-symmetry the specimen showed significant warping. Four type of *0*°-θ°interfaces were tested, θ = *0*°, *15*°, *30*°, and *45*°.

No relation between the fiber orientation and fracture toughness could be established as all specimen showed a toughness in the range of 1.4 to 1.6 kJ/m^2, which is comparable with the *0*°-*0*°interface found in the literature. In addition, the crack deviated into the peel-arm, away from the intended interface. It was stated that the results are most likely influenced by the warping of the specimen, as internal stresses are present. In addition, as all cracks propagate into *0*°orientation peel-arm it is also possible that this contributes to finding no relation between fiber angle and fracture toughness, as the material properties and therefore the fracture toughness of all pee-arms should be equal. Furthermore, the alignment force deviated during the experiments, introducing additional variations within the results [33].

Van den Boogert [34] continues the research with a similar objective and methodology as Forkink [33], but changed the carbon/PEEK lay-up to a symmetric one, namely [0 // θ /0_{14} /θ /0]. The alignment force and peeling rate were kept the same with 75 N and 15 mm/min, respectively. The radius of the mandrel is not stated. Four type of *0*°-θ°interfaces were tested, θ = *0*°, *60*°, *75*°, and *90*°. These angles were chosen expand the research of Forkink [33].

A relation between the fiber orientation and fracture toughness was found, namely that the *0*°-*60*°interfaces show an increase in the fracture toughness of 19% with respect to the *0*°-*0*°interface, whereas the *0*°-*75*°and *0*°-*90*°show an increase of 29%. However, it was found that the cracks of the *0*°-*0*°interface specimen migrated in both the peel-arm and substrate, while the cracks of the *0*°- θ°interface specimen tend to propagate into the peel-arm. Another observation of this research is that stick-slip seems to occur during the experiments and the author suggests additional research on this phenomenon. It is suggested that when the peel-arm conforms to the mandrel again after loosening it's grip, the crack propagates with a higher speed than the 15 mm/min, what could cause a sudden drop of the peeling and alignment force. The surface of the unstable crack propagation show no bare fibers, indicating that the crack propagates in the matrix, see figure 2.12 [34].

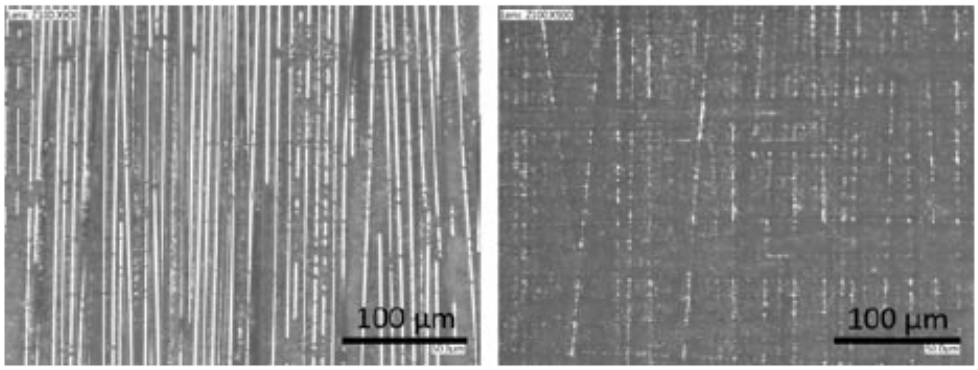

Figure 2.12: Difference in surfaces. Left) surface of normal crack propagation. Right) Surface of stick-slip behavior

2.3.4 Literature overview measured G_{Ic} mandrel peel

As the crack propagation is migrating away from the intended interface, or showed unstable crack propagation of most presented studies [9,21,33,34], the question arises if the measured G_{Ic} is valid, even if the obtained results are in line with the studied literature. In addition, the presence of stick-slip behavior [9,21,34] complicates the analyses. It is therefore important to understand the crack propagating behavior of the material when it is tested on the MP test together with the parameters of the MP test to see if the unstable

crack propagation can be avoided. When unstable crack propagation can be avoided, the MP test will be the best setup to test mode I fracture toughness of materials in comparison with the other methods due to its relative ease. This study will first analyse the MP setup to see if any parameters influence the measured G_{Ic} and crack propagation. After that, the crack propagation behavior of the specimen tested with the MP test will be studied to get a better understanding of its behavior. The next chapter will discuss the MP setup in detail together with more information on the stick-slip phenomenon and its causes.

Table 2.2: Overview results literature research MP test

Material	Interface	Lay-up	Width [mm]	G_{Ic}[J/m^2]	Method	Study
carbon/PPS weave	Midplane	5 Harness Satin	20	700	DCB	[8]
carbon/PPS weave	0°-(90/0)°	5 Harness Satin	8	975	MP	[8]
carbon/PPS UD	Midplane	UD	20	1080	DCB	[8]
carbon/PPS UD	0°-0°	UD	8	853	MP	[8]
carbon/PEEK weave	Midplane	$[(0/90)/(0/90)_r]_{4s}$	20	+- 1550	DCB	[9]
carbon/PEEK weave	(0/90)°-(0/90)°	$[(0/90)/(0/90)_r]_{4s}$	10	+- 1500	MP 3 mm/min	[9]
carbon/PEEK weave	(0/90)°-(0/90)°	$[(0/90)/(0/90)_r]_{4s}$	10	+-1490	MP 30 mm/min	[9]
carbon/PEEK weave	(0/90)°-(0/90)°	$[(0/90)/(0/90)_r]_{4s}$	18	+-1300	MP 30 mm/min	[9]
carbon/PEEK weave	(0/90)°-(0/90)°	$[(0/90)/(0/90)_r]_{4s}$	20	1650	DCB Parallel	[21]
carbon/PEEK weave	(0/90)°-(0/90)°	$[(0/90)/(0/90)_r]_{4s}$	20	2590	DCB Perpendicular	[21]
carbon/PEEK weave	(0/90)°-(0/90)°	$[(0/90)/(0/90)_r]_{4s}$	10	1500	MP Parallel	[21]
carbon/PEEK weave	(0/90)°-(0/90)°	$[(0/90)/(0/90)_r]_{4s}$	10	2290	MP Perpendicular	[21]
carbon/PEEK	0°-0°	[0-θ/0_{14}]	10	1490	MP	[33]
carbon/PEEK	0°-15°	[0-θ/0_{14}]	10	1540	MP	[33]
carbon/PEEK	0°-30°	[0-θ/0_{14}]	10	1450	MP	[33]
carbon/PEEK	0°-45°	[0-θ/0_{14}]	10	1400	MP	[33]
carbon/PEEK	0°-0°	[0$\|\|$ θ /0_{14} /θ /0]	10	1180	MP	[34]
carbon/PEEK	0°-60°	[0$\|\|$ θ /0_{14} /θ /0]	10	1410	MP	[34]
carbon/PEEK	0°-75°	[0$\|\|$ θ /0_{14} /θ /0]	10	1530	MP	[34]
carbon/PEEK	0°-90°	[0$\|\|$ θ /0_{14} /θ /0]	10	1520	MP	[34]

Chapter 3

Background: Mandrel Peel setup

The mandrel peel test has been introduced in section 2.2.3 as an alternative test method to characterize the interlaminar fracture toughness between two plies. There are many advantages of the mandrel peel test, such as that the tested interface can be isolated from the rest of the specimen [21], the peel curvature can be maintained while the risk of fiber breakage decreases [13], and the peel angle does not fluctuate. In addition, the MP test ensures more crack re-initiations per unit length after unstable crack propagation [9]. A schematic drawing of the mandrel peel test can be seen in figure 3.1. The setup bends the peel-arm of a sample around a mandrel while the peel-arm is fixed in a universal testing machine. This machine will peel with a set rate while applying an alignment force to the base of the sample in order to ease conformation of the peel-arm to the mandrel [32]. The mandrel peel setup is still at an early stage when it comes to measuring the fracture toughness of composite materials, which means that the settings used during the experiments and their effects on the measurement results are not fully understood yet. To measure the fracture toughness between two adjacent plies it is important that the crack propagates through the intended interface, otherwise an intralaminar fracture toughness will be measured. To avoid shifting of the delamination plane it is important to understand all the parameters of the setup. When looking at figure 3.1, it can be observed that three forces are of major importance, which are the peeling force (F_p), the alignment force (F_a) and the force the mandrel places on the specimen. The latter is dependent on the position of the mandrel with respect to the sample. The fracture toughness (G_c) can be determined via a relation between the width of the specimen, the internal friction, the peeling force and the alignment force via equation 2.10 [8], see section 2.2.3 for the full analysis of G_c. The effect of the specimen dimensions, internal friction, F_p, and F_a on the experimental results will be discussed in the next sections of this chapter.

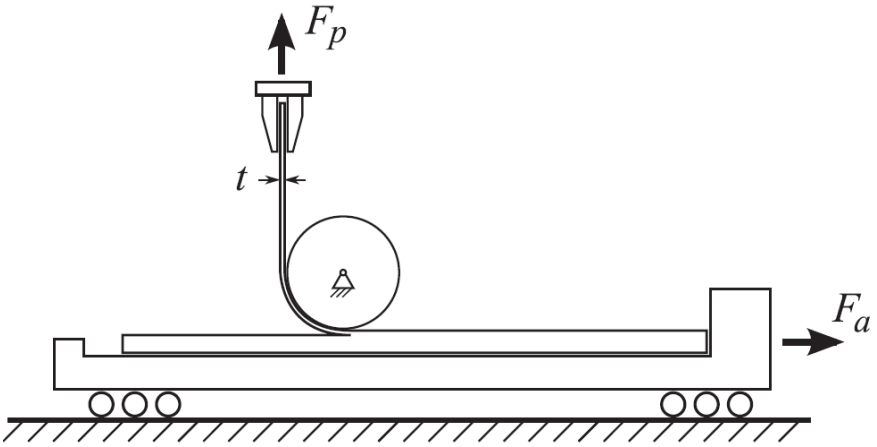

Figure 3.1: Schematic overview of the mandrel peel setup, from [8]

3.1 Stick-slip behavior

To study the fracture toughness (G_{Ic}) by means of the MP test it is important that the crack propagates through the intended interface and grows in a stable manner. It is already observed by Sacchetti et al. [21] that the crack propagation during the mandrel peel test can be unstable, such as crack jumping, crack migration away from the intended interface, and stick-slip behavior. Stick-slip behavior is best explained by the schematic image of figure 3.2 [21]: In the initial loading phase, the peel-arm conforms to the mandrel (stage A). As the loading increases, stick is observed as the crack does not propagate. As a result, conformation of the peel-arm to the mandrel cannot be maintained (stage B). The force keeps on increasing and when it reaches a peak load, the stored energy in the system is high enough to propagate the crack (stage C). Stick-slip behavior can occur suddenly and is accompanied by an abrupt drop in the peeling force (slip). When this sudden crack propagation comes to an end, the peel-arm conforms to the mandrel again (stage A) [21].

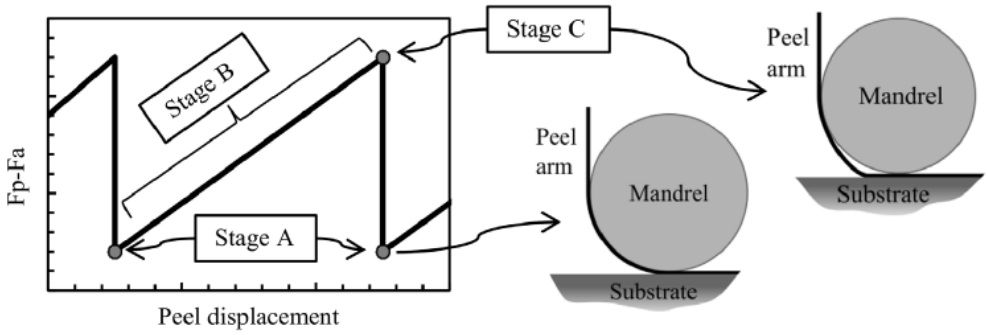

Figure 3.2: Schematic illustration of the stick-slip phenomenon [21]

Stick-slip behavior causes deviations in the crack propagation velocity, which therefore influences the results and in extreme cases causes the peel-arm to break [9]. As conformation of the peel-arm to the mandrel seems of importance in the stick-slip behavior, it should be noted that the stick-slip behavior is not only caused by an improper conformation of the peel-arm to the mandrel, but is rather an effect of a sudden change in crack propagation. The reason for this sudden change can originate from different factors. The first reason for stick-slip behavior is that it is caused by the non-uniform matrix to fiber ratio within the interface. As can be seen in figures 2.5 of section 2.1.2, the fiber to matrix ratio of carbon/PEEK UD laminates is non-uniform. As is discussed in section 2.1.2, the failure becomes more brittle as the crack accelerates through the material, resulting in intermediate-brittle (I-B) and fast-brittle (F-B) failure types [20]. This is prone to happen in fiber rich areas [25]. When the crack encounters a matrix rich region, the plastic deformation increases causing an absorption of the energy, which will rapidly decelerate the crack propagation to the slow-ductile (S-D) failure type [20]. The rapid deceleration of the crack propagation from F-B to S-D and vice versa is observed as stick-slip behavior, where the S-D failure type coincides with stick and the I/F-B types coincide with slip. The sudden changes of the toughness encountered by the crack contribute to unstable crack propagation [25] as is mentioned in section 2.1.2, so the presence of stick-slip is an indicator of unstable crack propagation.

Secondly, stick-slip can occur due to the damage zone at the crack tip of angled laminates. It was already described by Purslow [20] that F-B fractures prefer to propagate between plies of different angles where one ply contains the direction of propagation. As is explained in section 2.1.1, the damage zone around the crack tip exists out of micro-cracks and the intensity of the micro-cracking increases as the ply-angle of the plies increases. This leads to a drop in the toughness [16], resulting in F-B fracture propagation. When this type of crack propagates, the plastic deformation increases, which will again lead to the rapid deceleration of the crack propagation to the S-D failure type [20].

The last cause attributed to stick-slip behavior is due to the varying crystallinity of the polymer material as described in section 2.1.2. As the crystallinity is determined by the cooling rate during manufacturing, variations of the material properties are induced when the specimen have not been cooled sufficiently slow, or when the specimen significantly varies in thickness. The variations in the crystallinity cannot be controlled outside of the cooling rate. It is plausible that within a manufactured product that has significant variations in thickness, the crystallinity varies in toughness, causing either more S-D propagation or F-B propagation.

When the crack propagates and the crystallinity suddenly changes, stick-slip will occur. However, as this study will use specimen with an equal thickness throughout its length, variations of crystallinity are not expected to occur.

3.2 Forces and friction

The alignment force is used to ease the conformation of the peel-arm to the mandrel [32] and depends on the width of the specimen, the fracture toughness, the mandrel radius, the type of material, and the thickness of the material [35]. As already stated in the previous section, an improper conformation could result in stick-slip behavior, or vice versa, which can cause deviations in the crack propagation velocity and plane [9]. Even though the possibility exist that stick-slip is caused by sudden propagation of the delamination into neighboring interfaces, it is still important to avoid stick-slip based on improper mandrel conformation. It is found by Kawashita et al. [36] that higher alignment loads show a more consistent crack propagation plane for metal peel-arms, yet also result in a reduction of the fracture toughness value. The required alignment load cannot be determined yet by means of a protocol or formula, instead it requires experience according to the research of Kawashita et al. [35] and is obtained by means of trial experiments.

As in most experimental setups, the mandrel peel test deals with internal friction due to moving parts that can influence the results. The protocol for fracture toughness measurements by means of the mandrel peel test states that the total friction of the system cannot exceed 5% to avoid influencing the results [35]. To lower the friction as much as possible, the mandrel peel setup uses a linear bearing system for the sliding table and bearings as mandrels, as described by Kawashita et al. [32, 35]. The friction (μ) is dependent on the peeling and alignment force and can be determined through equation 3.1 [21]:

$$\mu = \frac{F_p - F_a}{F_p} \tag{3.1}$$

The friction can be measured by performing the mandrel peel experiment on a sample that has already been peeled [9]. However, due to the peeling fibers in the top and bottom ply are pulled out of the matrix and lie bare at the surface. When the plies are being stacked together again for the friction measurement, it is possible that the bare fibers might hook into each other, causing additional forces needed to separate the intertwined fibers on top of the friction force. To avoid this from happening, the friction measurement can take place in the pre-crack. Additional advantages of this technique is that the friction and peeling force can be measured in one motion, and the settings of the setup remain the same during both tests. To test the applicability of this new way of measuring the friction, a reproduction of the experiments of Forkink [33] are done with left over specimen from that research. It was determined that the friction coefficient can be determined by measuring the friction of the system in the pre-crack. The friction coefficient and fracture toughness value generated by the new way of testing differs less than 1% with respect to the values generated by Forkink [33].

3.3 The mandrel

Besides affecting the friction due to the rolling contact, the mandrel affects the shifting of the delamination plane. Sacchetti et al. [9] found that the distance of the unstable crack propagation is limited in comparison with the standard DCB test. The mandrel provides numerous crack re-initiation values per unit of crack length, as the mandrel arrests the unstable crack propagation each time it occurs [21].

The parameters related to the mandrel are the vertical placement and mandrel size. The vertical placement of the mandrel with respect to the specimen is an important parameter, as it can influence breakage of the peel-arm and the friction. When the mandrel is placed to far from the base of the sample, the alignment force, peeling force, and angle θ can make the peel-arm break, as can be seen in figure 3.3 [35]. In addition, when the mandrel is not firmly pressed against the base of the sample, the sample might lift from the sliding table, causing additional internal stresses within the specimen. When the mandrel is firmly pressed against the sample, the risk of breaking the peel-arm lowers together with the risk of unstable crack propagation. Nevertheless, the friction of the setup increases when the mandrel is firmly pressed against the sample. The vertical placement of the mandrel with respect to the specimen is a balance between the mandrel being

as near to the sample as possible but without the overall friction of the equipment to exceed the 5% [35], so it is recommended to experiment with the placement of the mandrel.

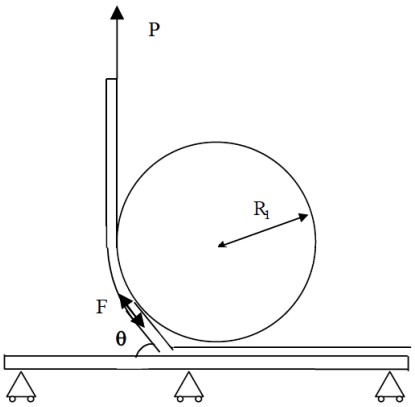

Figure 3.3: Peel-arm behavior when vertical placement of mandrel is 0.5 mm [35]

The diameter of the mandrel does not seem to influence the fracture toughness results according to Kawashita et al. [32], but affects the maximum bending strain of the peel-arm related to the thickness of the peel-arm [13]. Therefore, the mandrel radius (*R*) and peel-arm thickness (*h*) are closely related. To avoid peel-arm breakage, the maximum bending strain of the peel-arm (ϵ) can be determined through equation 3.2:

$$\epsilon = \frac{h}{2 * R} \tag{3.2}$$

3.4 Sample dimensions

The dimensions of the specimen to take into consideration are the width of the sample, the total thickness, and the thickness of the peel-arm. When looking at the formula for determining the fracture toughness, see equation 2.10, it can be seen that the forces are divided by the width of the specimen, meaning that the width should not be of influence on the fracture toughness value. Nonetheless, a study done by Sacchetti et al. [9] on carbon/PEEK 5 harness satin weave material showed contradicting results. It was found that the wider peel-arm results in a slightly lower fracture toughness value and decreases the standard deviation, but the authors did not give any plausible causation for this effect. The authors recommend further research to understand these results [9]. As this study uses UD material instead of weave material, the encountered dependence of the width on the fracture toughness value might differ. It is not expected that a wider peel-arm influences the fracture toughness, as the fracture toughness value is determined by dividing the value with the width of the specimen. Nonetheless, it is recommended to experiment with the width of the specimen to confirm its effect.

3.4.1 Thickness

The total thickness of the specimen also influences the global stiffness, therefore, it should be taken into account as a plausible influence on the delamination resistance. Davies et al. [10] already established a genuine effect of the specimen thickness on the propagation values in 1989 when testing with the DCB method. The authors state that the higher fracture toughness values of thicker specimen are the result of crack initiation and propagation on intralaminar level surrounding the initial crack plane, together with the increased contributions of fiber bridging and breakage. This effect casts doubt on the usefulness of propagation values to characterize delamination resistance in this type of material [10]. However, the base of the specimen during the mandrel peel test is fixed on the sliding table, theoretically only leaving the geometry of the peel-arm to be of plausible influence on the measured fracture toughness. As with different testing

methods the delamination interface cannot be isolated from the geometry of the specimen, comparison of results among different studies should therefore be treated with care.

3.4.2 Peel-arm

The peel-arm is an important parameter in the mandrel peel method, as the universal testing machine applies the peeling force on the peel-arm. Besides that the peel-arm influences the conformation to the mandrel, the thickness of the peel-arm can also influence the experiments. Kawashita et al. [36] studied the effect of the peel-arm thickness on the adhesive fracture toughness of rubber toughened epoxy-aluminium alloy laminates. The authors tested with peel-arms of 0.5, 1, and 1.5 mm in thickness. A smaller G_C was observed when the peel-arm thickness was 0.5 mm in comparison with the fracture toughness of the 1 mm and 1.5 mm peel-arm. It was mentioned that the interfacial fracture might be responsible for the lower G_C [36]. It is important to note that the peel toughness of metal peel-arms include other energies like plastic work in bending the the peel-arm around the mandrel [32], but this will not be the case for a peel-arm with a fiber direction parallel to the peeling force. Nonetheless, the thickness of a carbon/PEEK peel-arm still influences the stiffness of the peel-arm and could therefor influence the measured fracture toughness.

3.5 Preliminary study: Mandrel peel test

The theory described in this chapter states the different aspects and parameters of the mandrel peel setup needed to measure the fracture toughness of carbon/PEEK UD material. Together with the theory mentioned in chapter 2, the hypothesis of this study is that the MP method is applicable to establish a relation between the interlaminar fracture toughness and a *0°*-θ°interface. It is expected that with increasing ply-angle, the fracture toughness increases as well. However, the mentioned theory is not exclusive enough to state the correct parameters of the setup and dimensions of the specimen to make sure the experiments can be performed correctly. To find if the MP setup is applicable to measure the fracture toughness of *0°*-θ°interfaces correctly, it is of most importance to find the best experimental settings and specimen dimensions to see if they influence the results. This will be done in the preliminary study.

3.5.1 Preliminary study: Objective and outline

The preliminary study will answer the following sub-questions in order to perform the experimental part of this research:

1. *"What are the best settings of the mandrel peel setup to measure the fracture toughness between two plies of carbon/PEEK UD without inducing crack migration?"*

2. *"What are the best dimensions of the carbon/PEEK UD specimen to measure the fracture toughness between two plies with the mandrel peel setup without inducing crack migration?"*

3. *"Do the settings of the mandrel peel setup influence the measured fracture toughness values?"*

4. *"Do the dimensions of the carbon/PEEK UD specimen influence the measured fracture toughness values?"*

5. *"Do the settings of the mandrel peel setup influence the crack initiation?"*

6. *"Do the dimensions of the carbon/PEEK UD specimen influence the crack initiation?"*

The needed theory to design the experiments for the preliminary study are given in the previous chapters. The methodology for the preliminary study can be found in Appendix A and the results in Appendix B. The results of the preliminary study are a direct input to the methodology of this research and will therefor be repeated in the next section.

3.5.2 Preliminary study: Conclusion

The preliminary study found no visible trend between the used parameters and crack propagation. During the experiments it was found that the crack can propagate away from the delamination interface, while no stick-slip behavior occurred. The reason that no stick-slip behavior is found during these experiments might be due to the UD lay-up. The specimen are all build from UD material in the *0°*direction. During consolidation, it is common for UD laminates that fibers of adjacent plies nest together, causing fiber bridging [18]. When fiber bridging occurs, the interfaces of the laminates are more blend together. This blending of the interfaces make it challenging to track the delamination propagation interface and make the laminate more uniform in general. The damage zone in front of the crack tip will therefore be more uniform as well, which will decrease the risk of stick-slip and other unstable crack propagation behavior. Furthermore, Ramji et al. [14] found that migration of the delamination plane into a neighboring interface happens more sudden, while migration into the ply of the delamination interface happens gradually. As the ply interfaces of a UD laminate are more blend together, it makes sense that migration to other interfaces happen more gradually than when the laminate is multidirectional, thus lessening the risk of stick-slip behavior. However, as this study will focus on MD laminates, stick-slip behavior may be experienced when MD carbon/PEEK specimen are tested.

The preliminary study is performed to answer the sub-questions about the specimen dimensions and mandrel peel settings as stated in section 3.5.1. An overview of the measured average G_{Ic} with the standard deviation, together with the effect of the tested parameters on the G_{Ic} and crack propagation can be found in table 3.1.

It was found that the thickness of the peel-arm (PA) affects the measured G_{Ic}, where a thicker peel-arm increases the G_{Ic}. This could be due to the different global stiffness of the peel-arm or due to more fiber migration. The overall best choice is to use 10 mm wide samples with a peel-arm of one ply thick. The vertical adjustment of the mandrel with respect to the specimen should be set to 0 mm, while using an alignment force of 100 N. The pneumatic cylinder used to establish the alignment force should be changed, as the cylinder was unable to maintain a stable alignment force. On a side note, the used pre-crack of 10 mm was barely enough to mount the peel-arm around the mandrel, therefore it is recommended to have a pre-crack of at least 12 mm for mounting convenience. It is important to note that the used test quantities of this study are not enough to make this experiment significant, therefore all results should be treated with care. However, as goal to understand the MP set-up and testing parameters the quantities of this study are sufficient.

Table 3.1: Overview averaged results preliminary study

	F_a 125 N	**F_a 75 N**	**HM 0 mm**	**HM 0.5 mm**	**peel-arm 1 ply**	**peel-arm 2 plies**	**Width 10 mm**	**Width 17 mm**
G_{Ic}	1.56	1.60	1.56	1.61	1.43	1.72	1.58	1.59
Std.Dev.	0.169	0.159	0.1711	0.1524	0.0722	0.049	0.1663	0.1645
Effect on G_{Ic}	No effect		No effect		Thicker PA causes higher G_{Ic}		No effect	
Effect on crack propagation	Higher F_a shows less intralaminar propagation		No effect		No effect		No effect	

Chapter 4

Methodology

This study examines if the mandrel peel setup is applicable to establish a relation between the interlaminar fracture toughness and an $0°$- $\theta°$interface of carbon/PEEK UD laminates. The previous chapters discussed the required theory. Based on this theory, together with the outcome of the preliminary study, the methodology is created.

4.1 Materials and specimen manufacturing

A total of four laminates will be made from carbon/PEEK UD Cetex TC1200 composite material, produced by Toray [37]. The lay-up will be a 16 layered laminate with a total of 14 0°-layers. Of each laminate, the second and 15th layer will have a different fiber direction, as can be seen in the grey area of figure 4.1. The different fiber direction of the 15th layer is needed for the required symmetry of the specimen. If the specimen are not symmetric, warping is expected to occur which can cause undesirable internal stresses when the sample is clamped into the MP setup [34]. The fiber directions that will be tested are 90°, 60°, 30°and 45°, each laminate containing a different fiber direction. See table 4.1 for an overview on the specimen dimensions. See preliminary study, section B.1 for the choice on peel-arm thickness and specimen width. In this table, the location of the pre-crack within the lay-up is denoted by //.

The laminates will be assembled in a 12 inch picture frame and consolidated at TPRC in Enschede. The consolidation process goes according to the standard press cycle of carbon/PEEK, the details can be found in table 4.2. The laminates will have a 12 cm long and 12 μm thick polyimide film between the 15th and 16th ply to serve as an initial crack. The position of the polyimide film is visualized as a thick-red line in figure 4.1. The polyimide film should not affect the stacking quality, but this will be checked with fractographic research, see section 4.4. It is possible however that the polyimide film affects the initiation toughness value, as the film has a square tip which affects the stresses around the crack-tip in comparison with a crack that initiates without a pre-crack. After consolidation, the laminates are checked for the consolidation quality by means of an ultrasonic C-scan. After the quality check, the samples are cut into the desired widths of 10 mm and the polyimide film will be removed. Each group will have 10 samples to test, creating a total of 40 samples in total. In addition to the ultrasonic quality check, the consolidation of some specimen are checked under the microscope after peeling, as will be discussed in section 4.4.

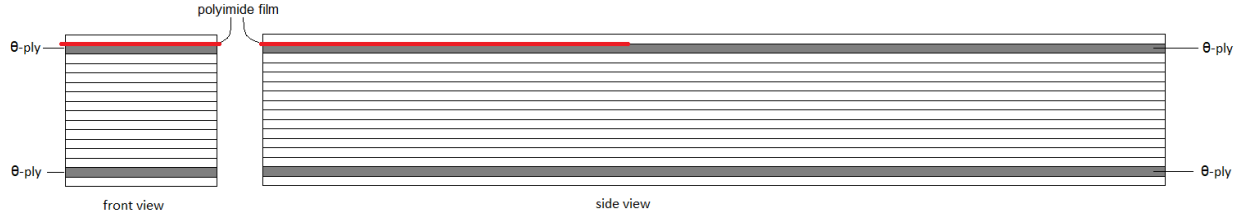

Figure 4.1: Front and side view of specimen lay-up

Table 4.1: Dimensions of specimen

Width	Peel-arm thickness	Lay-up
10 mm	1 ply	$[0//\theta/0_6]_{sym}$

Table 4.2: Standard press cylce Carbon/PEEK material

Pressure	Temperature	Dwell time	Total cycle time
20 bar	385	No dwell	8635 sec

4.2 Mandrel peel setup

The mandrel peel (MP) setup can be used to measure the fracture toughness value by means of peeling the top ply from a laminate. The MP setup that is used during this work is the same as used in among others the work of Forkink [33] van den Boogert [34], and Sacchetti et al. [9, 21]. A schematic overview of the MP setup can be found figure 4.2a [8], where the alignment force and peeling force are denoted as F_a and F_p respectively. The specimen is clamped on the sliding table and the peel-arm (top-ply) is wrapped around the mandrel. The peel-arm is clamped by a gripper which is attached to a Zwick universal testing machine. The universal testing machine will pull upwards, resulting that the base of the specimen and sliding table want to move to the left of figure 4.2a. The alignment force will counteract this movement and will keep the peel-arm conformed to the mandrel at all times [34]. The alignment force is applied by means of a pneumatic cylinder attached to the sliding table and is set to 100 N as is discussed in the preliminary study, see section B.5. The alignment force will be monitored during the test and adjusted accordingly in case needed. In addition, the conformation of the peel-arm to the mandrel is monitored by means of a camera which is placed parallel to the mandrel, see figure 4.2b. The generated video captures the movement of the sliding table, mandrel, and peel-arm. During the experiments, the alignment and peeling forces are measured by means of 200 N force cells. A 10 mm radius mandrel will be used with a width of 18 mm. The peeling rate will be set at 15 mm/min, as with the research of Forkink [33], van den Boogert [34], Grouve et al. [8], and Su et al. [13]. The vertical adjustment of the mandrel with respect to the sample is set to be 0 mm, as is found in the preliminary study, see appendix B.4. An overview of all the settings are summed in table 4.3. The experiments will be performed according to the '*protocol for determination of adhesive fracture toughness of flexible laminates by peel testing: mandrel peel method*' designed by Kawashita et al. [35]. An overall step-by-step guide on how to operate the mandrel-peel setup can be found in appendix D. As described in section 3.2, the friction and fracture toughness of each sample will be measured in the same stroke.

Table 4.3: Settings of mandrel peel setup

Alignment	Peeling rate	Force cells	Mandrel	Vertical mandrel placement
100 N	15 mm/min	2x 200 N	18 mm wide ⌀20 mm	0 mm

4.3 Data reduction

During the mandrel peel test the peeling and alignment forces are being measured. Based on these values the friction (μ) of the experimental setup can be determined through equation 3.1 together with the fractural toughness (G) of the specimen by means of equation 2.10. For completeness, these equations are repeated here:

$$\mu = \frac{F_p - F_a}{F_p} \tag{4.1}$$

$$G = \frac{1}{b}[F_p(1-\mu) - F_a] \tag{4.2}$$

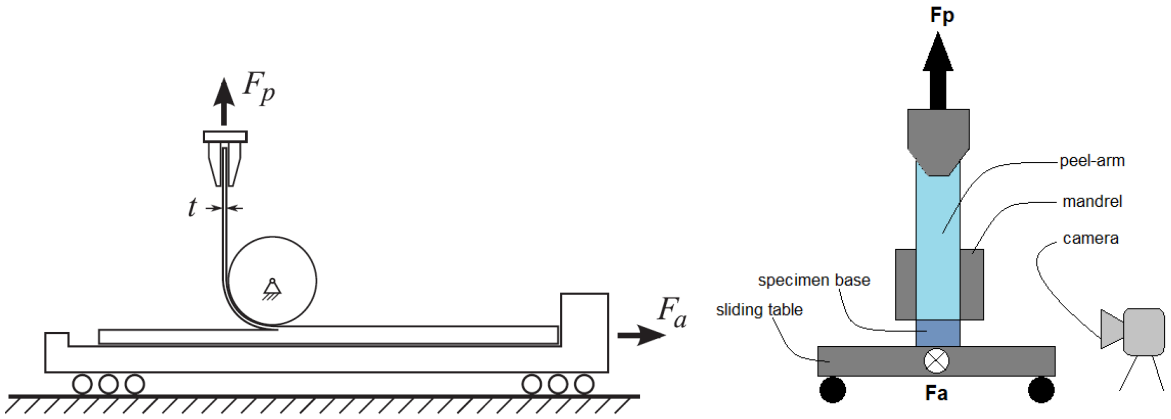

(a) Side view mandrel peel setup [8]

(b) Front view mandrel peel setup

Figure 4.2: Side and front view of the mandrel peel setup

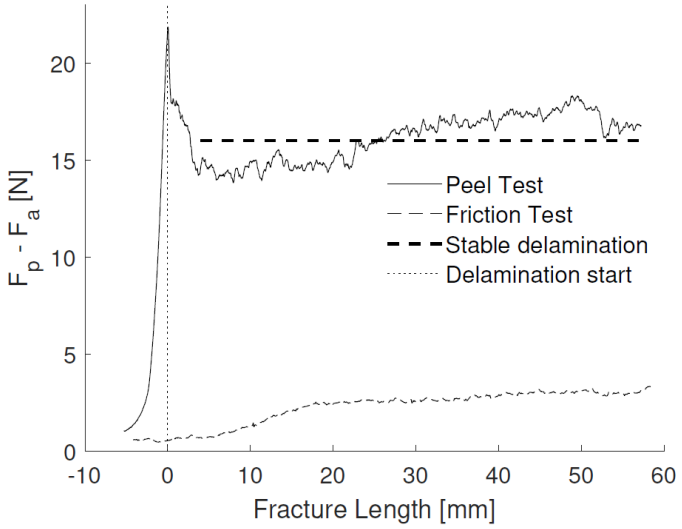

Figure 4.3: Example force-displacement graph [33]

Once all experiments are performed, the data will be translated to graphs by means of MATLAB. An example graph of how the result potentially looks like can be seen in figure A.3 [33], where the alignment, peeling, and friction forces are visualized. It can be seen that there is an initial peak that marks the start of the delamination. After the crack initiation, the crack propagation stabilises around a plateau value of 17 N. The fracture toughness value G_c is determined from this plateau value [33]. To see if the fiber direction has an influence on the fracture toughness, the values of each sample will be compared. The crack initiation force (F_{peak}) will also be analysed together with the initial peak force (F_{ip}) to see if the fiber angle influences these results. However, these results should be treated with care as the polyimide film might influence the these forces. The F_{ip} is determined by dividing the F_{peak} by the width of the specimen, as the width of the specimen influences the induced forces. The following formula is used to determine F_{ip}:

$$F_{ip} = \frac{F_p - F_a}{b} \tag{4.3}$$

4.4 Fractography

The aim of the microscopic research is to examine the fracture surface and propagation plane. After the experiments the specimen are taken to a Keyence VHX-5000 digital microscope where the specimen and propagation plane will be examined. Figures 4.4a and 4.4b show where the samples will be examined. Places A and B are intended to study the crack propagation interface, where point A shows the crack tip and point B shows the fracture surface. To get a better view of the crack tip, a cross-section of the area around the red box at arrow A will be cut out, containing both the peel-arm and substrate around the crack tip. The stacking sequence and consolidation quality is studied by means of places C, D, and E. Point C studies if the polyimide film influences the lay-up, point D shows how the layers are stacked from a side view and point E shows a cross section of the stacking sequence. The microscopic images of places B and D will be generated directly from the specimen, without any polishing or the like. For the other places, the cut sections are embedded in clear epoxy and cured for at least 24 hours. After the curing, the samples are polished and prepared for the digital microscope.

In addition, the failure type of the fracture surface will be studied by means of SEM fractographic research. Samples at point B will be cut out at the desired place and will be cleaned with ethanol and dried in the oven for two hours at 50°Celsius before being placed in the holder. The samples will undergo a gold coating before the SEM analysis starts.

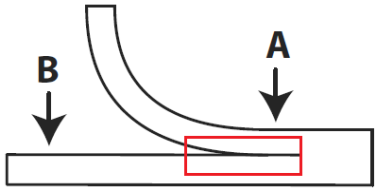

(a) Microscopic analysis of crack propagation plane

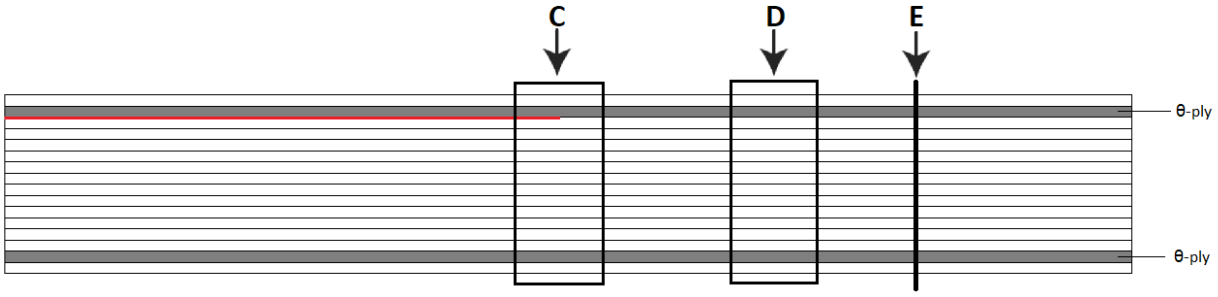

(b) Example force-displacement graph [33]

Figure 4.4: Microscopic images

Chapter 5

Results and discussion

The results of the mandrel peel (MP) experiments are presented in this chapter. First, the force-displacement graphs will be discussed, followed by the crack propagation. The fracture toughness analysis and applicability of the MP setup are discussed at the end of this chapter. The fractographic research is stated throughout the chapter. The shown results of the *0°-0°*interfaces originate from the preliminary study, where the samples of the one-ply thick peel-arm are used.

5.1 Force-displacement analysis

The forces measured of all samples, including their friction measurements, can be found in appendix F. Representative examples of each *0°-θ°*group can be found in figure 5.1. Each of the representative graph examples show an initial peak which marks the start of the delamination, followed by a plateau value which determines the fracture toughness value. Stick-slip behavior and unstable crack propagation was found in most specimen and can be recognized by sudden drops of the forces as can be seen in the force displacement graphs of 0-45-4, 0-60-5, and 0-90-5 in figure 5.1. More information on the stick-slip behavior will be given in section 5.2.1. Besides the stick-slip behavior, no abnormalities were found in the force-displacement graphs of each sample and the friction of all samples stayed below the 1%.

5.1.1 Initiation toughness

The initiation toughness is the resistance of the delamination to initiate and could be affected by the fiber direction. Within this work it was found that the initial peak of the *0°-90°*samples are not as elevated as with the other *0°-θ°*interfaces, as can be seen in figure 5.1d. The *0°-60°*interfaces also show the same phenomenon of less elevated initial peaks. Figure 5.2 shows the initial peak force values per group. In this figure, it can be seen that the *0°-90°*and *0°-60°*interfaces show a decrease in initiation toughness, while the *0°-45°*and *0°-30°*interfaces show an increase. However, the standard deviation is rather large. The results of the initiation toughness should be treated with care as the 12 μm polyimide (PI) film used as an insert for the pre-crack influences the initiation toughness. The PI film has a square tip, which influences the stress field around the crack tip. In addition, the delamination interface region right after the PI film shows more matrix material than further along the interface, which also influences the results, as can be seen in the microscopic images of figure 5.3. Here, the PI film is marked with a blue rectangle. The image shows that the fibers do not bend around the PI film, as the matrix material seems to have filled the surrounding space. As this additional amount of matrix material right after the PI film is equal for all groups except the *0°-0°*group, a definite conclusion on the influence of the fiber angle on the initiation value cannot be drawn.

Even though conclusions on the influence of the fiber angle on the initiation toughness cannot be drawn, the influence of the PI film on the stacking sequence will be explained in more detail, as it could influence the crack propagation. When looking further into the pre-crack interface, it can be found that the matrix material right after the PI film is larger than further along the interface. The matrix rich region right after the PI film is as thick as the PI film itself, roughly 0.012 mm, which gradually decreases along the interface. This larger matrix rich zone influences the plastic yield zone (r_y) around the crack tip, as a matrix rich interface allows for a larger r_y [25] as was already discussed in section 2.1.2. Here it is stated that Sacchetti et al. [25] has determined that the r_y of PEEK material is 0.225 mm. When the plastic yielding zone is larger

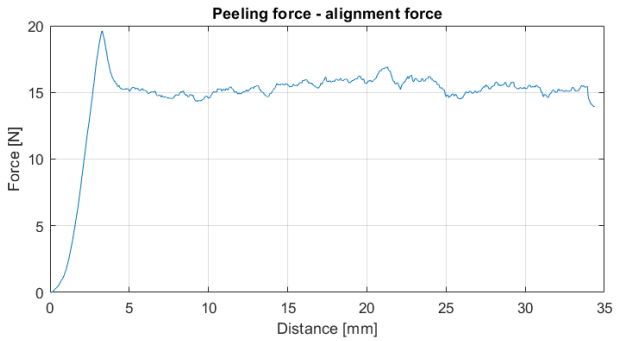

(a) Force displacement graph of 0-30-1 sample

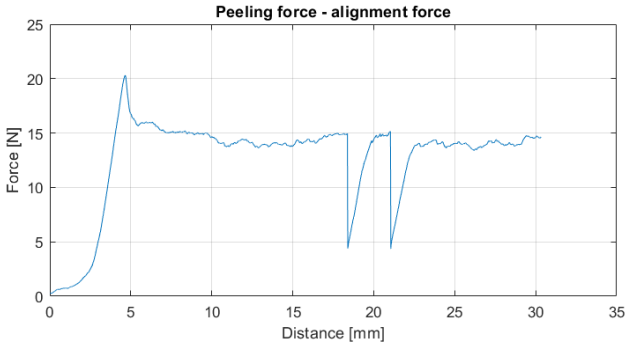

(b) Force displacement graph of 0-45-4 sample

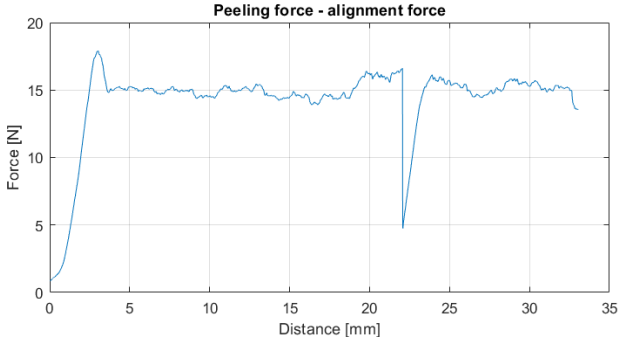

(c) Force displacement graph of 0-60-5 sample

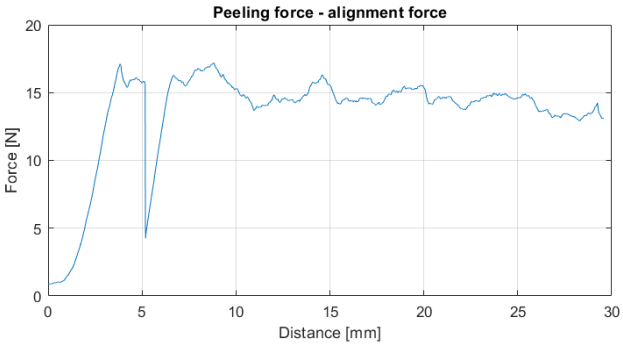

(d) Fracture toughness values of 0-90-5 sample

Figure 5.1: Force-displacement examples of each interface group

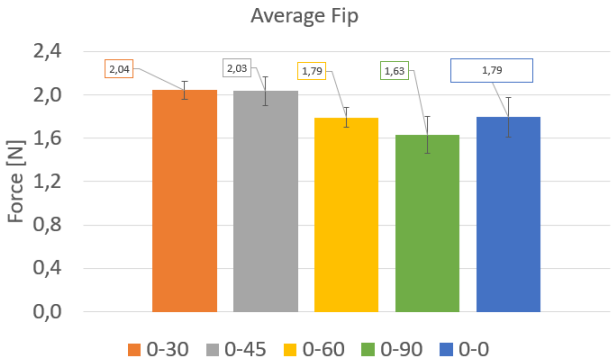

Figure 5.2: Average initial peak force value (F_{ip}) per fiber-direction group

than the matrix rich region, the crack will migrate towards the weakest region within the interface resulting in unstable crack growth. When the matrix region is larger than r_y, the crack will propagate within the matrix rich region [25]. As the matrix rich region at the start of the crack initiation is smaller than the required 0.225 mm, unstable crack propagation might occur. As the matrix region gradually decreases in size as well, it makes sense that the unstable crack propagation could worsen over the length of its interface. As this study together with the research of both Forkink [33] and van den Boogert [34] all use a pre-crack generated by means of a PI film, the experienced migration of the crack away from its intended interface encountered by all studies could be explained by the lack of sufficient matrix material and decrease of this material within the intended propagation interface. However, as the amount of matrix material cannot be changed without affecting the fracture toughness value, it is suggested to experiment with a more brittle material than PEEK as then the r_y is smaller.

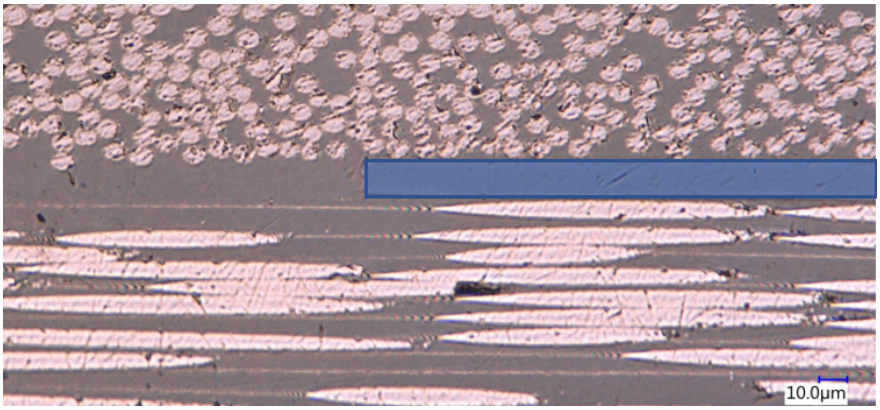

(a) Effect of polyimide film (blue rectangle) on *0°-90°* stacking

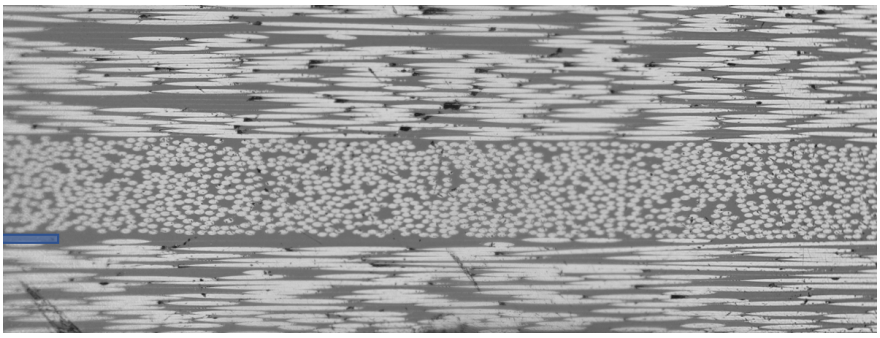

(b) Influence PI film on *0°-45°* stacking

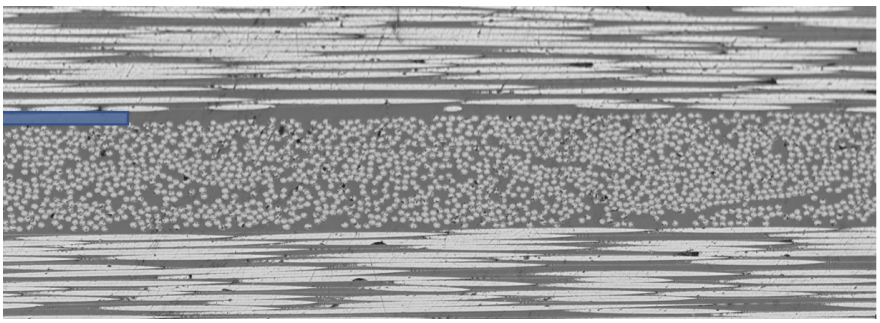

(c) Influence PI film on *0°-30°* stacking

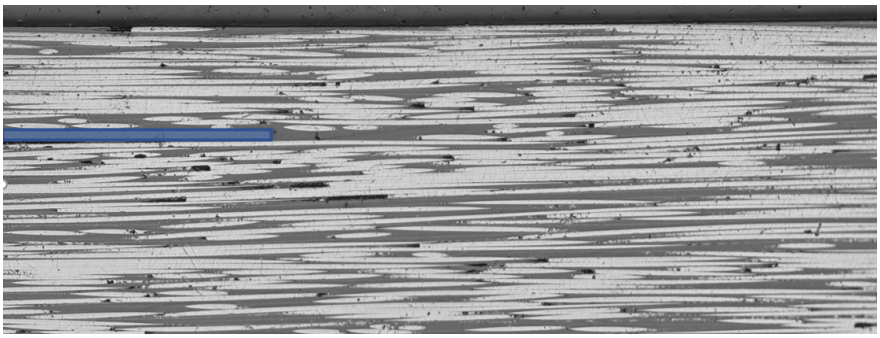

(d) Influence PI film on *0°*-0° stacking

Figure 5.3: Influence of polyimide (PI) film in stacking sequence, shown by the blue square with thick outlining

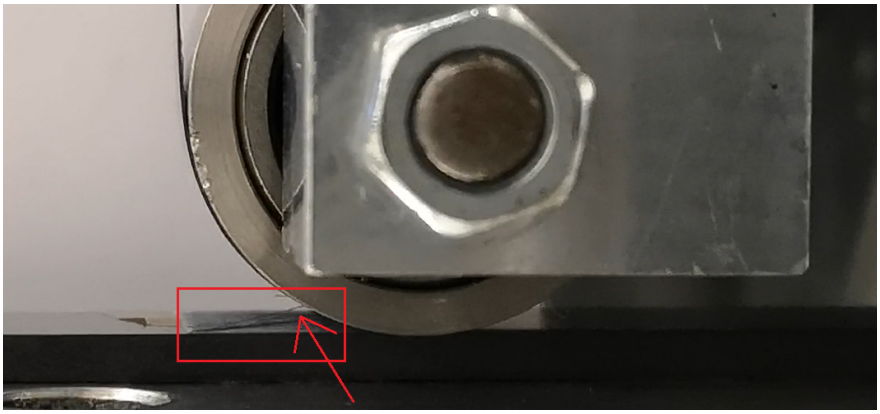

Figure 5.4: Screenshot from conformation video sample 0-45-5. Fiber jumping is visible at the arrow within the red square.

5.2 Crack propagation

After reviewing the video material of all specimen, it can be concluded that the peel-arm visibly had proper conformation with the mandrel at all times and that no irregularities were found during the peeling. In addition, it was found that fibers of the peel-arm sometimes jump towards the base, or vice versa. An example of this fiber jumping can be seen in a screenshot made from sample 0-45-5, see figure 5.4. This phenomenon can be confirmed by the fractography images, where each specimen shows fibers of the peel-arm that are stuck on the substrate, as can be seen in figure 5.5a.

The fibers of the peel-arm that are found on the base could be an indication that the crack plane moves from the intended interface into the peel-arm. In addition, the crack sometimes propagates into the substrate as well. Fractographic images of crack propagation into the peel-arm and substrate can be found in figure 5.5b and 5.5c, respectively. The fibers that get stuck on the base of the specimen seems to start directly at the beginning of the crack propagation, as can be seen in figure 5.5a. This is the same for all studied interfaces. This phenomenon does not intensify with the crack propagation, as the number of peel-arm fibers left on the surface do not seem to increase along the crack propagation path. However, fibers that are stuck on the base of the specimen do not necessarily imply that the crack migrated into the peel-arm: when looking at figure 5.7a it can be seen that the crack mostly propagates along the intended interface of sample 0-30-3, while fibers of the peel-arm still get stuck on the base (see figure 5.7b). However, it should be noted that most samples do show crack migration away from the intended interface. When looking at figures 5.7c and 5.6, it is visualized that the crack suddenly can change its propagation path into the peel-arm, or vice versa. The reason for this sudden change could lie with fiber bridging, where fibers will be either pulled out of their position or they must be broken when the crack surface separates [38]. When the fibers are pulled out or broken, energy is released which may interfere with the crack propagation direction. More on fiber bridging will be discussed in section 5.3.1. As fibers bridge over the delamination interface, the crack could move its propagation course. The sudden crack migration is common behavior for crack propagation in MD laminates. Khan et al. [18] already stated that the relative angle of adjacent plies induces the delamination to deviate from the intended interface into neighboring plies and interfaces, as the direction of the crack propagation is not parallel to the fiber axis. The tendency of the crack to migrate away from the intended interface makes it difficult to find the interlaminar delamination resistance between angled plies by any type of measurement method.

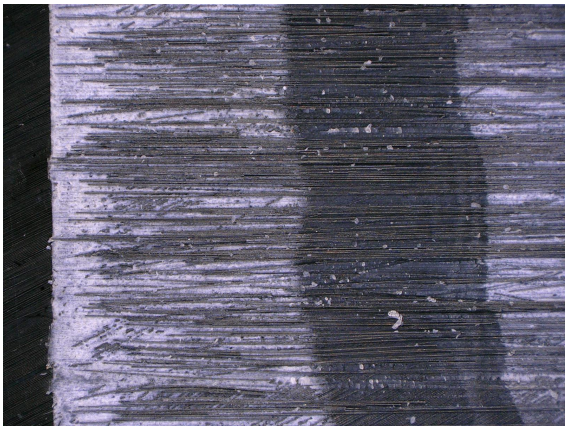

(a) Fibers of the peel-arm (*0°* direction) are stuck on the substrate, visible as the darker horizontal lines. Stick-slip behavior is visible by means of the black vertical line across the base of the sample.

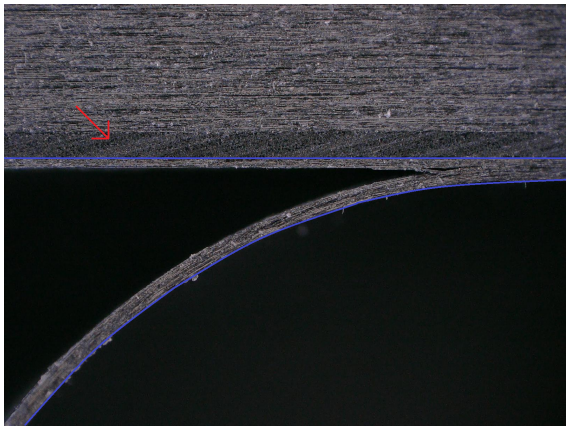

(b) Crack propagates in peel-arm of sample 0-45-6. The peel-arm is between the blue lines, while the angled ply is marked by the red arrow. The crack should propagate between the angled ply and peel-arm, but instead propagates through the peel-arm itself.

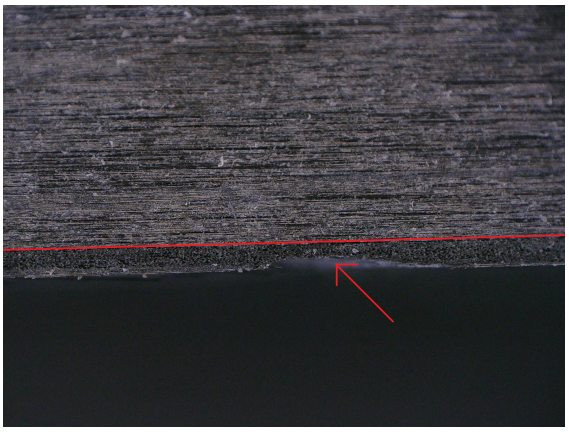

(c) Crack propagates in substrate of sample 0-30-5. The red line marks the transition of the angled ply to the base of the specimen. The red arrow shows that a chunk of the angled ply is missing from the delamination plane.

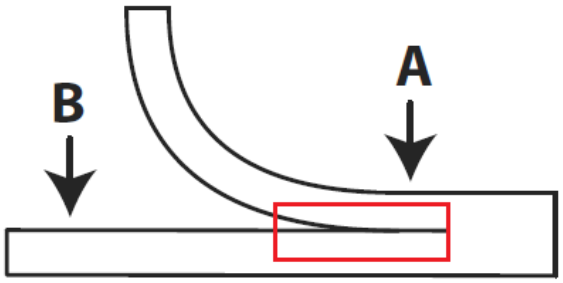

(d) Location of crack propagation examples: Image (a) is taken at arrow B, while images (b) and (c) are taken perpendicular to arrow A.

Figure 5.5: Crack propagation examples. With all samples, the crack propagated from left to right.

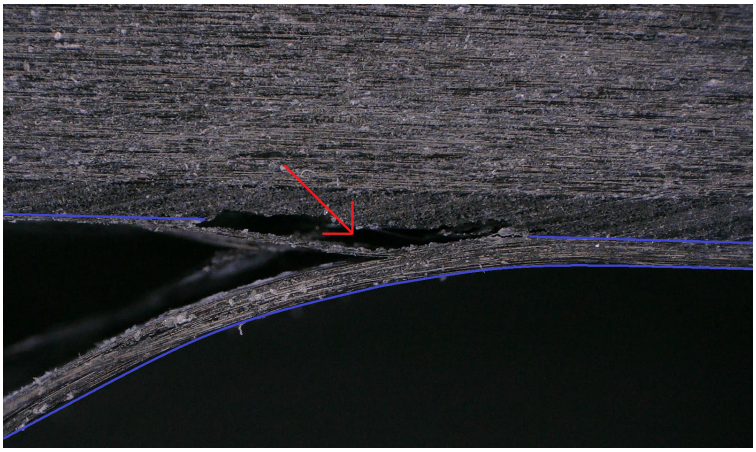

Figure 5.6: Delamination interface of sample 0-45-8 at crack tip. The crack suddenly jumps from propagating through the peel-arm (marked between the blue lines) to the base of the material (red arrow). The crack propagation is from left to right.

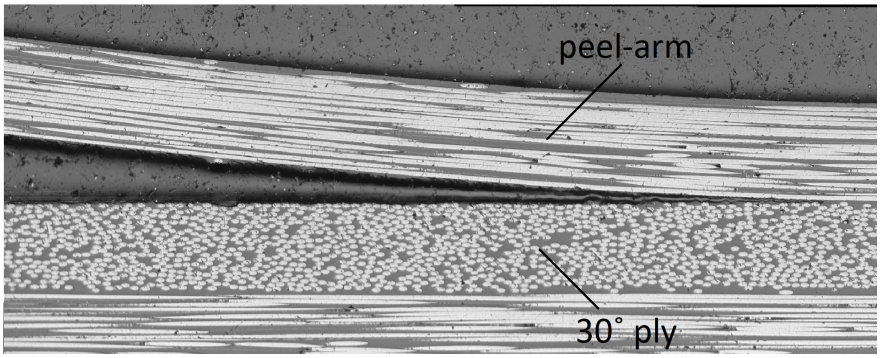

(a) Crack propagation of crack-tip along the intended interface of sample 0-30-3

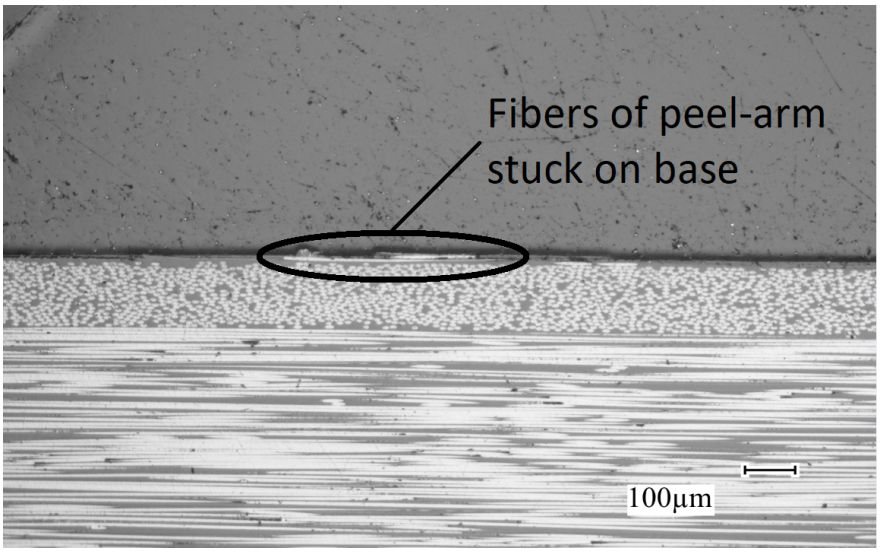

(b) Fibers of peel-arm are stuck on the base of sample 0-30-3

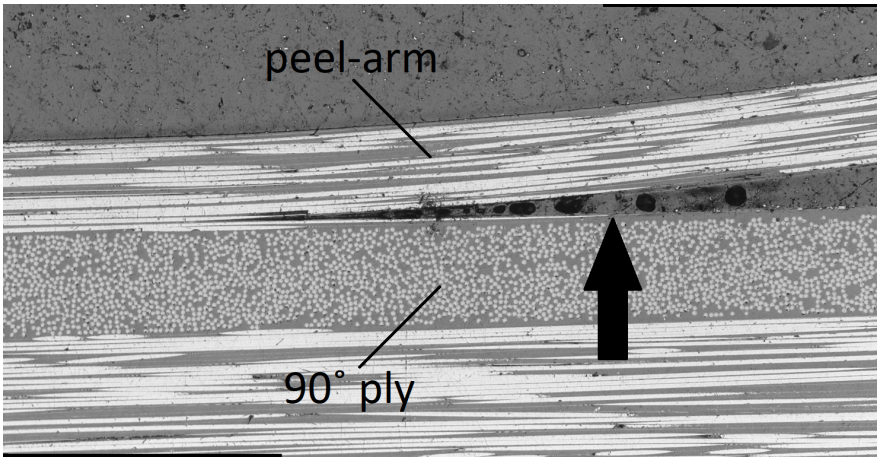

(c) Crack migrating from intended interface into the peel-arm of sample 0-90-3. The arrow marks the spot where the crack migrates away into the peel-arm

Figure 5.7: Crack propagation examples

5.2.1 Stick-slip behavior

Table 5.1: Overview of samples with stick-slip behavior

0-0	0-30	0-45	0-60	0-90
-	0-30-4	0-45-1	0-60-1	0-90-3
-	0-30-6	0-45-2	0-60-2	0-90-5
-	0-30-7	0-45-3	0-60-3	0-90-6
-	0-30-9	0-45-4	0-60-5	0-90-7
-	-	0-45-5	0-60-8	0-90-9
-	-	0-45-6	0-60-9	0-90-11
-	-	0-45-7	0-60-10	-
-	-	0-45-8	-	-
-	-	0-45-9	-	-

As already stated before, stick-slip behavior and unstable crack propagation were found in most specimen samples and can be recognized by the sudden drop of peeling forces. An overview of the samples showing stick-slip behavior is stated in table 5.1. After reviewing the experimental images from the videos, the conformation of the peel-arm to the mandrel seemed good at all times, as already stated in section 5.2. However, it seems unlikely that the peel-arm stays conform to the mandrel when stick-slip occurs. Only very small or fast stick can already affect the crack propagation, suggesting that the stick could be small or fast enough to not be detected by the current means of filming.

The stick-slip is accompanied by black lines on the specimen of a couple of millimeters in width, as can be seen on the microscopic image of sample 0-30-5 in figure 5.5a. During stick-slip, the crack propagation differs from the stable crack growth, which leaves a different type of peeling surface. Van den Boogert [34] also encountered sudden drops in the peeling force, accompanied by a different peeling surface shown by black lines existing solely of matrix material. The stick-slip surfaces are analyzed by means of SEM fractography, see figure 5.8. The red arrows in this figure indicate the studied transition of the surface. The SEM images of the studied surfaces are presented in figure 5.9. Here, a clear distinction can be seen between the surface of the stick-slip behavior, denoted by the word 'Line' and the rest of the fracture surface, denoted by the word 'Laminate'. When comparing these images with the fractographic images of figure 2.10 of section 2.2.4 it can be seen that the stick-slip behavior shows the same surface characteristics as a fast-brittle (F-B) fracture type, while the other type is similar to the slow-ductile (S-D) failure type. The F-B failure type shows more scarps, rivers and cusps, while the S-D failure type shows more matrix deformation as can be seen in figure 5.9c.

To understand better the cause of the stick-slip behavior, fractographic images are made to study the lay-up and intended interface of the specimen. A cross section of an unpeeled interface (0°-90°) can be seen in figure 5.10a. No irregularities can be found in the lay-up in any of the studied cross sections, such as cavities or broken fibers, which was the case for all studied interfaces. It can be seen that the interface between the adjacent plies shows no nesting, the phenomenon where fibers migrate to neighboring plies during the consolidation cycle [18]. For MD laminates, this is also not expected. However, it was found that the fibers within a ply are not equally distributed, which can be seen in figure 5.10b. This uneven distribution causes spots in the samples where only matrix material is located. In the case of figure 5.10b, this matrix-spot is quite severe, almost splitting the ply in half. These (severe) matrix-spots are not uncommon as they were found in all generated microscopic cross-sections. Less severe matrix-spots can be seen in figure 5.10c, where the spots are mostly located at the ply interfaces. The uneven divisions of the fiber volume fraction causes the crack to encounter different type of materials, which would increase the risk of stick-slip, crack jumping or migration outside of the intended interface. In the figures 5.10c and 5.10a it can be seen that the matrix-spots envelope fibers. When the crack propagates trough these area's, the crack has to either break the fiber or pull it out of its position. This phenomenon is called fiber bridging and will be discussed in more detail in section 5.3.1. As the crack pulls or break the fibers during propagation, the enveloped fibers will remain stuck on either the substrate or the peel-arm, which can be found in the studied interfaces such as figure 5.10d. In addition, the pulling and breaking of the fibers could cause the crack to deviate from its intended interface, or cause stick. The uneven distribution of fibers within a ply are generated during the production of the prepreg carbon/PEEK UD material. Matrix-spots are therefore unavoidable when products or samples are made from this material.

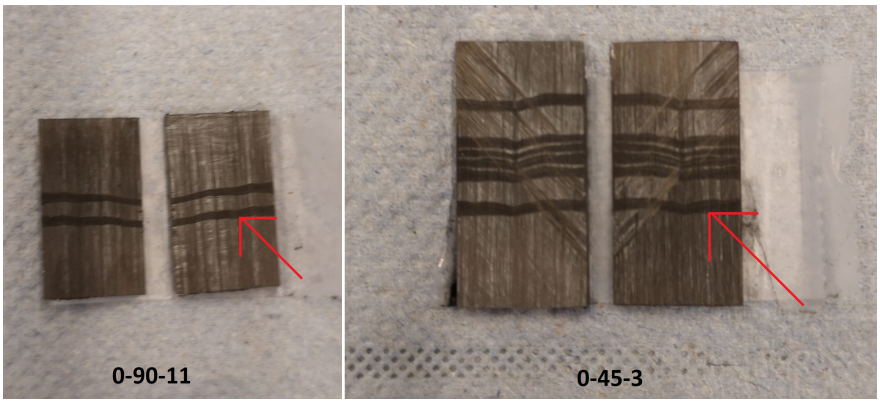

Figure 5.8: Analyzed surfaces of samples 0-45-3 and 0-90-11 to study the stick-slip behavior. The stick-slip behavior are accompanied by the visible darker lines on the surface. The red arrow indicates the transition that is studied

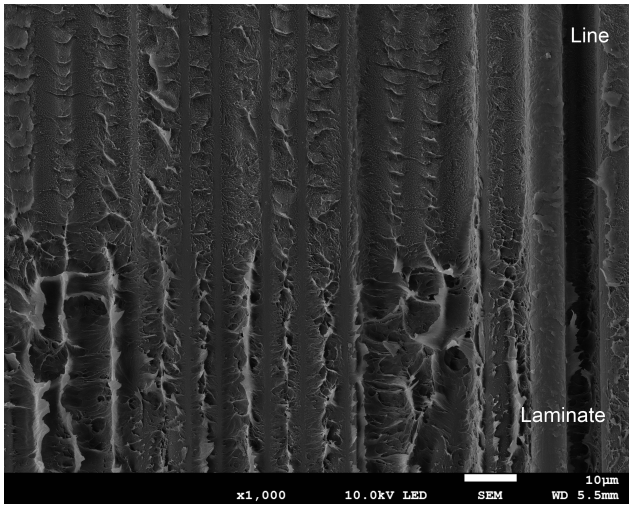

(a) Transition to stick-slip of 0-90-11 sample, x1000

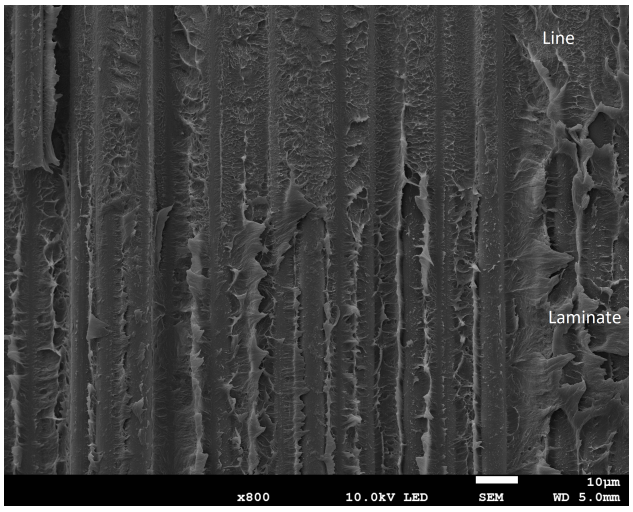

(b) Transition to stick-slip of 0-45-3 sample, x800

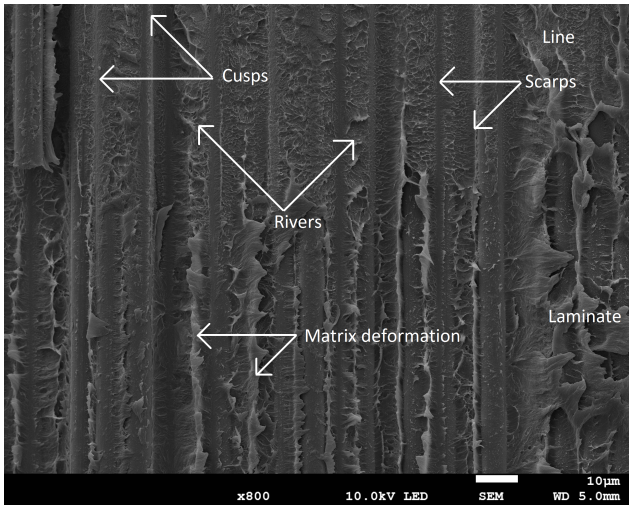

(c) Transition to stick-slip of 0-45-3 sample, x800

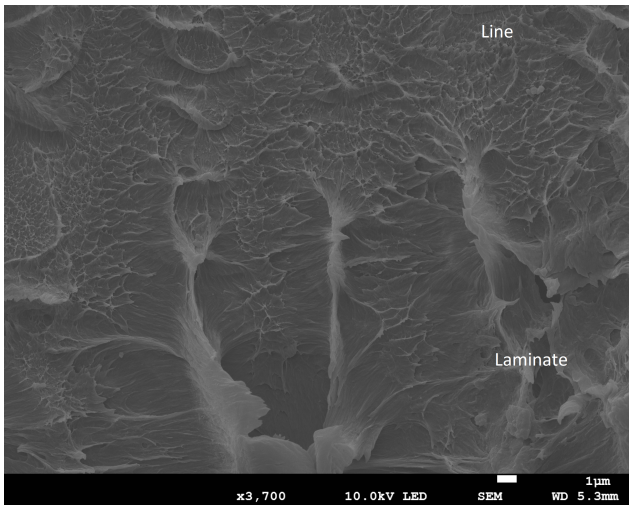

(d) Transition to stick-slip of 0-45-3 sample x3700

Figure 5.9: SEM images of the transition to stick-slip behavior (denoted by 'Line').

Combining the found results an indication of the unstable crack growth and propagation can be made: as the pre-crack ends in the matrix material as can be seen in figure 5.3a, the crack will initiate in an S-D manner, resulting in a ductile peeling surface. Local variations in fiber volume fraction are encountered throughout the crack propagation interface. When the fiber volume changes or when fibers need to be pulled out of their position, stick could occur. As the peeling continues, energy is build up for the crack to propagate until it slips. During slip, the crack propagates in an unstable manner where the strain rate is higher, which result in a more brittle fracture surface until the mandrel arrests the unstable crack propagation. Sacchetti et al. [21] already mentioned that unstable crack propagation is easier stopped due to the mandrel, meaning that the stick-slip arrest position will not necessarily be in a tough matrix rich region. This would lower the impact of the matrix rich regions within the laminate, which is beneficial as the matrix rich regions are an effect of the manufacturing process. This would make the MP method more suitable to measure the fracture toughness of MD laminates than the DCB test, as there the unstable crack propagation has to be stopped by a matrix rich region. In addition, the changes of fiber-to-matrix rich regions could cause the crack to jump or migrate away from the intended delamination interface.

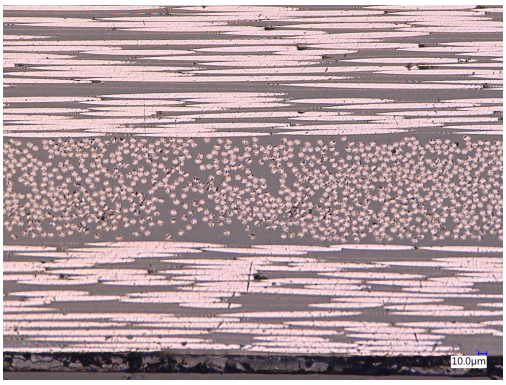

(a) Fiber division between peel-arm and adjacent ply

(b) Uneven fiber division within each ply causes severe matrix spots across the width of the ply.

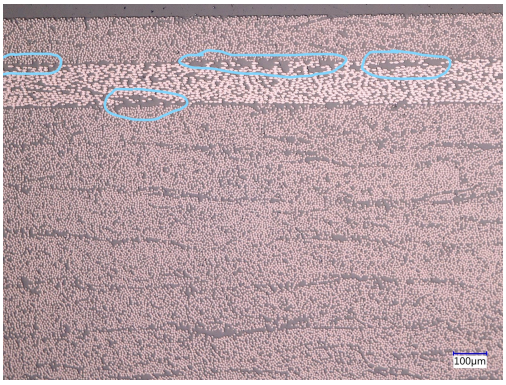

(c) Matrix-spots at the adjacent ply interfaces

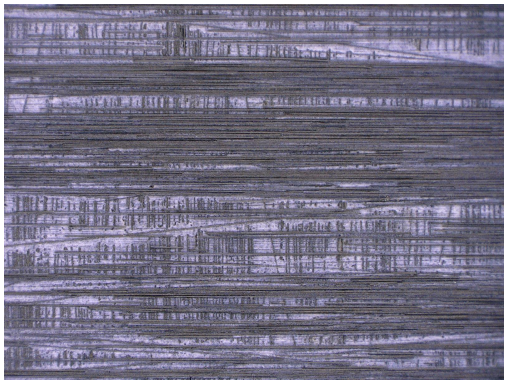

(d) Fibers of *0°* peel-arm are stuck on base of a *0°*-*90°* sample. The peel-arm fibers are visible as the horizontal darker lines on top of the lighter base with *90°* fibers.

Figure 5.10: Microscopic images of ply division

5.3 Fracture toughness analysis

For most of the cases the fracture toughness is determined excluding stick-slip, since there is sufficient stable crack growth to exclude stick-slip. For some specimen the stick-slip happened across the entire measurement, which makes it not possible to determine the fracture toughness excluding stick-slip. However, the fracture toughness value does not seem to change significantly when stick-slip is included. To illustrate, the fracture toughness value of sample 0-30-9 (see figure 5.11) excluding the stick-slip is 1.20

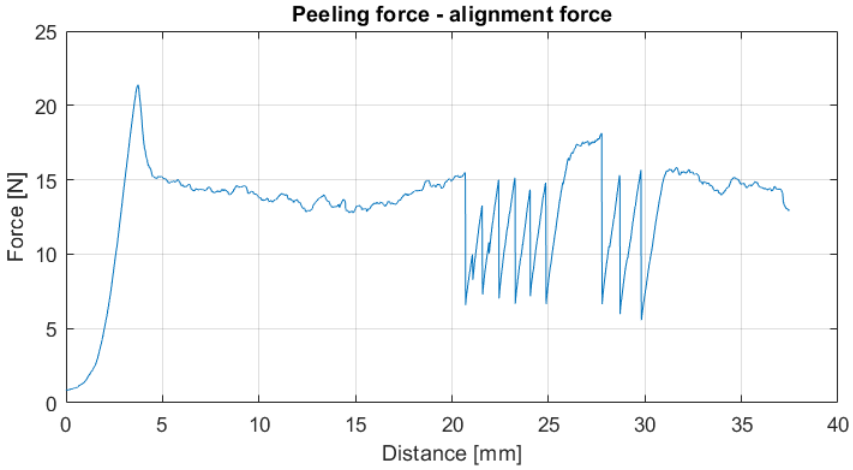

Figure 5.11: Force displacement graph of sample 0-30-9 with intensive stick-slip

Table 5.2: Overview results measurement category

Series	G_{Ic} [kJ/m^2]	StdDev. G_{Ic}	μ [%]	F_{ip} [N/mm]	StdDev. F_{ip}
0-0	1.43	0.07	0.27	1.79	0.17
0-30	1.34	0.11	0.47	2.04	0.09
0-45	1.30	0.12	0.53	2.03	0.19
0-60	1.24	0.09	0.47	1.79	0.13
0-90	1.18	0.10	0.50	1.63	0.09

kJ/m^2 and including stick-slip the value is 1.18 kJ/m^2. With a standard deviation of 0.10 from that group the difference of 0.02 kJ/m^2 is insignificant. The insignificant change of fracture toughness value is explained by the fact that the mandrel arrests unstable crack propagation, as found by Sacchetti et al. [21]. As the mandrel arrests unstable crack propagation, the crack arrest position will not necessarily be in a though region and thus not affect the fracture toughness value. When the stick-slip is stopped by means of a tough region, such as with the DCB test, the measured fracture toughness value would be higher (see section 2.2.4).

The averaged fracture toughness values of all groups, together with their averaged standard deviation, friction, and initial peak forces, can be found in table 5.2. An overview of all measured results can be found in table E.1 of appendix E. The averaged *0°-0°*interface results are based on the preliminary study. The averaged fracture toughness values per interface group can be found in figure 5.12a. The latter figure shows that the measured G_{Ic} decreases when the ply-angle increases, however, due to the standard deviation the significance of this decrease is questionable. Figure 5.12b show the percentages of the decrease with respect to the *0°-0°*interface per group.

The findings of this study are not in line with the results of van den Boogert [34], as there an increase of fiber angle increases the measured G_{Ic}. In addition, Bin Mohamed Rehan et al. [16] successfully established to isolate the delamination interface during the DCB test and also found that G_{Ic} increases with the ply-angle. It should be noted that comparing results among studies is difficult, as composite material show an inherent variability due to the manufacturing process. Furthermore, the sample size of this study together with the study of van den Boogert [34] are rather low. In addition, the lay-up of the latter mentioned study differs, as van den Boogert uses a lay-up of 18 plies ([*0*//θ/0_{14}/θ/*0*]) and this study uses a lay-up of 16 plies ([*0*//θ/0_{12}/θ/*0*]). However, as the base of the specimen is fixed to the sliding table, the delamination interface should be isolated and therefore not interfere with the delamination propagation. Nonetheless, additional research is needed to see if the thickness of the specimen during the MP test influences the results. It should also be noted that the results of Forkink [33] are to be taken with care, as the specimen showed significant warping. Warping is the result of the non-symmetric lay-up, as this induces higher internal stresses. The difference in internal stress causes difference in the plastic yielding zone near the crack tip, and thus affects the fracture toughness [25].

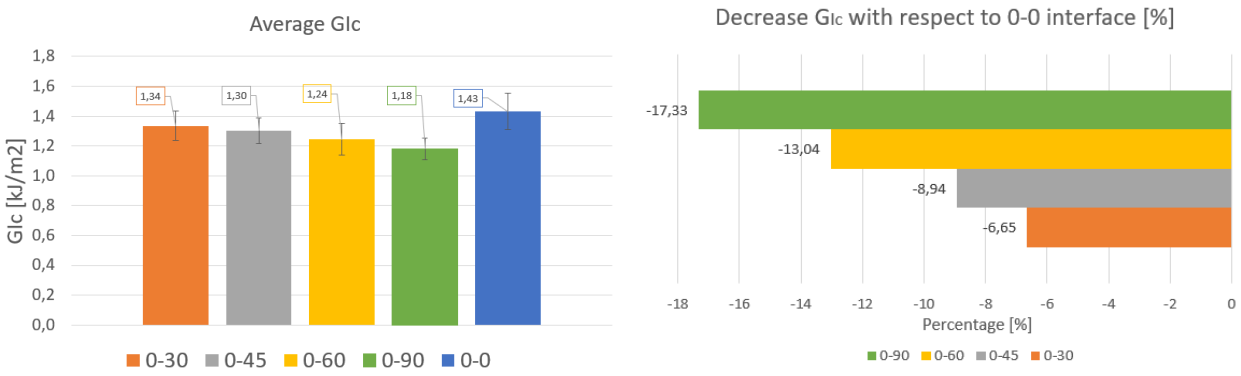

(a) Average fracture toughness value (G_{Ic}) per fiber-direction group *(b)* Difference of fracture toughness (G_{Ic}) *0°-θ°* group with respect to *0°-0°* group

Figure 5.12: Fracture toughness values (G_{Ic})

Table 5.3: Comparing results

Interface	van den Boogert [34]	Forkink [33]	This study	Difference [%]
0-0	1.18	-	1.43	21.2
0-0	-	1.49	1.43	-4.0
0-30	-	1.45	1.34	-7.9
0-45	-	1.40	1.30	-7.0
0-60	1.41	-	1.24	-11.8
0-90	1.52	-	1.18	-22.2

5.3.1 Fiber bridging

The mentioned inherent variability between laminates is mostly caused by the manufacturing process. One of those variabilities among laminates is fiber bridging and fiber nesting. Fiber bridging attributes to among others fiber nesting of adjacent plies, weak interfaces, extended crack tip yield zones, larger fiber volume fraction, and crack branching in angled laminates. Nesting is common in UD laminates due to which the adjacent fibers migrate during the consolidation cycle [18], see figure 5.13. As the plies during fiber nesting are not well defined, the fibers from various layers tend to intermingle. When a crack propagates through this area, the crack needs to pull or break fibers from one ply out of the adjacent ply in order to propagate, this effect is called fiber bridging [38]. Due to the large-scale fiber bridging across the delamination plane, the apparent fracture toughness is frequently found to increase as the delamination increases, as the adjacent fibers bridge over the delamination plane and therefore arrest the crack propagation [18]. De Moura et al. [2] found that 60% of the energy being dissipated during interlaminar crack propagation is responsible from fiber bridging and is therefore an important crack shielding mechanism during the delamination growth in laminates and consequently for the fracture toughness [11].

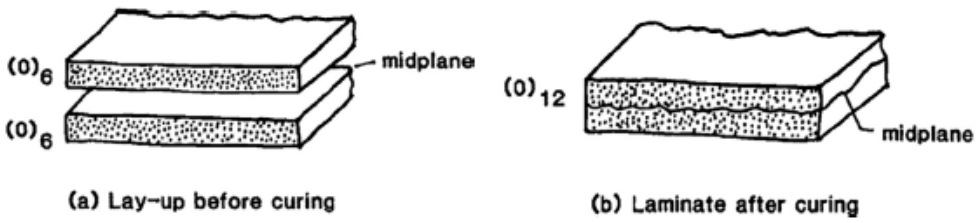

Figure 5.13: Schematic overview of fiber nesting during laminate manufacturing, adapted from [18]

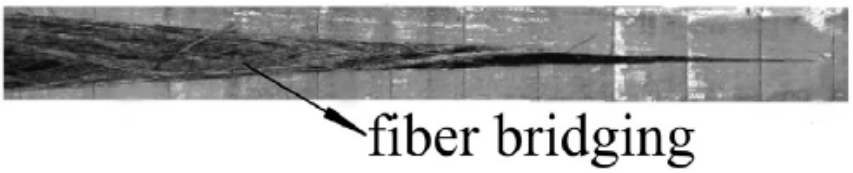

Figure 5.14: Fiber bridging at wake of mode I delamination front of an MD laminate [11]

Laminates that have a relative angle between adjacent plies reduce fiber nesting, but do not completely eliminate the bridging. When the crack migrates away from the intended interface into the neighboring plies, fiber bridging in the delamination plane can occur [18]. As the fiber bridging is not a parameter that can be controlled during manufacturing, it can therefore be expected that the measured fracture toughness of different laminates will generate varying results among samples and different studies. When the fracture toughness is more dominated by the presence of fiber nesting and bridging, it does not imply the the fiber orientation does not have an effect on the toughness. It rather implies that when the effect of fiber orientation is analyzed for $0°$-$\theta°$interfaces, fiber bridging should be eliminated. This can be done by cutting the bridging fibers [39] and then analyzing the fracture toughness. As only three studies have been performed on measuring $0°$-$\theta°$interfaces by means of the MP test and all show contradicting results, a valid conclusion on the fracture toughness of $0°$-$\theta°$interfaces cannot be drawn without additional research.

5.3.2 Applicability of the mandrel peel setup

The deviating results between this study and the studies of Forkink [33] and van den Boogert [34] would question the applicability of the MP setup to measure a correct fracture toughness value. However, when looking at table 2.1 of section 2.2.1, the DCB setup also shows significant deviating results. The deviating results of the DCB test are assigned to the difference of stiffness of the specimen arms [16], but this theory does not add up for the MP studies, as all studies use the same material and thickness of the peel-arm. In addition, the deviating results of the DCB test can also originate from the inherent variability of the laminates among the different studies, different processing effects that determine the properties of the laminate, or slight differences in the testing procedures. The latter mentioned factors on its own make it already difficult to compare results among studies.

As all measurement methods show deviating results, it is likely that different mechanisms influence the results outside the fiber orientation and the applicability of the MP setup is therefore not undermined. Such mechanisms are fiber bridging due to the pulling and breaking of fibers when the crack migrates away from the intended interface and the presence of stick-slip behavior. Furthermore, the insufficient amount of matrix material around the crack initiation causes the plastic yield zone around the crack-tip to be larger than the matrix zone, causing unstable crack propagation. Combined with the uneven division of matrix to fiber rich regions within the delamination interface, the crack might propagate in an unstable manner.

All these mentioned mechanisms that influence the crack propagation are not specific for the MP setup, but will be present within other testing methods as well. As the mandrel arrests unstable crack propagation more easily than the DCB test, the MP method is more favorable to measure the fracture toughness of MP laminates. Therefore it can be concluded that the MP setup is more favorable to measure the fracture toughness of $0°$-$\theta°$interfaces than other testing methods, but additional research to the mechanism that causes the crack to propagate in an unstable manner is required.

Chapter 6

Conclusion

This research analyses the applicability of the mandrel peel setup to measure the interlaminar fracture toughness of 0°-θ° interfaces of carbon/PEEK UD laminates. The conclusion will be presented in this chapter.

6.1 Fracture toughness

The measured fracture toughness of this study shows to decrease with increasing fiber angle. Due to the high standard deviation, however, the significance of these findings are questionable. These findings are not in line with the hypothesis that an increase in ply-angle will increase the fracture toughness. The measured fracture toughness of the 0°-0° interfaces deviates slightly from the values of comparable research [33, 34]. The different results among the studies can have several causes, where the most plausible causes are due to the inherent variability of composite laminates due to the manufacturing process and the low sample sizes. Furthermore, a suggested cause for the different results is that the fracture toughness value is not dominated by the fiber orientation, but rather by fiber bridging. As fiber bridging changes with the ply-angle and each fracture, the fracture toughness is therefore indirectly related to the ply-angle. As De Moura et al. [2] found that 60% of the energy being dissipated during the interlaminar crack propagation is due to fiber bridging, an increased fiber angle should therefore reduce the fracture toughness. Fiber nesting is most common in UD laminates and increases the fracture toughness, making 0°-0° tougher than angled laminates. The quantities of the fiber bridging depends on the fiber nesting, stacking sequence, manufacturing process, and crack propagation can differ significantly between different studies and laminates. In addition, the presence of stick-slip behavior and crack migration away from the intended interface also influence the purity of the measured fracture toughness, as not the intended interface is measured.

6.2 Crack propagation

This study encountered crack migration and stick-slip behavior, which means that the measured fracture toughness is not from the intended delamination interface. A possible reason for the unstable crack propagation is due to the pre-crack and matrix-to-fiber rich regions within the intended interface. As the pre-crack ends in a higher matrix rich region, the crack will initiate in a slow-ductile (S-D) manner. Due to the possible induced micro-cracking of the plastic deformation zone around the crack tip with insufficient matrix material surrounding it, the crack may deviate following the weakest link [25]. Within this path the crack will encounter fiber-rich areas. When this happens, the crack propagation changes to a fast-brittle (F-B) manner. In addition, the changes of fiber-to-matrix rich regions could cause the crack to jump or migrate away from the intended delamination interface. The presence of severe matrix-spots make it almost impossible for the crack to avoid these matrix richer regions, which would suddenly change the propagation behavior again to an S-D failure type. The sudden changes of S-D to F-B failure propagation results in stick-slip behavior. However, Sacchetti et al. [21] already mentioned that unstable crack propagation is easier stopped due to the mandrel, meaning that the stick-slip arrest position will not necessarily be in a tough matrix rich region. This would lower the impact of the matrix rich regions within the laminate, which is beneficial as the matrix rich regions are an effect of the manufacturing process. This would make the MP method more

suitable to measure the fracture toughness of MD laminates than the DCB test, as there the unstable crack propagation has to be stopped by a matrix rich region.

6.3 Overall conclusion

As this study showed crack behavior with the tendency to propagate away from the intended interface, the fracture toughness that is measured is not directly related to the interlaminar fracture toughness. This result means that the mandrel peel setup was not able to measure the delamination resistance of carbon/PEEK MD interfaces. However, the crack behavior of carbon/PEEK UD found in this study is similar to other studies and measurement methods, since crack propagation away from the intended interface is found regularly. As the crack behavior is found the be similar, the applicability of the mandrel peel setup to measure non-symmetric interfaces is quite favorable over for example the DCB test for many reasons. First, the manufacturing of the specimen is relatively easy as symmetry is not required. This is due to the fact that the base of the specimen is clamped and the peel-arm is only one-ply thick. The DCB test requires the peel-arms to be symmetric, which favors the mandrel peel setup as then non-symmetric interfaces can be tested. Secondly, the test procedure itself is rather simple and straightforward. With the DCB test, the crack propagation has to be monitored at all times, while that is not the case for the mandrel peel test. It was already found by Sacchetti et al. [21] that the mandrel arrest unstable crack propagation, which generates more valuable data points to analyze the fracture toughness.

Chapter 7

Recommendations

As this is only the third study to measure the delamination resistance of non-symmetric carbon/PEEK UD interfaces by means of the mandrel peel setup and all studies show contradicting results, a definite conclusion cannot be given yet without additional research. The following recommendations are made to study the mandrel peel setup and crack propagation behavior of multidirectional interfaces:

1. To understand the behavior of stick-slip behavior better, it is recommended to film the experiments with a slow-motion camera to capture any small or fast movements of the peel-arm away from the mandrel when stick-slip behavior occurs.

2. The effect of the base thickness of the specimen on the measured fracture toughness by means of the mandrel peel setup should be tested. The base of the specimen is fixed on the sliding table and is expected to have no influence on the fracture toughness, but this should be verified nonetheless.

3. The effect of fiber orientation without fiber bridging on MD laminates with a $0^\circ - \theta^\circ$ interface should be tested. This can be done bu cutting by cutting the bridging fibers [39]. When fiber bridging is eliminated, the effect of a 0°-θ interface on the measured fracture toughness by means of the mandrel peel setup can be analysed. In addition, better filming appliances could also capture the bridging zone size.

4. The influence of an angled ply on the initiation toughness with the mandrel peel setup should be analyzed. Within this work the shape of the polyimide film served as a pre-crack influences the initiation toughness. This can be forestalled by first initiating the crack a couple of millimeters and then reversing the experiment to let the peel-arm roll back. After the first initiation, the experiment has to start again, but now a more natural initiation toughness is measured without the influence of the polyimide film.

5. As the matrix material within the delamination interface of this work is smaller than the plastic yielding zone of the crack-tip, the crack most likely propagates in an unstable manner because of this. It should be tested if an additional band of matrix material within the interface solves unstable crack propagation. Another and more favorable option is to experiment with a more brittle matrix material to reduce the plastic deformation zone, as the mentioned additional matrix material will influence the fracture toughness value.

Acknowledgements

This work is performed in order to finish my master in mechanical engineering at the University of Twente, but could not have been completed without the help of some amazing people. To start, I would like to state my gratitude towards my supervisor, Wouter Grouve. For his guidance during the process, knowledge, and constant support even in difficult times got me to keep on working and finish this work. To continue, I would like to thank Nich Helthuis for his guidance and knowledge on everything that was needed to perform the fractographic research. A special thanks also goes to the people from TPRC: Vanessa Marinosci, thank you for your patience and help with getting to know the mandrel peel setup; Gert Jan Navenzel and Edwar Boer, thank you for your time, help, and advice regarding the manufacturing process of the specimen.

Furthermore, I want to dedicate some words towards the most amazing friends, who never seem to fail in supporting me and whom I hope to always have in my life. I do not think the words I write on this page will ever come close to how I feel towards you, but I will try my best. Fernanda Leticia Dos Santos, I have never met a friend who gets me on the level that you do. Your wise words, warm smile, and humor heightens my highs and flattens my lows. You even make me want to wake up in the morning a little bit earlier than I am used to on holidays, and that says a lot. Mark Huizingh and Lars van der Woude, without you guys I would not have gotten this far into the master, thank you so much for that. Our study sessions seemed stressful at the time, but when I am looking back they were one of the most precious moments and I will miss them. Thank you for bearing with me with my endless rants on what was bothering me, supporting me with my work, exploring intriguing ideas and all the fun conversations and times we had and hopefully continue to have. And last but not least, Clara Torrico, thank you for keeping me sane the moments I thought I had lost it all and for making me feel more at home in my own house, you truly are an amazing person and housemate. I hope our endless talks and pizza nights will never end.

Bibliography

[1] J. Puishys, S. Haldar, and H. A. Bruck, "Characterization of mixed-mode energy release rates for carbon fiber/epoxy composites using digital image correlation," in *Experimental Mechanics of Composite, Hybrid, and Multifunctional Materials, Volume 6*. Springer, 2014, pp. 109–115.

[2] M. F. de Moura, R. D. Campilho, A. M. Amaro, and P. N. Reis, "Interlaminar and intralaminar fracture characterization of composites under mode I loading," *Composite Structures*, vol. 92, no. 1, pp. 144–149, 2010. [Online]. Available: http://dx.doi.org/10.1016/j.compstruct.2009.07.012

[3] P. Hu, D. Pulungan, R. Tao, and G. Lubineau, "An experimental study on the influence of intralaminar damage on interlaminar delamination properties of laminated composites," *Composites Part A: Applied Science and Manufacturing*, vol. 131, no. October 2019, p. 105783, 2020. [Online]. Available: https://doi.org/10.1016/j.compositesa.2020.105783

[4] T. Jollivet, C. Peyrac, and F. Lefebvre, "Damage of composite materials," *Procedia Engineering*, vol. 66, pp. 746 – 758, 2013.

[5] H. Chai, C. D. Babcock, and W. G. Knauss, "One dimensional modelling of failure in laminated plates by delamination buckling," *International Journal of Solids and Structures*, vol. 17, no. 11, pp. 1069–1083, 1981.

[6] D. Svensson, "Experimental methods to determine model parameters for failure modes of CFRP," 2013. [Online]. Available: https://www.his.se/PageFiles/4666/Experimental{_}methods{_}to{_}determine{_}model{_}parameters{_}for{_}failure{_}models{_}of{_}CFRP.pdf

[7] P. Prombut, L. Michel, F. Lachaud, and J. J. Barrau, "Delamination of multidirectional composite laminates at 0/θ ply interfaces," *Engineering Fracture Mechanics*, vol. 73, no. 16, pp. 2427–2442, 2006.

[8] W. J. Grouve, L. L. Warnet, and R. Akkerman, "Critical assessment of the mandrel peel test for fiber reinforced thermoplastic laminates," *Engineering Fracture Mechanics*, vol. 101, pp. 96–108, 2013. [Online]. Available: http://dx.doi.org/10.1016/j.engfracmech.2012.07.005

[9] F. Sacchetti, W. J. Grouve, L. L. Warnet, and I. F. Villegas, "Woven fabric composites: Can we peel it?" *Procedia Structural Integrity*, vol. 2, pp. 245–252, 2016.

[10] P. Davies, W. Cantwell, C. Moulin, and H. H. Kausch, "A study of the delamination resistance of IM6/PEEK composites," *Composites Science and Technology*, vol. 36, no. 2, pp. 153–166, 1989.

[11] Y. Gong, L. Zhao, J. Zhang, Y. Wang, and N. Hu, "Delamination propagation criterion including the effect of fiber bridging for mixed-mode I/II delamination in CFRP multidirectional laminates," *Composites Science and Technology*, vol. 151, pp. 302–309, 2017. [Online]. Available: https://doi.org/10.1016/j.compscitech.2017.09.002

[12] J. Andersons and M. König, "Dependence of fracture toughness of composite laminates on interface ply orientations and delamination growth direction," *Composites Science and Technology*, vol. 64, no. 13-14, pp. 2139–2152, 2004.

[13] Y. Su, M. De Rooij, W. Grouve, and L. Warnet, "Characterisation of metal-thermoplastic composite hybrid joints by means of a mandrel peel test," *Composites Part B: Engineering*, vol. 95, pp. 293–300, 2016. [Online]. Available: http://dx.doi.org/10.1016/j.compositesb.2016.03.055

[14] A. Ramji, Y. Xu, M. Yasaee, M. Grasso, and P. Webb, "Delamination migration in CFRP laminates under mode I loading," *Composites Science and Technology*, vol. 190, no. June 2019, p. 108067, 2020. [Online]. Available: https://doi.org/10.1016/j.compscitech.2020.108067

[15] X. J. Gong, A. Hurez, and G. Verchery, "On the determination of delamination toughness by using multidirectional DCB specimens," *Polymer Testing*, vol. 29, no. 6, pp. 658–666, 2010. [Online]. Available: http://dx.doi.org/10.1016/j.polymertesting.2010.04.007

[16] M. S. Bin Mohamed Rehan, J. Rousseau, S. Fontaine, and X. J. Gong, "Experimental study of the influence of ply orientation on DCB mode-I delamination behavior by using multidirectional fully isotropic carbon/epoxy laminates," *Composite Structures*, vol. 161, pp. 1–7, 2017. [Online]. Available: http://dx.doi.org/10.1016/j.compstruct.2016.11.036

[17] N. Sela and O. Ishai, "Interlaminar fracture toughness and toughening of laminated composite materials: a review," *Composites*, vol. 20, no. 5, pp. 423–435, 1989.

[18] R. Khan, "Fiber bridging in composite laminates : A literature review," *Composite Structures*, vol. 229, no. December 2018, 2019.

[19] B. W. Kim and A. H. Mayer, "Influence of fiber direction and mixed-mode ration on delamination fracture toughness of carbon/epoxy laminates," *Composites Science and Technology*, 2003.

[20] D. Purslow, "Matrix fractography of fibre-reinforced thermoplastics, part 1. peel failures," *Composites*, vol. 18, no. 5, pp. 365–374, 1987.

[21] F. Sacchetti, W. J. Grouve, L. L. Warnet, and I. Fernandez Villegas, "Interlaminar fracture toughness of 5HS Carbon/PEEK laminates. A comparison between DCB, ELS and mandrel peel tests," *Polymer Testing*, vol. 66, no. December 2017, pp. 13–23, 2018. [Online]. Available: https://doi.org/10.1016/j.polymertesting.2017.12.005

[22] M. J. Laffan, "Testing the toughness of polymer matrix composites," *Failure Mechanisms in Polymer Matrix Composites: Criteria, Testing and Industrial Applications*, pp. 110–128, 2012.

[23] H. K. Adluru, K. H. Hoos, E. V. Iarve, and J. G. Ratcliffe, "Delamination initiation and migration modeling in clamped tapered laminated beam specimens under static loading," *Composites Part A: Applied Science and Manufacturing*, vol. 118, no. June 2018, pp. 202–212, 2019.

[24] R. Khan, R. Alderliesten, S. Badshah, M. A. Khattak, M. S. Khan, and R. Benedictus, "Experimental investigation of the microscopic damage development at mode i fatigue delamination tips in carbon/epoxy laminates," *Jurnal Teknologi*, vol. 78, no. 11, pp. 33–40, 2016.

[25] F. Sacchetti, W. J. Grouve, L. L. Warnet, and I. F. Villegas, "Effect of resin-rich bond line thickness and fibre migration on the toughness of unidirectional Carbon/PEEK joints," *Composites Part A: Applied Science and Manufacturing*, vol. 109, no. February, pp. 197–206, 2018. [Online]. Available: https://doi.org/10.1016/j.compositesa.2018.02.035

[26] D. Stevanovic, S. Kalyanasundaram, A. Lowe, and P. Y. Jar, "FEA of crack-particle interactions during delamination in interlayer toughened polymer composites," *Engineering Fracture Mechanics*, vol. 72, no. 11, pp. 1738–1769, 2005.

[27] F. Cepero, I. G. García, J. Justo, V. Mantič, and F. París, "An experimental study of the translaminar fracture toughnesses in composites for different crack growth directions, parallel and transverse to the fiber direction," *Composites Science and Technology*, vol. 181, no. February, p. 107679, 2019. [Online]. Available: https://doi.org/10.1016/j.compscitech.2019.107679

[28] A. Sekulic, "Experimental Identification of Adhesive Properties between Epoxy and Glass," Ph.D. dissertation, 2008.

[29] C. T. Sun and S. Zheng, "Delamination characteristics of double-cantilever beam and end-notched flexure composite specimens," *Strain*, vol. 56, pp. 451–459, 1996.

[30] F. Daghia and C. Cluzel, “The Climbing Drum Peel Test: An alternative to the Double Cantilever Beam for the determination of fracture toughness of monolithic laminates,” *Composites Part A: Applied Science and Manufacturing*, vol. 78, pp. 70–83, 2015. [Online]. Available: http://dx.doi.org/10.1016/j.compositesa.2015.07.010

[31] A. Rudawska, *Assessment of surface preparation for the bonding/adhesive technology*, 2019.

[32] L. F. Kawashita, D. R. Moore, and J. G. Williams, “The development of a mandrel peel test for the measurement of adhesive fracture toughness of epoxy-metal laminates,” *Journal of Adhesion*, vol. 80, no. 3, pp. 147–167, 2004.

[33] L. Forkink, “Fracture Toughness Measurement of Multi-Directional Laminates with the Mandrel Peel Test,” Thesis, University of Twente, 2017.

[34] K. R. van den Boogert, “Delamination Resistance Experiments of Multi-directional C-PEEK Laminates using the Mandrel Peel Test,” Thesis, University of Twente.

[35] J. G. W. L. F. Kawashita, D. R. Moore, “A protocol for determination of adhesive fracture thoughness of flexible laminates by peel testing: Mandrel peel method,” 2005. [Online]. Available: http://www3.imperial.ac.uk/pls/portallive/docs/1/4631904.PDF

[36] L. F. Kawashita, A. J. Kinloch, D. R. Moore, and J. G. Williams, “The influence of bond line thickness and peel arm thickness on adhesive fracture toughness of rubber toughened epoxy-aluminium alloy laminates,” *International Journal of Adhesion and Adhesives*, vol. 28, pp. 199–210, 2008.

[37] Toray, “Toray Cetex TC1200 PEEK,” pp. 1–5. [Online]. Available: https://www.toraytac.com/media/7765d981-1f9f-472d-bf24-69a647412e38/8InI2A/TAC/Documents/Data{_}sheets/Thermoplastic/UDtapes,prepregsandlaminates/Toray-Cetex-TC1200{_}PEEK{_}PDS.pdf

[38] N. J. Johnston, *Toughened Composites: Symposium on Toughened Composites*. ASTM International, 1987, no. 937.

[39] M. Iwamoto, Q.-Q. Ni, T. Fujiwara, and K. Kurashiki, “Intralaminar fracture mechanism in unidirectional cfrp composites: Part i: Intralaminar toughness and ae characteristics,” *Engineering Fracture Mechanics*, vol. 64, no. 6, pp. 721–745, 1999.

[40] P. P. Parlevliet, H. E. Bersee, and A. Beukers, “Residual stresses in thermoplastic composites-A study of the literature-Part I: Formation of residual stresses,” *Composites Part A: Applied Science and Manufacturing*, vol. 37, no. 11, pp. 1847–1857, 2006.

[41] M. A. Umarfarooq, P. S. Shivakumar Gouda, G. B. Veeresh kumar, N. R. Banapurmath, and A. Edacherian, “Impact of process induced residual stresses on interlaminar fracture toughness in carbon epoxy composites,” *Composites Part A: Applied Science and Manufacturing*, vol. 127, no. August, p. 105652, 2019. [Online]. Available: https://doi.org/10.1016/j.compositesa.2019.105652

Appendix A

Preliminary study: Methodology

Before the experiments on the relation between the interlaminar fracture toughness and fiber orientation will start, the preliminary study is designed to test the influence on the crack propagation of the peel-arm thickness, specimen width, alignment force and vertical adjustment of the mandrel with respect to the specimen, while generating knowledge and experience with the setup. Each tested parameter will be explained in this chapter, while an overview of the parameters is stated in table A.2. The required theory for this study is stated in chapter 3. The outcome of the preliminary study answers the sub-questions as stated in section 3.5.1 and is a direct input to the methodology of the experimental part of this research.

A.1 Specimen

Most research known for testing the fracture toughness by means of the mandrel peel setup use specimen of 10 mm in width ([33], [34], [13], and [21]), making this width a favorite option. Nonetheless, widths of 16 mm [32] and 18 mm [9] are also found. The width of the specimen is limited to the maximum width of the mandrel, which is for the current research 18 mm. It is advised to stay at least 1 mm below the width of the mandrel, to avoid that the specimen is wider than the mandrel due to cutting tolerances, leaving the second choice to be 17 mm. It is expected that a wider sample affects the fracture toughness value, as the global stiffness of the peel-arm is different in comparison with a smaller sample, see section 3.4.2.

The choice for the peel-arm thickness can be based on the mandrel diameter and manageability of mounting the peel-arm around the mandrel. There are two different mandrel sizes available at the laboratory of the University of Twente; radii of 10 and 20 mm. Using equation 3.2 it can be calculated that a maximum thickness of 0,36 mm (2.8 plies) and 0,72 mm (5.5 plies) can be used with a maximum elongation of 1.8%, respectively to the mandrel radius. However, a peel-arm thicker than two plies might be too stiff to bent around the mandrel. Based on these findings it is recommended to compare the fracture toughness results of specimen with a peel-arm of 0.13 mm (one ply) and 0.26 mm (two plies). Both thicknesses can be tested on a 10 mm radius mandrel. It is expected that the fracture toughness of the samples with a thicker peel-arm show more difficulties mounting around the mandrel, but will show a more stable crack propagation due to the fact that the peeling and alignment forces are distributed over two plies instead of one. In addition, it is expected that a thicker peel-arm affects the measured fracture toughness value, as a thicker peel-arm has a different global stiffness.

A.1.1 Production

The used material for the specimen is carbon/PEEK unidirectional composite material, produced by Toray [37]. The lay-up will be a 16 layered laminate with 0°with respect to each ply. The 0°direction of each layer is chosen to ease the production process of the laminate, and the 0°generated fracture toughness of the specimen can easily be compared with the available material properties from Toray [37], which can confirm the applicability of the used parameters on the mandrel peel setup. The laminates will be assembled in a 12 inch picture frame and consolidated at TPRC in Enschede. The consolidation process goes according to the standard press cycle of carbon/PEEK, see table A.1. The first laminate will have a 10cm long 12 μm thick polyimide film between the 15^{th} and 16^{th} ply to serve as an initial crack, while the second laminate will

have the film between the 14th and 15th ply, see figure A.1. After consolidation, the samples are cut into the desired widths of 10 and 17 mm and the polyimide film will be removed.

Table A.1: Standard press cylce carbon/PEEK material

Pressure	Temperature	Dwell time	Total cycle time
20 bar	385	Cooling directly	8635 sec

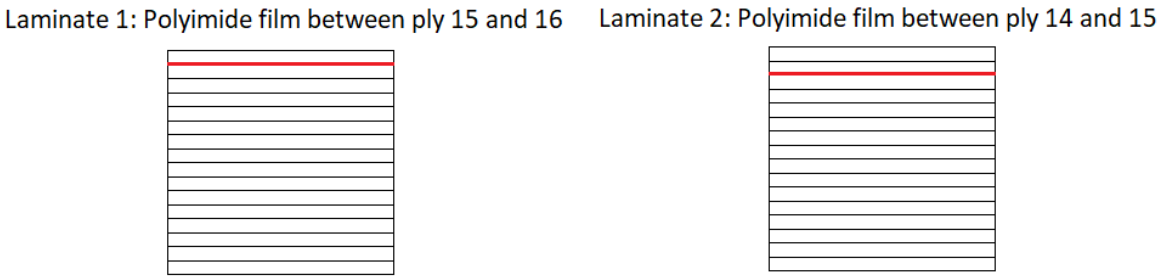

Figure A.1: Front view placement of polyimide film of laminate 1 and 2

A.2 Mandrel peel experiments

The experiments will be performed according to the '*protocol for determination of adhesive fracture toughness of flexible laminates by peel testing: mandrel peel method*' designed by Kawashita et al. [35]. An overall step-by-step guide on how to operate the mandrel-peel setup can be found in appendix D. A schematic overview of the mandrel peel setup can be found in figure A.2a. To monitor the conformation of the peel-arm to the mandrel, a camera will be placed parallel to the mandrel to capture the movement of the peel-arm, see figure A.2b. As described in section 3.2, the friction and fracture toughness of each sample will be measured in the same stroke.

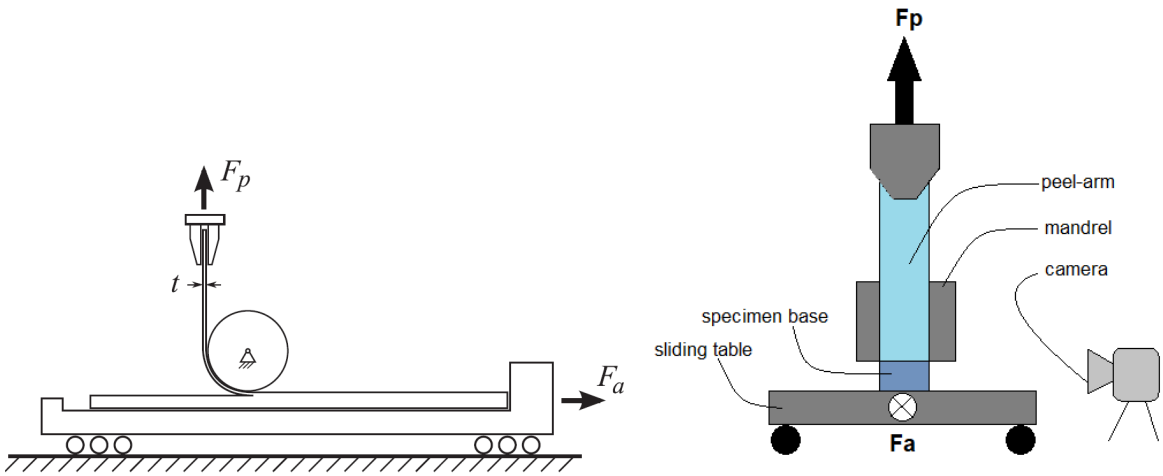

(a) Side view mandrel peel setup [8]

(b) Front view mandrel peel setup

Figure A.2: Side and front view of the mandrel peel setup

As written in section A.1, a 10 mm radius mandrel will be used as the mandrel diameter is of no influence

on the fracture toughness [32] and only influences the maximum bending strain of the peel-arm [13]. The rate at which the crack can propagate will be set at 15mm/min, as then the results can easily be compared with the research of Forkink [33], van den Boogert [34], Grouve et al. [8], and Su et al. [13]. The peeling rate will not be varied, as Sacchetti et al. [9] already examined the effect of the peeling rate on the measured fracture toughness and found no significant influence. The effect of a different vertical adjustment of the mandrel on the crack propagation will be examined, together with the effect of the alignment force. These factors will be discussed in the next sections.

A.2.1 Vertical adjustment of the mandrel

The vertical adjustment of the mandrel is related to the total amount of internal friction and cannot exceed the 5% [35]. For the current research, it is recommended to experiment with a placement of 0 mm and 0.5 mm between sample and mandrel. It is expected that conformation of the peel-arm to the mandrel will be best with the 0 mm placement, together with the crack propagation plane. When the mandrel is placed 0.5 mm above the sample, the force *F* and angle θ can make the peel-arm break as can be seen in figure 3.3 [35], but the total amount of friction should be lower.

A.2.2 Alignment force

When looking at the studies of both Forkink [33] and van den Boogert [34] as described in section 2.3, it can be suggested that their used alignment force was not sufficient with the knowledge that a higher alignment force contributes to a more consistent crack propagation [36]. Van den Boogert found crack migration to the base of the specimen [34], and Forkink found that the crack deviated into the peel-arm [33]. In addition, van den Boogert [34] also experienced stick-slip behavior, but this is most likely caused by the migration of the delamination into the neighboring interface [14], as discussed in chapter 3. Nonetheless it is recommended to test if an increase in the alignment force counteracts the shifting of the delamination plane away from the intended interface. The forces that will be used are 75 N as a reproduction of previously mentioned research and 125 N as increase. It is expected that samples tested with the alignment load of 125 N will show interlaminar crack growth, while the crack propagation of the samples tested with 75 N will deviated from the intended interface.

Table A.2: Overview of experimental settings

Peel-arm	Sample width	Alignment force	Vertical adjustment mandrel
1-ply	10 mm	75 N	0 mm
2-ply	17 mm	125 N	0.5 mm

A.3 Data reduction

During the mandrel peel test the peeling and alignment forces are being measured. Based on these values the friction (μ) of the experimental setup can be determined through equation 3.1 together with the fractural toughness (*G*) of the specimen by means of equation 2.10. For completeness, these equations are repeated here:

$$\mu = \frac{F_p - F_a}{F_p} \tag{A.1}$$

$$G = \frac{1}{b}[F_p(1-\mu) - F_a] \tag{A.2}$$

Once all experiments are performed, the data will be translated to graphs by means of MATLAB. An example graph of how the result potentially looks like can be seen in figure A.3 [33], where the alignment, peeling, and friction forces are visualized. It can be seen that there is an initial peak that marks the start of the delamination. After the crack initiation, the crack propagation stabilises around a plateau value of 17 N. The fracture toughness value G_c is determined from this plateau value [33]. To see if the fiber direction has

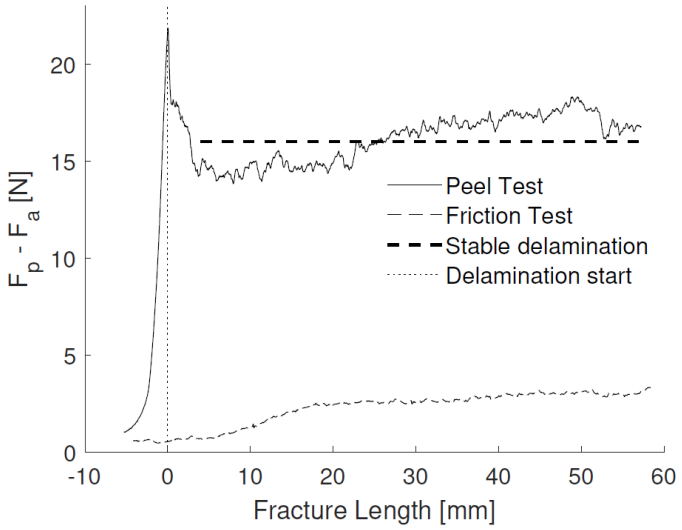

Figure A.3: Example force-displacement graph [33]

an influence on the fracture toughness, the values of each sample will be compared. The crack initiation force (F_{peak}) will also be analysed together with the initial peak force (F_{ip}) to see if the fiber angle influences these results. However, these results should be treated with care as the polyimide film might influence the these forces. The F_{ip} is determined by dividing the F_{peak} by the width of the specimen, as the width of the specimen influences the induced forces. The following formula is used to determine F_{ip}:

$$F_{ip} = \frac{F_p - F_a}{b} \tag{A.3}$$

A.4 Microscopy

The aim of the microscopic research is to examine the crack propagation plane at the position shown in the red square of figure 4.4a. The red square of figure 4.4a will be cut out, containing both the peel-arm and substrate just behind the crack tip. The cut sections of each sample are embedded in clear epoxy and cured for at least 24 hours. After the curing, the samples are polished and prepared for the digital Keyence VHX-5000 microscope.

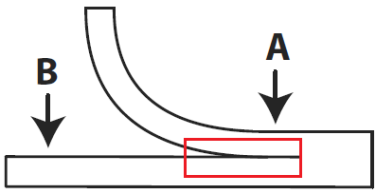

Figure A.4: Microscopic analysis of crack propagation plane

Appendix B

Preliminary study: Experimental

An overview of all results can be found in table B.1. The name of the specimen describes the used dimensions and parameters as follows: vertical adjustment of mandrel (0 or 5*10^{-1} mm) - alignment force (75 or 125 N) - specimen width (10 or 17 mm)- peel-arm thickness (1 or 2 plies). The mode I fracture toughness (G_{Ic}) is given, together with the peak force (F_{peak}), initial peak force (F_{ip}), and friction (μ). It is stated whether the peel-arm conformed to the mandrel or not, how the crack propagated and if there are any other remarks.

Table B.1: Results trial experiments

Sample	G_{Ic} [kJ/m^2]	F_{peak} [N]	F_{ip} [N]	μ	μ [%]	Conform to mandrel	Crack propagation	Remarks
0-75-10-1	1.5032	20.412	2.041	0.0040	0.27	yes	interlaminar	-
0-75-10-2	1.7287	21.189	2.120	0.0078	0.45	yes	into substrate	-
0-75-17-1	1.3513	27.888	1.640	0.0057	0.42	yes	into peel-arm	Difficult to hold grip
0-75-17-2	1.7499	34.092	2.005	0.0040	0.23	-	interlaminar	-
0-125-10-1	1.3854	19.936	1.994	0.0029	0.21	yes	interlaminar	-
0-125-10-2	1.6404	18.119	1.812	0.0059	0.36	yes	into substrate	-
0-125-17-1	1.3811	27.866	1.639	0.0023	0.17	yes	-	Difficult to hold grip
0-125-17-2	1.7171	33.751	1.985	0.0057	0.33	yes	into substrate	-
5-75-10-1	1.4668	17.936	1.793	0.0011	0.07	yes	interlaminar	Sample got lifted
5-75-10-2	1.7872	22.111	2.211	0.0038	0.21	yes	into substrate	Sample got lifted
5-75-17-1	1.5393	28.086	1.652	0.0014	0.09	yes	interlaminar	Sample got lifted
5-75-17-2	1.7040	37.369	2.198	0.0043	0.25	yes	into peel-arm	Sample got lifted
5-125-10-1	1.3844	17.939	1.794	0.0011	0.08	yes	interlaminar	Sample got lifted
5-125-10-2	1.7533	18.642	1.864	0.0026	0.15	yes	interlaminar	Sample got lifted
5-125-17-1	-	-	-	-	-	-	-	Difficult to hold grip
5-125-17-2	1.6580	27.850	1.638	0.0018	0.11	yes	interlaminar	Sample got lifted

B.1 General results

The generated graphs of all samples can be found in appendix C and show no irregularities, such as the stick-slip behavior as described by van den Boogert [34]. This is as expected, as the conformation of the peel-arm to the mandrel was good and stick-slip and both Forkink [33] and van den Boogert [34] did not encounter stick-slip with their 0°//0°interface specimen. The reason for the lack of stick-slip behavior when it comes to UD laminates might be due to the lay-up. During curing, it is common for UD laminates that fibers of adjacent plies nest together, causing fiber bridging [18]. When fiber bridging occurs, the interfaces of the laminates are more blend together. This blending of the interfaces make it challenging to track the delamination propagation interface and make the laminate more uniform in general. The damage zone in front of the crack tip will therefore be more uniform as well, which will decrease the risk of stick-slip and other unstable crack propagation behavior. Furthermore, Ramji et al. [14] found that migration of the delamination

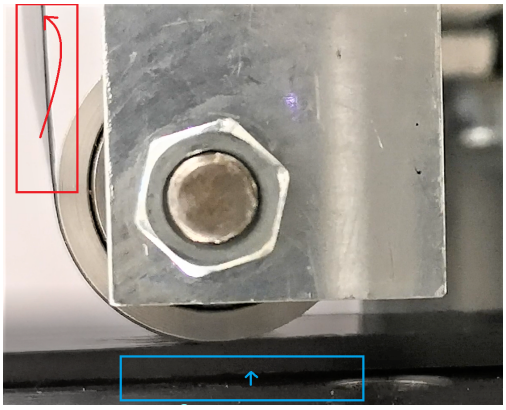

Figure B.1: Screenshot from experimental film 5-75-17-2. The blue arrow at the bottom shows that the substrate is lifted from the base during peeling, while the red arrow shows the twisting effect

plane into a neighboring interface happens more sudden, while migration into the ply of the delamination interface happens gradually. As the ply interfaces of a UD laminate are more blend together, it makes sense that migration to other interfaces happen more gradually than when the laminate is multidirectional, thus lessening the risk of stick-slip behavior. However, stick-slip behavior will most likely be experienced with the MD carbon/PEEK specimen.

The interlaminar fracture toughness of the total tested samples lies in the range of 1.6 $\pm 0.2 kJ/m^2$ with a total standard deviation of 0.16. The interlaminar fracture toughness given by the manufacturer of the carbon/PEEK material is 1.6 kJ/m^2 [37] as well, tested with the DCB test (ASTM D 5528). However, as the fracture toughness is influenced by the global stiffness of the specimen and testing method [16], this comparison should be taken with care. In addition, if any of the MP parameters or sample dimension influence the measured G_{Ic}, the samples will be taken out of the average which would change the averaged value. The standard deviation per parameter is given in table B.2, together with the found average G_{Ic}. The differences between each parameter is not very high, making the standard deviation not a suitable tool to choose the best settings for the mandrel-peel set-up. In addition, based on the standard deviation a peel-arm with a thickness of 2 plies and a width of 17 mm is more favorable than 1 ply and 10 mm respectively, even though it is already discussed that these parameters should not be used due to the twisting of the peel-arm and mounting difficulties.

Despite the lack of irregularities in the generated results, the samples with a peel-arm of 2 plies were more difficult to mount into the gripper than the 1 ply variants, since they are stiffer and therefore more difficult to bend around the mandrel. This gave as a result that most of these peel-arms were a bit twisted, due to lack of proper alignment. The same twisting effect was seen with the samples that are 17 mm wide, also due to alignment reasons, as it showed difficulties with the smaller fixation clamp of the peeling force, resulting in a twisted fixation. This twisting effect can be seen in figure B.1, where the red arrow in the left upper corner shows the location. This effect made it easy for the peel-arm to slip out of the clamp. The twisting effect can induce improper force distribution at the peeling surface what might interfere with the crack propagation plane, making the 2 ply thick peel-arm and 17 mm wide samples less suitable for the mandrel peel-test.

B.2 Peel-arm thickness

When looking at the peel-arm thickness, the average fracture toughness values are 1.72 and 1.43 kJ/m^2 for a peel-arm of two plies and one ply respectively, with a standard deviation of 0.049 and 0.0722 respectively. This can be seen in figure B.2a. This result suggest that the fracture toughness is related to the thickness of the peel-arm, but can also be explained by the different laminates the specimen were made from. Nonetheless, this finding is in line with the study done by Kawashita et al. [32], that related a thicker peel-arm to a higher fracture toughness value as already discussed in section 3.4.2. In addition, as the global stiffness of the specimen affects the G_{Ic} as is discussed in chapter 2, the higher measured G_{Ic} of the two ply peel-arm specimen can be related to that as well. Furthermore, fiber migration might be different between the two

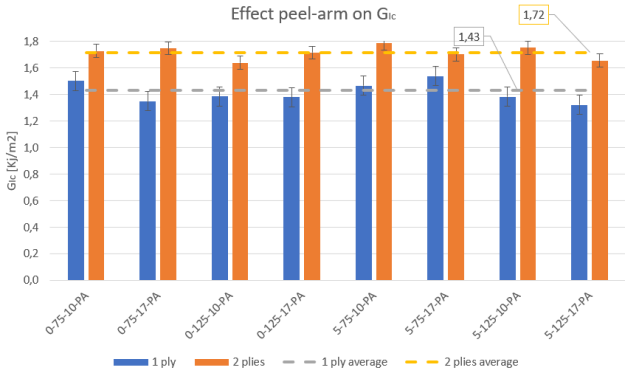

(a) Influence of PA on fracture toughness

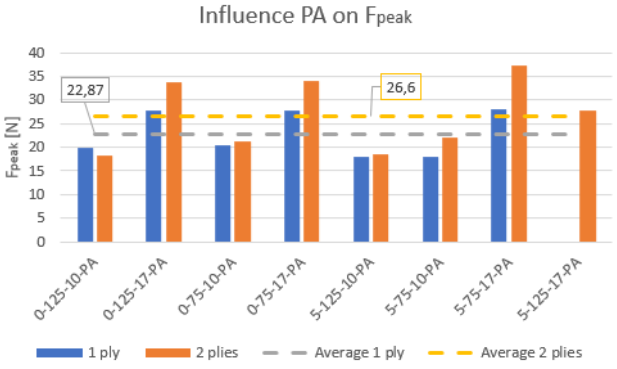

(b) Influence of PA on peak force

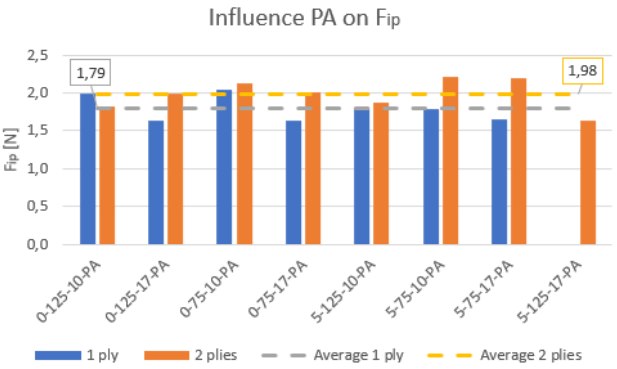

(c) Influence of PA on initial peak force

Figure B.2: Influence of peel-arm (PA) on the measured fracture toughness (G_{Ic}), crack initiation force (F_{peak}), and initial peak force (F_{ip})

peel-arms, which could also lead to the findings. The influence of the peel-arm thickness on the fracture toughness suggests that a one ply thick peel-arm should be used, especially when the results of this study need to be compared with the studies of Forkink [33] and van den Boogert [34] who both use a peel-arm thickness of one ply.

The effect of the peel-arm on the initial peak (F_{peak}) and initial peak force (F_{ip}) can be found in figures B.2b and B.2c. Here it can be seen that the F_{peak} does seem to differ significantly depending on the peel-arm thickness, with values of 22.87 N and 26.6 N for respectively a 1-ply to 2-plies thick peel-arm. However, when the F_{peak} is divided by the width of the specimen, the F_{ip} shows to decrease the significance of the difference, namely 1.79 N/mm and 1.98 N/mm for respectively a 1-ply to 2-plies thick peel-arm. It can therefore be concluded that the peel-arm thickness has a direct influence on the measured G_{Ic}, but not so much on the crack initiation.

B.3 Specimen width

No effect of the specimen width on the measured G_{Ic} can be found, as can be seen in figure B.3a. The average G_{Ic} is 1.58 and 1.59 for specimen with a width of 10 mm and 17 mm, respectively. The standard deviation is 0.1663 and 0.1645 for a width of 10 mm and 17 mm, respectively. This is not in line with the results found by Sacchetti et al. [9], as there it was found that a wider peel-arm results in a slightly lower fracture toughness value and decreases the standard deviation. The authors did not expect this result and recommended further research to explain these findings. As Sacchetti et al. [9] used carbon/PEEK 5 Harness Satin Weave samples and this preliminary study carbon/PEEK UD it is possible that the contradicting results are due to the type of material. As a wider specimen weave specimen contains more weave units, the directional stiffness of the peel-arm is therefore higher than the smaller specimen. This effect is not that extreme when it comes to UD material, as the directional stiffness does not change significantly when the peel-arm is a bit wider.

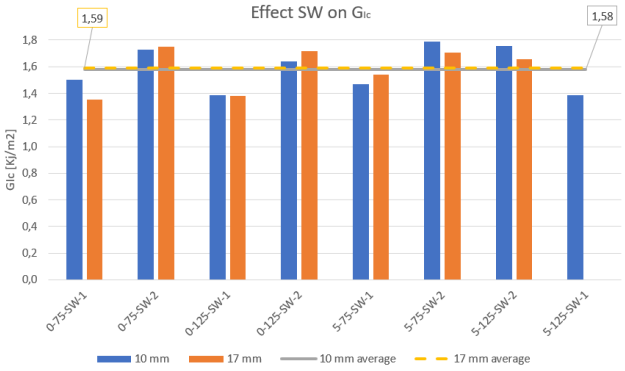

(a) Influence of SW on fracture toughness

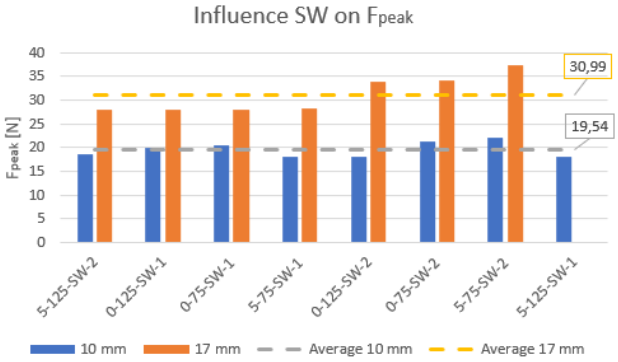

(b) Influence of SW on peak force

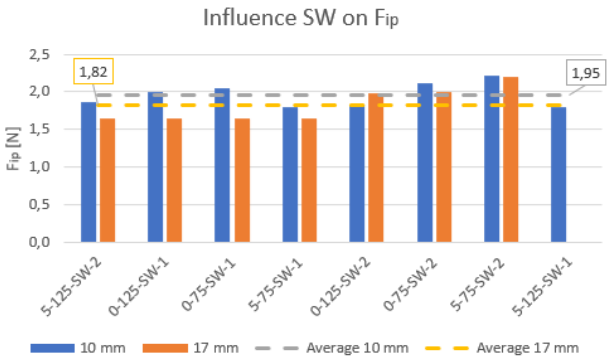

(c) Influence of SW on initial peak force

Figure B.3: Influence of specimen width (SW) on the measured fracture toughness (G_{Ic}), crack initiation force (F_{peak}), and initial peak force (F_{ip})

As expected, the specimen width increases the initial peak when the samples are wider, but this influence vanished when the initial peak is divided by the width of the specimen.The F_{peak} is 19.54 N and 30.99 N for a width of 10 mm and 17 mm, respectively. For the F_{ip}, the values are 1.95 and 1.82 for a width of 10 mm and 17 mm, respectively. It can be concluded that the specimen width does not seem to influence the measured G_{Ic} and crack initiation. The results of the initiation toughness should be treated with care as the 12 μm polyimide (PI) film used as an insert for the pre-crack influences the initiation toughness. The PI film has a square tip, which influences the stress field around the crack tip.

B.4 Friction and mandrel placement

When looking at figures B.4b, B.4c, and B.4d it can be seen that the vertical placement of the mandrel with respect to the sample does not influence the measured G_{Ic}, F_{peak}, and F_{ip}. The average value for the friction coefficient was found to be 0.0036, or 0.23% with a 0.12% deviation from the average. This means that the friction stays below the 5% as mentioned by [35]. As stated in section 3.3, the vertical placement of the mandrel with respect to the specimen was expected to influence the friction, where a distance of 0.5 mm would generate lower friction values. This expectation is confirmed when looking at the results in figure B.4a, where the average friction percentage of the 0.5 mm mandrel height is substantially lower than those of the 0 mm height. The standard deviation of the 0 mm height difference is 0.110, while the 0.5 mm has a standard deviation of 0.070. Based on these findings it can be stated that for friction purposes a mandrel height of 0.5 mm with respect to the sample is more favorable than a height of 0 mm. However, since the friction percentage of both heights are below the stated 5% [35], both heights could be used.

Nonetheless, when looking at the conformation of the peel-arm to the mandrel, the results show that when the height of the mandrel with respect to the specimen is 0.5 mm, the sample is being lifted from the base until it touches the mandrel. This lifting is visible at the blue arrow of figure B.1. The lifting of the sample towards the mandrel makes the height difference of 0.5 mm from mandrel to sample irrelevant,

since the distance is 0 mm the moment the peeling starts. In addition, the lifting increases the changes of alignment faults, especially with the wider samples of 17 mm and peel-arm thicknesses of 2 plies as discussed earlier. Finally, the lifting activates the presence of the global stiffness of the specimen into the measurement, which can influence the measured fracture toughness as is stated in section 3.3. Based on these findings it can be concluded that the height of the mandrel should be set to 0 mm with respect to the sample. Besides the lifting effect, it is found that all samples have a good conformation of the peel-arm to the mandrel. This result means that the chosen parameters do not seem to affect the conformation of the peel-arm to the mandrel, nor does it affect the measured G_{Ic}, F_{peak}, and F_{ip}.

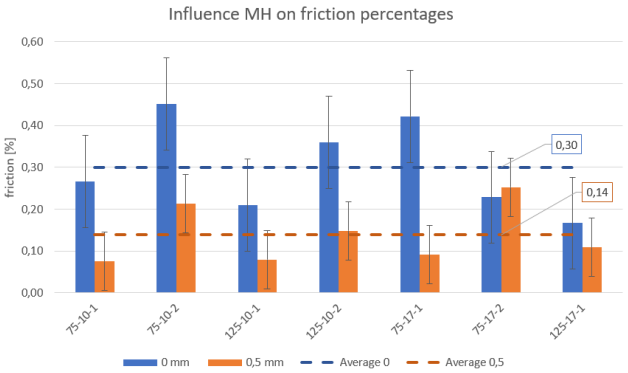

(a) Influence of MH on friction percentages

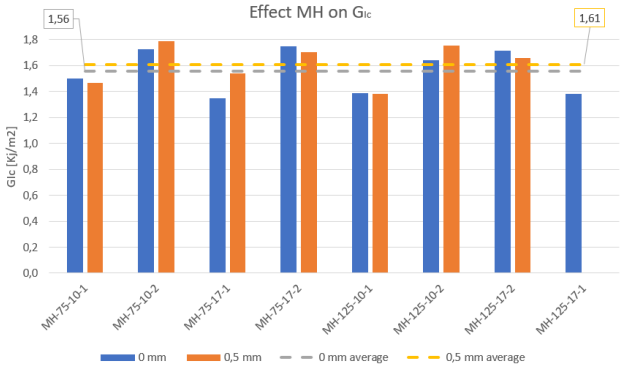

(b) Influence of MH on G_{Ic}

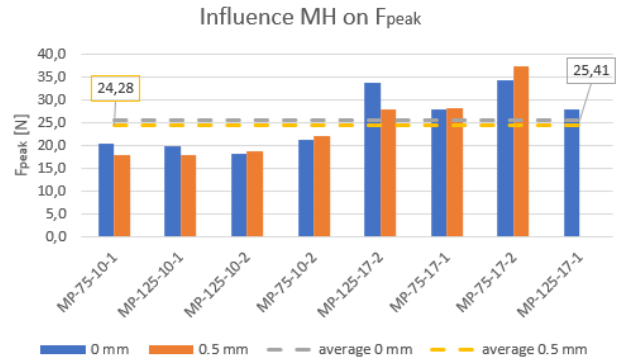

(c) Influence of MH on F_{peak}

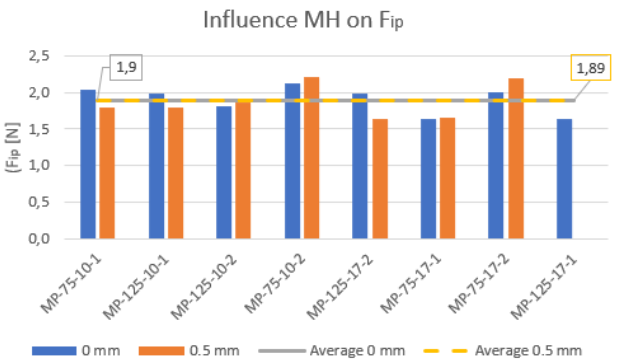

(d) Influence of MH on F_{ip}

Figure B.4: Influence of mandrel height (MH) on friction values (μ), fracture toughness (G_{Ic}), crack initiation force (F_{peak}), and initial peak force (F_{ip})

B.5 Alignment force

The alignment force is established by means of a pneumatic cylinder attached to the sliding table and the pressure is set manually. During the experiments it was observed that the pressure deviates from the fixed value, requiring that the alignment force needs adaptation during the experiment, inducing additional variables. It was found that the alignment force was easier to maintain stable with higher forces (125 N) and with the mandrel distance being 0 mm with respect to the sample.

When taking into account the manual fixation of the peeling clamp as discussed in the beginning of this chapter, it is better to use an alignment force of 75 N. A higher alignment force induces higher internal forces, making it easier for the peel-arm to slip out of the clamp. In addition, the used force cells to measure the peeling and alignment force are made for 200 N. With the idea in mind that a different fiber angle might induce a higher fracture toughness, an alignment force of 125 N might not be suitable. A 0°//0°fiber arrangement already induces 147.2 N with an alignment force of 125 N, while an alignment force of 75 N induces only 96.4 N. However, this argument can also be in favor for an alignment force of 125 N, since a different fiber angle is expected to induce a higher fracture toughness, what will relate to a higher peeling

force and is therefore in need of a higher alignment force to keep the peel-arm conformed to the mandrel. In addition, when looking at the generated results, four out of six samples that showed intralaminar crack propagation were from an alignment force of 75 N, even though the conformation of the peel-arm to the mandrel was proper at all times.

Another argument in favor of a higher alignment force lies in the mechanics of the specimen. Thermoplastic composites need high temperature processing and this induces residual stresses on a micro-mechanical level due to mismatch in thermal expansion coefficients of the fibres and matrix. Since residual stresses are present in virtually all composite materials it is therefore an important factor [40], especially since it is shown by Umarfarooq et al. [41] that the presence of residual stresses in UD carbon/Epoxy $[0]_8$ have a positive effect on the mode I fracture toughness. When looking at a macro-mechanical level, lamination residual stresses are present due to lamina anisotropy on a ply-to-ply scale. The stresses are induced due to a difference in the longitudinal and transverse ply coefficients of thermal expansion [40]. This means that when experiments are done on specimen with different fiber directions, the residual stresses might be higher and therefore have a higher fracture toughness, needing a higher alignment force to keep the peel-arm conformed to the mandrel.

Based on these findings it can be argued that an alignment force of 75 N is too low and 125 N is too high. Referring back to the theory given in section 3.2 that a higher alignment load contributes to a crack that propagates more consistently along the interface, it is chosen to use an alignment force of 100 N for the upcoming experiments. This change can be applied, since the fracture toughness value does not seem to depend on the alignment force when looking at the results in figure B.5a. Here it can be seen that the average fracture toughness is 0.07 kJ/m^2 higher for the samples with 75 N. The standard deviation is 0.159 and 0.169 for an alignment force of 75 N and 125 N, respectively, making the alignment force independent for the fracture toughness. Furthermore, the F_{peak} and F_{ip} does seem to differ, but the question remains whether this is a significant difference, see figures B.5b and B.5b. It can be concluded that the alignment force does not influence the measured G_{Ic}, but might influence the F_{peak}, and F_{ip}. The chance of crack migration decreases when a higher alignment force is used.

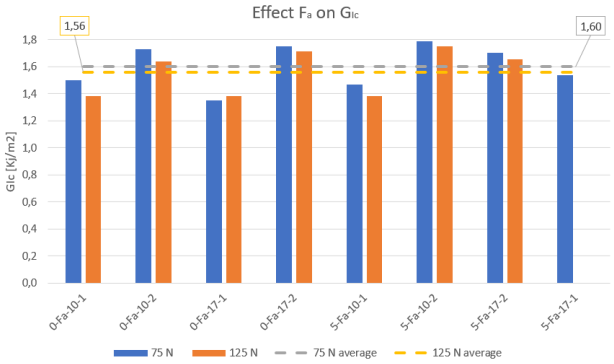

(a) Influence of Fa on the measured G_{Ic}

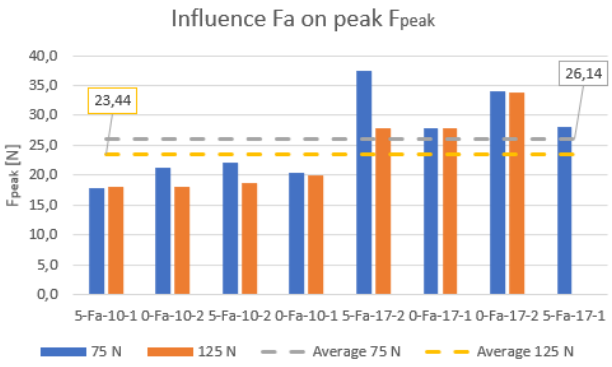

(b) Influence of Fa on the F_{peak}

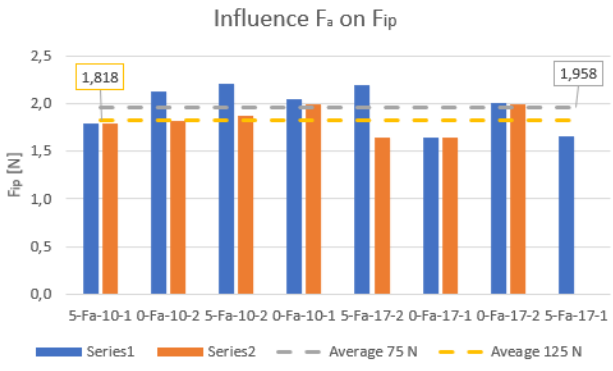

(c) Influence of Fa on the F_{ip}

Figure B.5: Influence of alignment force (Fa) on the measured fracture toughness (G_{Ic}), crack initiation force (F_{peak}), and initial peak force (F_{ip})

B.6 Microscopic results

The crack propagation plane is analyzed by making microscopic images and the results are summed up in table B.1. Based on these images it is found that samples 0-75-10-2, 0-125-10-2, 0-125-17-2, and 5-75-10-2 show crack migration into the substrate, as can be seen for sample 0-75-10-2 in figure B.6a. For the 5-75-17-2 and 0-75-17-1 samples, the crack propagated into the peel-arm, as can be seen in figure B.6b. The crack migration most likely happens due to the difference in fiber to matrix ratio's inside the propagation interface. As is suggested by Sacchetti et al. [25], the crack migrates to the weakest region when the plastic deformation zone is larger than the matrix zone, which can lead to migration and unstable crack propagation. Nonetheless, no visible trend between the used parameters and the interlaminar crack propagation is found, but a higher alignment force might increase the chance of stable crack propagation.

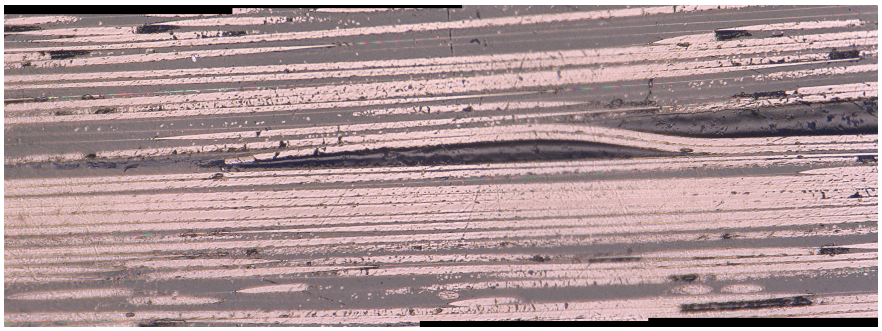

(a) Crack jumping of sample 0-75-10-2 into the substrate

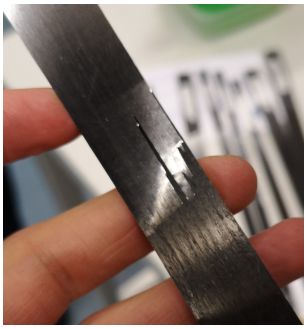

(b) Crack propagating into the peel-arm of sample 0-75-17-1

Figure B.6: Crack propagation

B.7 Conclusion and discussion preliminary study

The preliminary study found no visible trend between the used parameters and crack propagation. During the experiments it was found that the crack can propagate away from the delamination interface, while no stick-slip behavior occurred. The reason that no stick-slip behavior is found during these experiments might be due to the UD lay-up. The specimen are all build from UD material in the 0°direction. During curing, it is common for UD laminates that fibers of adjacent plies nest together, causing fiber bridging [18]. When fiber bridging occurs, the interfaces of the laminates are more blend together. This blending of the interfaces make it challenging to track the delamination propagation interface and make the laminate more uniform in general. The damage zone in front of the crack tip will therefore be more uniform as well, which will decrease the risk of stick-slip and other unstable crack propagation behavior. Furthermore, Ramji et al. [14] found that migration of the delamination plane into a neighboring interface happens more sudden, while migration into the ply of the delamination interface happens gradually. As the ply interfaces of a UD laminate are more blend together, it makes sense that migration to other interfaces happen more gradually than when the laminate is multidirectional, thus lessening the risk of stick-slip behavior. However, as this study will focus on MD laminates, stick-slip behavior will most likely be experienced when MD carbon/PEEK specimen are tested.

The preliminary study is performed to answer the sub-questions about the specimen dimensions and mandrel peel settings as stated in section 3.5.1. An overview of the measured average G_{Ic} with the standard deviation, together with the effect of the tested parameters on the G_{Ic} and crack propagation can be found in table B.2.

It was found that the thickness of the peel-arm (PA) affects the measured G_{Ic}, where a thicker peel-arm increases the G_{Ic}. This could be due to the different global stiffness of the peel-arm or due to more fiber migration. The other tested parameters do not show to have an effect on the G_{Ic}.

The overall best choice is to use 10 mm wide samples with a peel-arm of one ply thick. The vertical adjustment of the mandrel with respect to the specimen should be set to 0 mm, while using an alignment force of 100 N. The pneumatic cylinder used to establish the alignment force should be changed, as the cylinder was unable to maintain a stable alignment force. On a side note, the used pre-crack of 10 mm was barely enough to mount the peel-arm around the mandrel, therefore it is recommended to have a pre-crack of at least 12 mm for mounting convenience. It is important to note that the used test quantities of this study are not enough to make this experiment significant, therefore all results should be treated with care. However, as goal to understand the MP set-up and testing parameters the quantities of this study are sufficient.

Table B.2: Overview averaged results preliminary study

	F_a 125 N	**F_a 75 N**	**HM 0 mm**	**HM 0.5 mm**	**peel-arm 1 ply**	**peel-arm 2 plies**	**Width 10 mm**	**Width 17 mm**
G_{Ic}	1.56	1.60	1.56	1.61	1.43	1.72	1.58	1.59
Std.Dev.	0.169	0.159	0.1711	0.1524	0.0722	0.049	0.1663	0.1645
Effect on G_{Ic}	No effect		No effect		Thicker PA causes higher G_{Ic}		No effect	
Effect on crack propagation	Higher F_a shows less intralaminar propagation		No effect		No effect		No effect	

Appendix C

Preliminary: Measured forces and friction

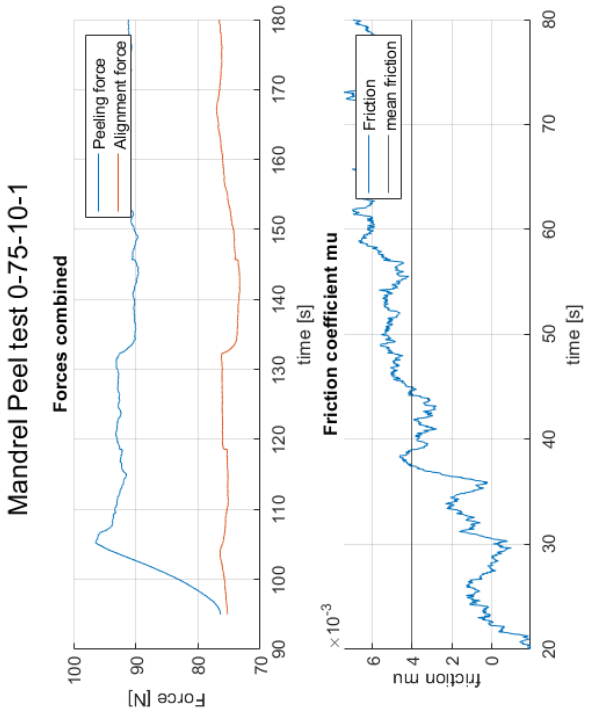

(a) 0-75-10-1, averagely μ is 0.004 and the G_A is 1.5032

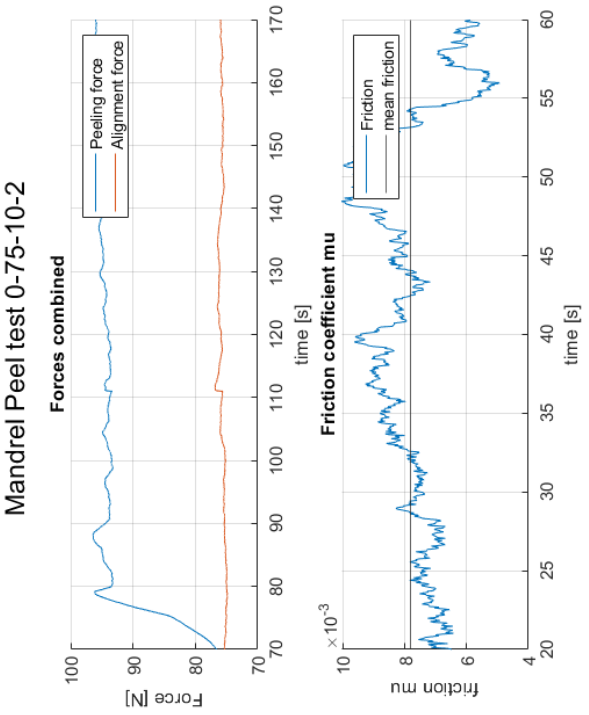

(b) 0-75-10-2, averagely μ is 0.0078 and the G_A is 1,7287

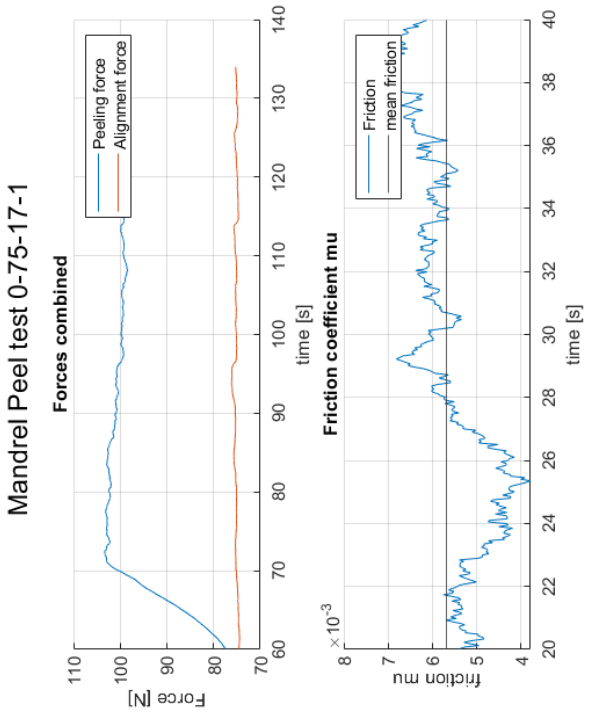

(c) 0-75-17-1, averagely μ is 0.0057 and the G_A is 1.3513

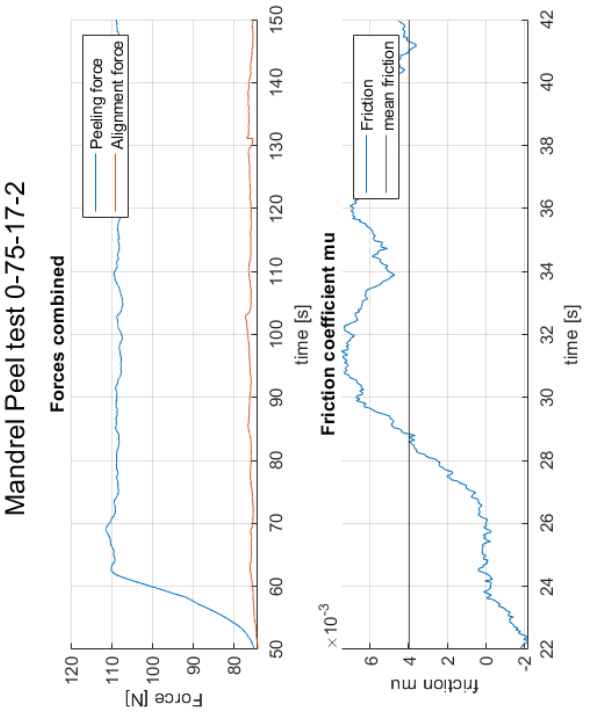

(d) 0-75-17-2, averagely μ is 0.004 and the G_A is 1.7499

Figure C.1: Friction and peeling force measurement F_a of 75 N and mandrel peel distance of 0 mm with respect to the sample.

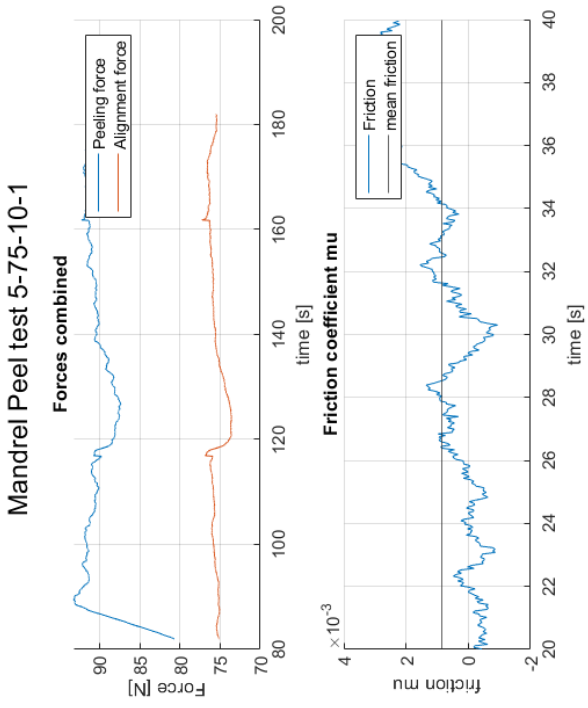

(a) 5-75-10-1, averagely μ is 0.0011 and the G_A is 1.4668

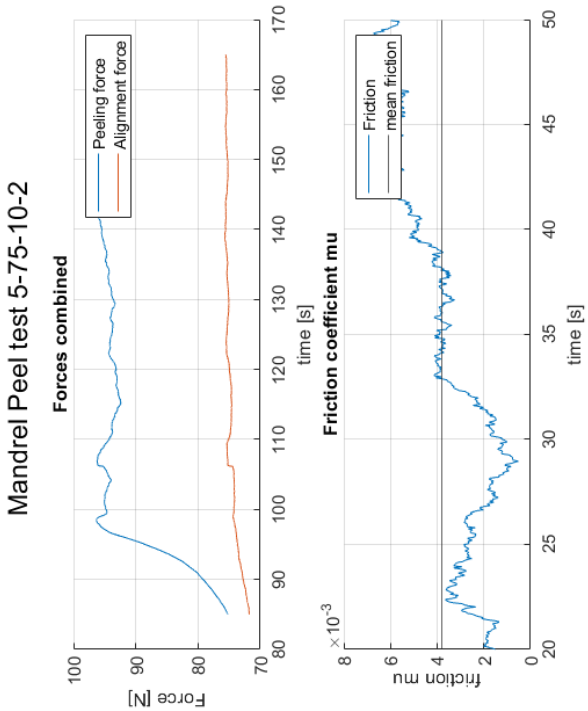

(b) 5-75-10-2, averagely μ is 0.0038 and the G_A is 1,7872

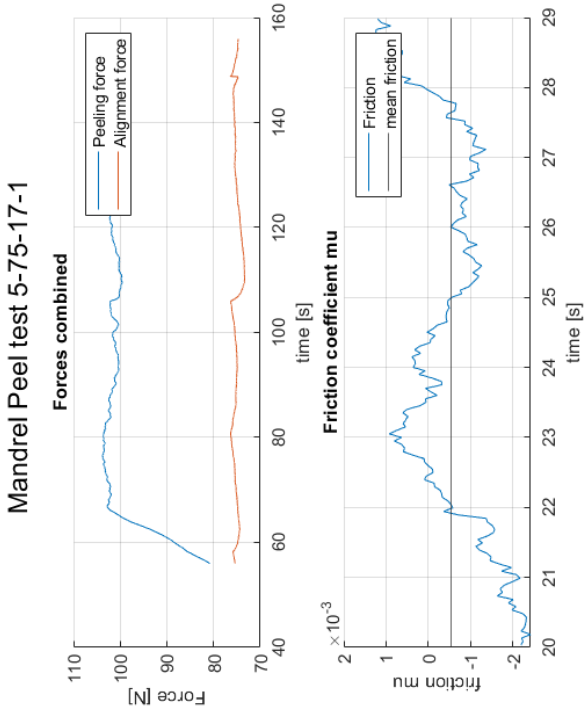

(c) 5-75-17-1, averagely μ is 0.0014 and the G_A is 1.5393

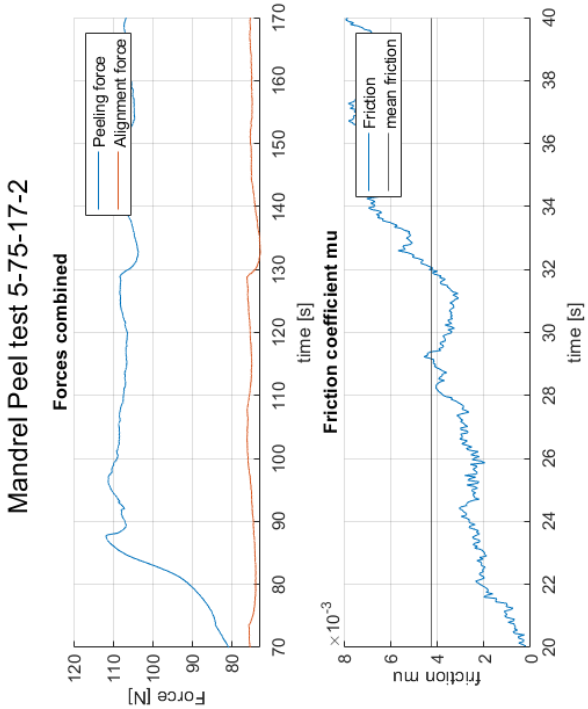

(d) 5-75-17-2, averagely μ is 0.0043 and the G_A is 1.7040

Figure C.2: Friction and peeling force measurement F_a of 75 N and mandrel peel distance of 5 mm with respect to the sample.

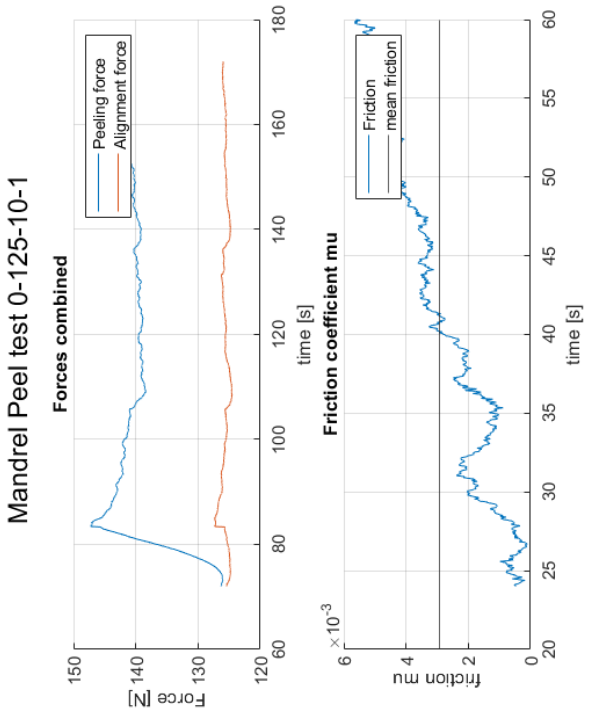

(a) 0-125-10-1, averagely μ is 0.0029 and the G_A is 1.3854

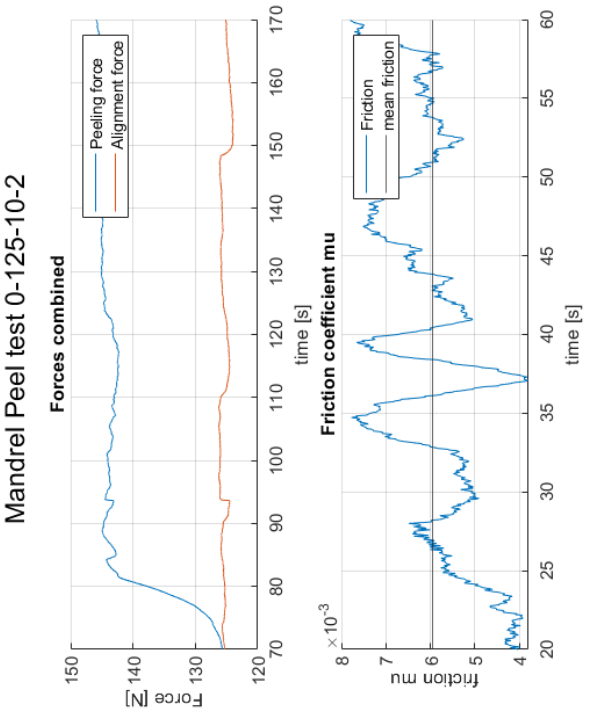

(b) 0-125-10-2, averagely μ is 0.0059 and the G_A is 1,6404

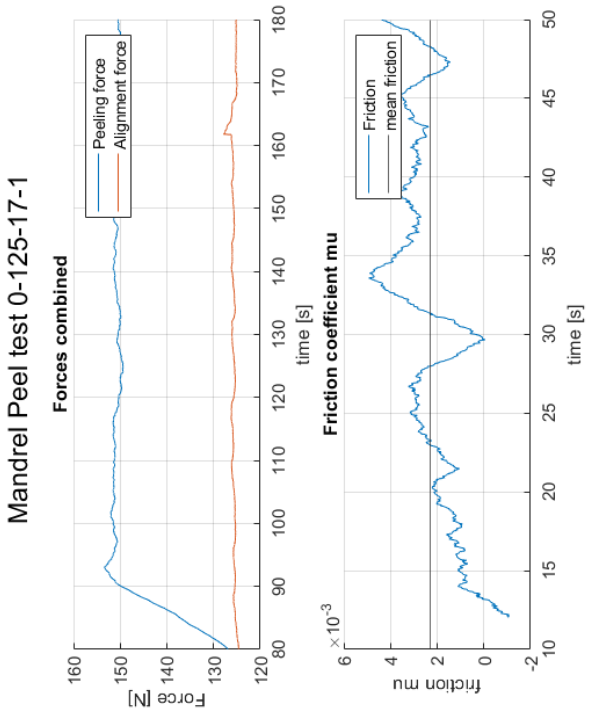

(c) 0-125-17-1, averagely μ is 0.0023 and the G_A is 1.3811

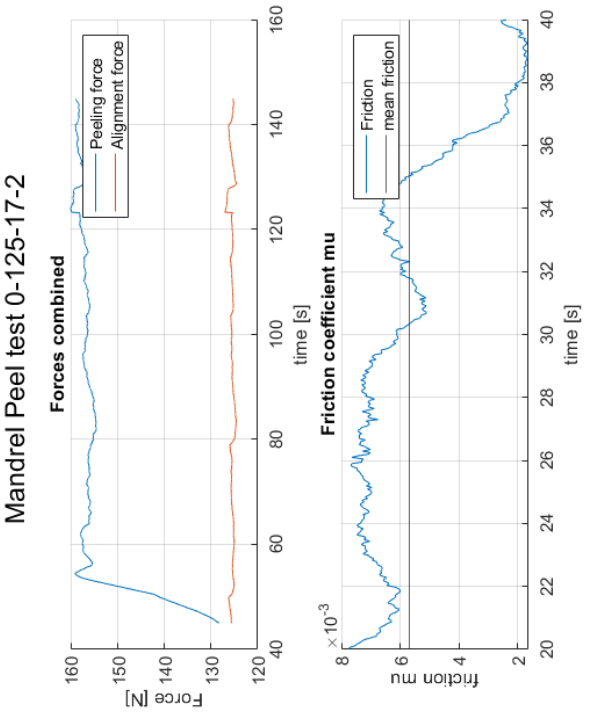

(d) 0-125-17-2, averagely μ is 0.0057 and the G_A is 1.7171

Figure C.3: Friction and peeling force measurement F_a of 125 N and mandrel peel distance of 0 mm with respect to the sample.

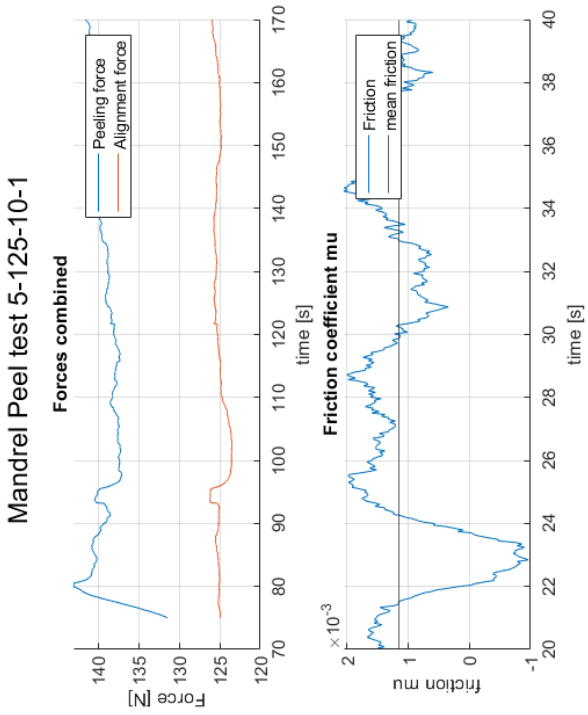

(a) 5-125-10-1, averagely μ is 0.0011 and the G_A is 1.3844

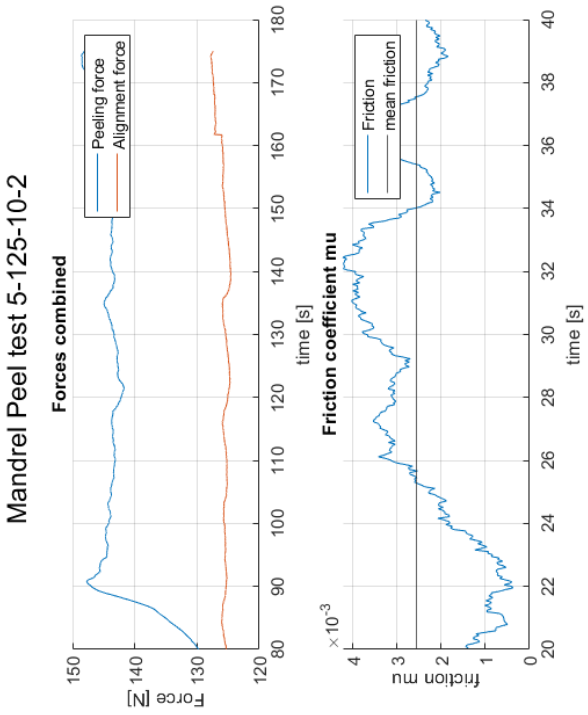

(b) 5-125-10-2, averagely μ is 0.0026 and the G_A is 1,7533

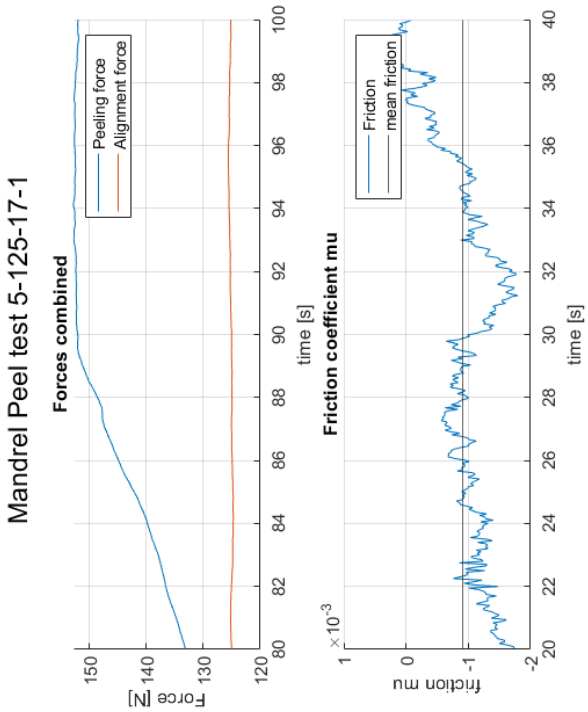

(c) 5-125-17-1, could not be fixed properly, therefor its results cannot be used

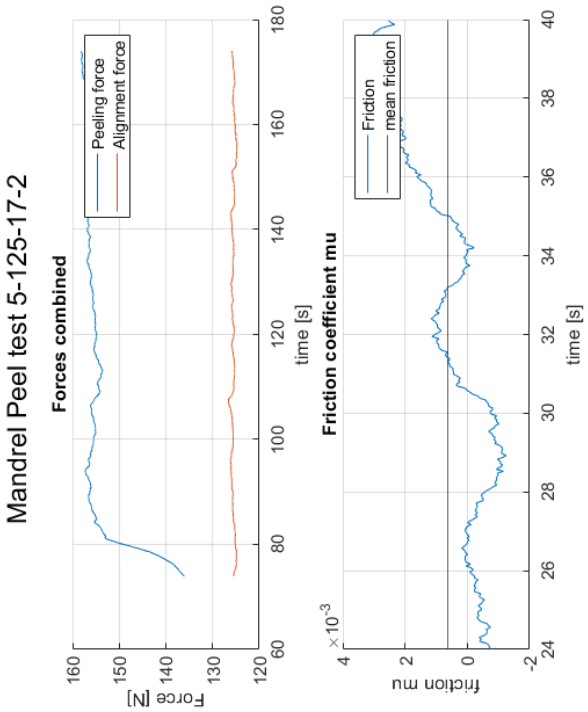

(d) 5-125-17-2, averagely μ is 0.0018 and the G_A is 1.6580

Figure C.4: Friction and peeling force measurement F_a of 125 N and mandrel peel distance of 5 mm with respect to the sample.

Appendix D

Step by step guide mandrel-peel test

Steps for performing the mandrel peel test:

1. Press Cl.-Lp. + type 15 4x till all V-lights are on. This step is only required by start-up of the set-up.
2. Set height of mandrel and fixate. This should be done once for all experiments that require that specific height to reduce variables.
3. Height of tensile testing machine can be changed by pressing position. The turning knob can be used to increase speed.
4. Fix sample on table. Make sure there is sufficient space to test friction before the peeling (at least 20 seconds should be available)
5. Put peel-arm in fixture
6. Put pressure on cylinder
7. Set video-camera ready, video zoom 2.5x, do not use flash
8. Place white paper behind set-up to increase contrast for the video images
9. Select right folder on Zwick system PC
10. Put in the specimen name in Zwick. If the name does not change, it will overwrite without saving old data
11. Start video
12. Start Zwick
13. Start Peeling
14. Set right alignment force and keep adjusting if necessary
15. Stop the peeling when there is sufficient data (at least 100 seconds should be available)
16. Stop Zwick
17. Stop video
18. Lower pressure on cylinder to 0
19. Demount peel-arm from fixture
20. Demount sample from table
21. Load all data to MATLAB once all experiments are done

Appendix E

Overview results

Table E.1: Overview of all results

Specimen	Peak force [N]	G_c [KJ/m2]	mu	mu [%]
0-30-1	19.4618	1.4830	-0.0079	0.5327
0-30-2	18.9487	1.3925	-0.0086	0.6176
0-30-3	21.0455	1.2822	0.0063	0.4913
0-30-4	20.0732	1.4821	0.0026	0.1754
0-30-5	21.4958	1.2871	0.0068	0.5283
0-30-6	19.8804	1.3695	0.0066	0.4819
0-30-7	20.2277	1.2663	-0.0061	0.4817
0-30-8	21.3289	1.2169	0.0047	0.3862
0-30-9	21.3695	1.2020	0.0068	0.5709
0-45-1	19.3428	1.3305	-0.0093	0.6990
0-45-2	18.0295	1.1084	-0.0059	0.5323
0-45-3	19.7853	1.4016	-0.0060	0.4281
0-45-4	20.2287	1.2543	0.0064	0.5102
0-45-5	21.3869	1.4419	0.0068	0.4716
0-45-6	19.2294	1.1824	0.0064	0.5413
0-45-7	19.5212	1.2471	0.0068	0.5453
0-45-8	24.508	1.4497	0.0076	0.5242
0-45-9	21.0123	1.2133	0.0066	0.5440
0-60-1	16.6878	1.1943	-0.0075	0.6280
0-60-2	19.3893	1.3166	-0.0068	0.5165
0-60-3	15.3648	1.1962	-0.0060	0.5016
0-60-4	18.178	1.1684	0.0056	0.4793
0-60-5	17.8559	1.3156	0.0028	0.2128
0-60-7	17.2349	1.1082	0.0071	0.6407
0-60-8	18.7401	1.2127	0.0032	0.2639
0-60-9	19.8225	1.3731	0.0054	0.3933
0-60-10	17.8917	1.2547	0.0068	0.5420
0-60-11	17.9375	1.2414	0.0062	0.4994
0-90-2	15.8054	1.2443	-0.0061	0.4902
0-90-3	16.5272	1.1485	-0.0063	0.5485
0-90-4	15.0753	1.1311	0.0059	0.5216
0-90-5	17.1113	1.2913	0.0055	0.4259
0-90-6	17.6268	1.3508	0.0056	0.4146
0-90-7	15.3872	1.0777	0.0050	0.4640
0-90-9	16.656	1.1323	0.0056	0.4946
0-90-11	16.2039	1.1928	0.0066	0.5533

Appendix F

Measured forces and friction

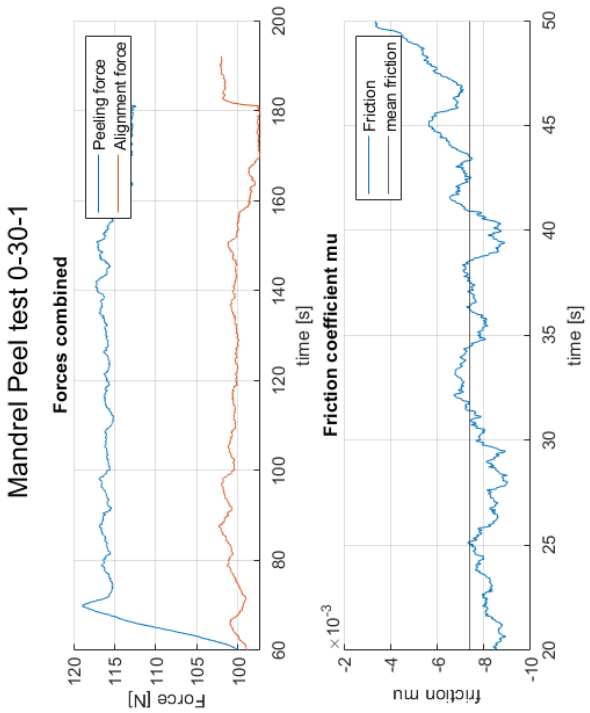

(a) Measured forces and friction 0-30-1

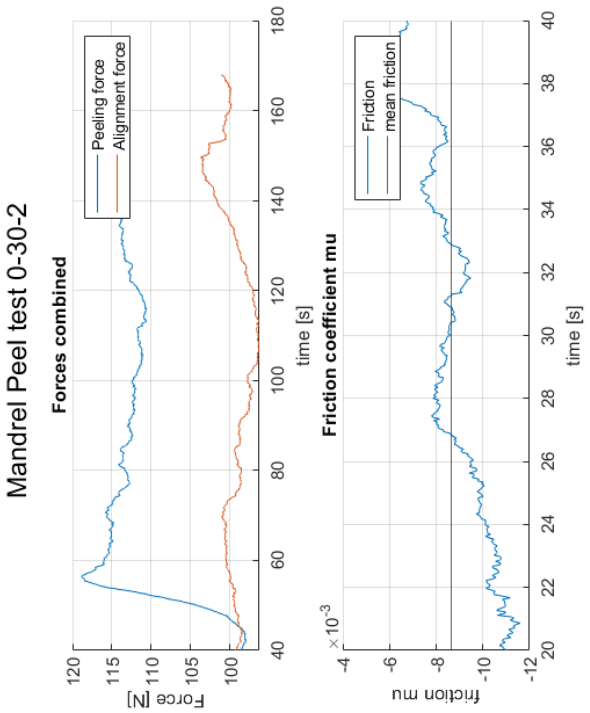

(b) Measured forces and friction 0-30-2

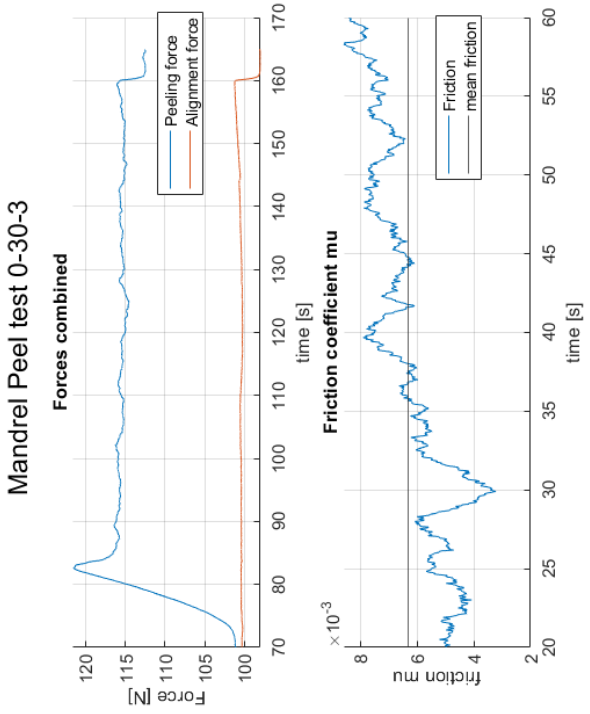

(c) Measured forces and friction 0-30-3

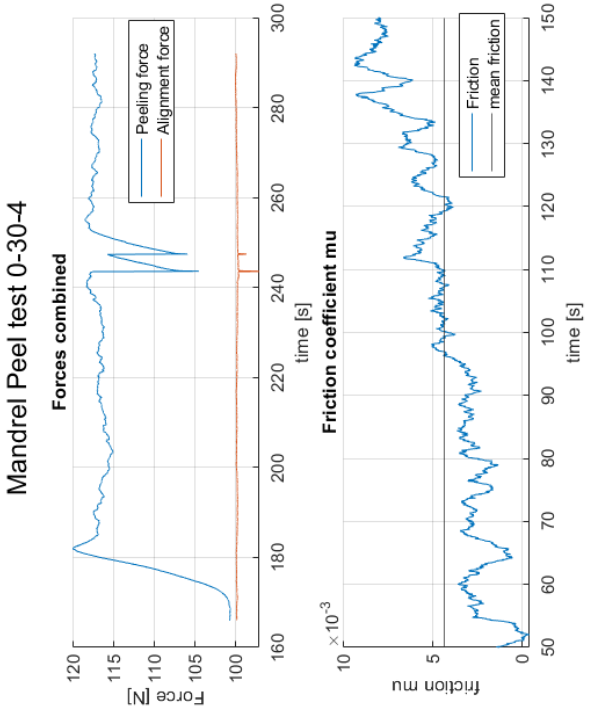

(d) Measured forces and friction 0-30-4

Figure F.1: Measured forces and friction 0-30 specimen

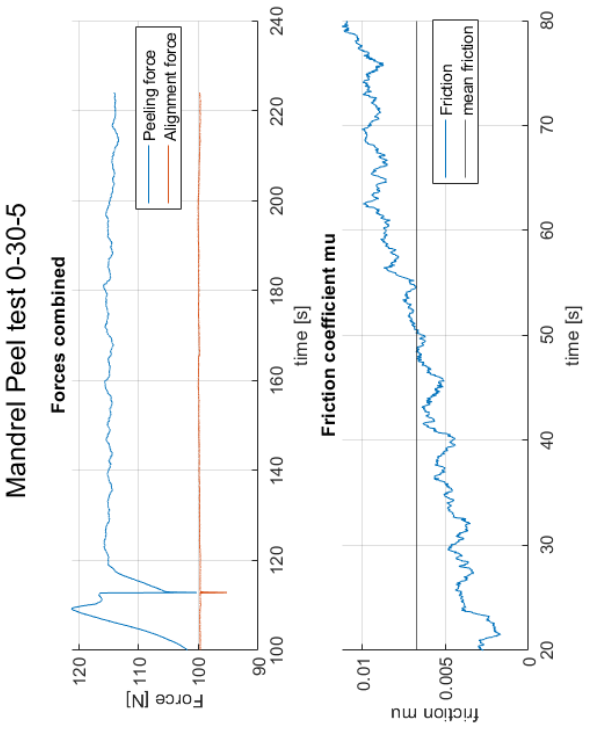

(a) Measured forces and friction 0-30-5

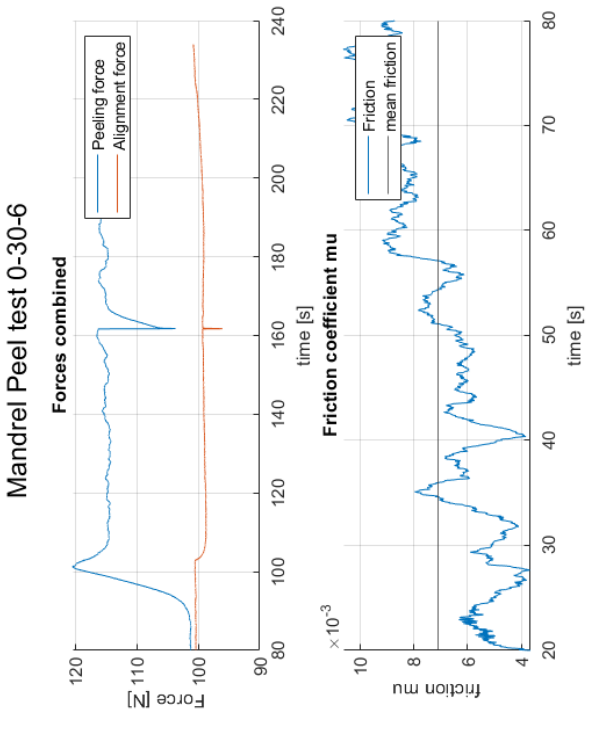

(b) Measured forces and friction 0-30-6

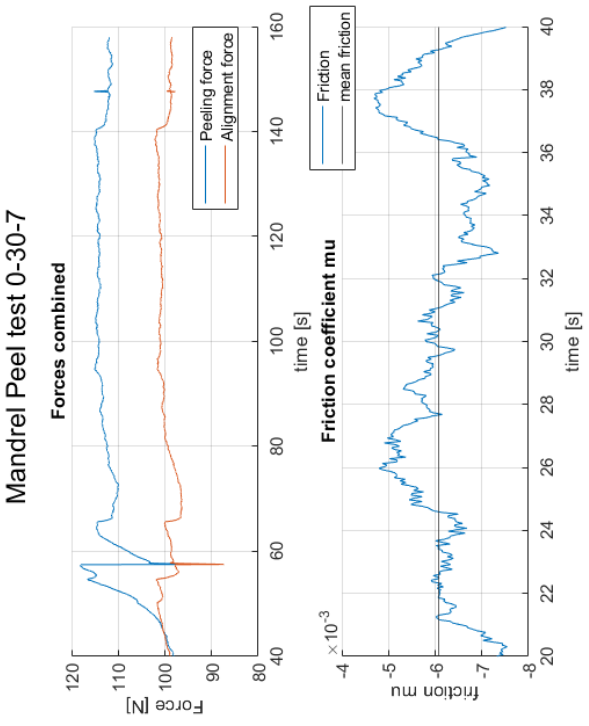

(c) Measured forces and friction 0-30-7

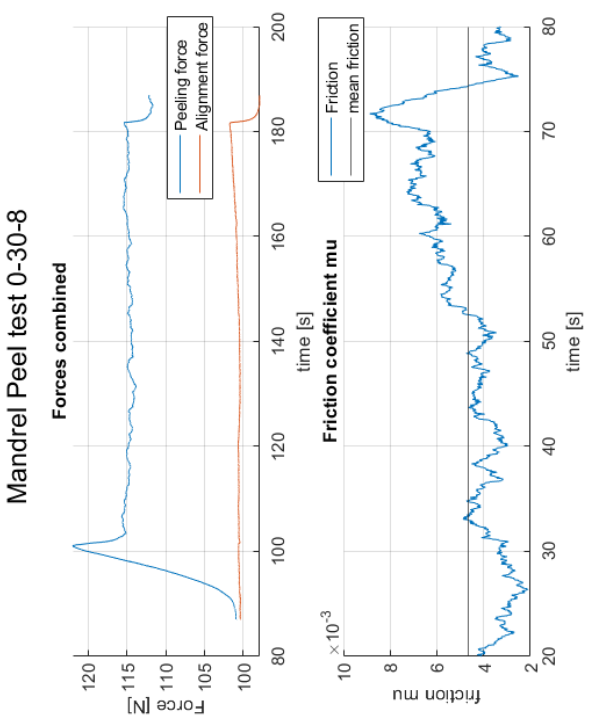

(d) Measured forces and friction 0-30-8

Figure F.2: Measured forces and friction 0-30 specimen

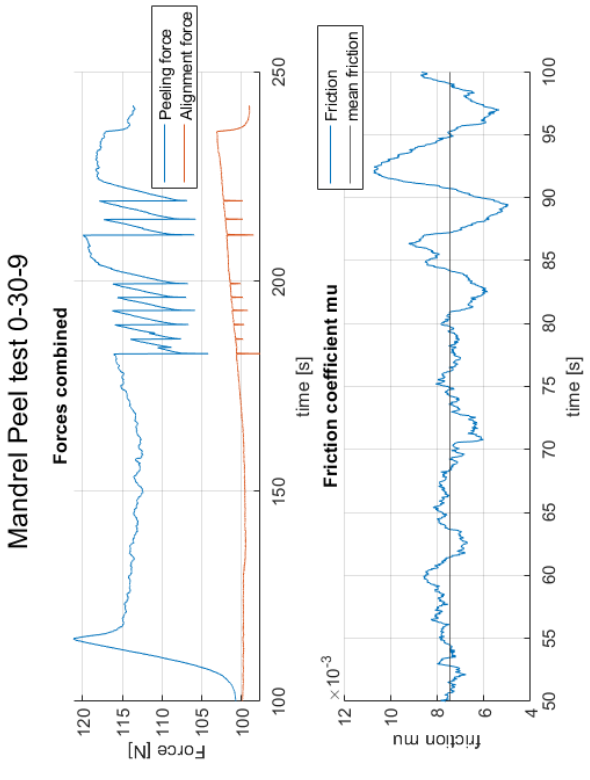

(a) Measured forces and friction 0-30-9

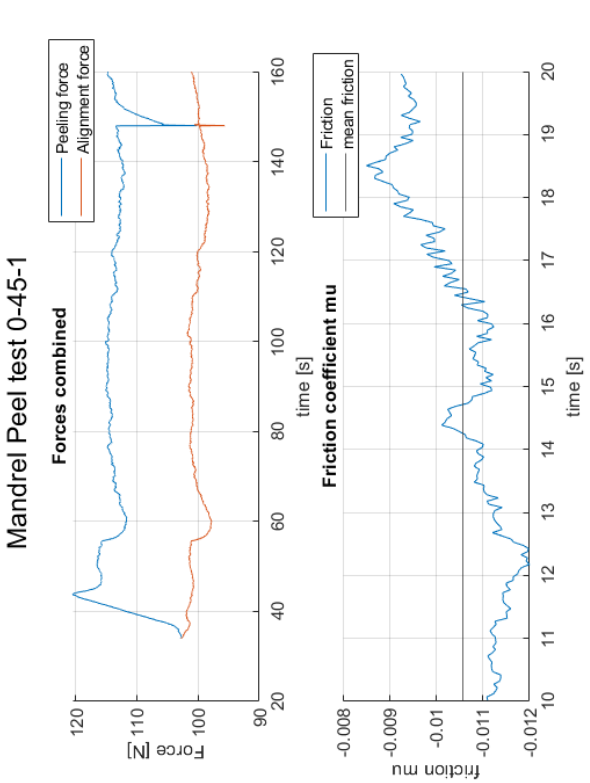

(b) Measured forces and friction 0-45-1

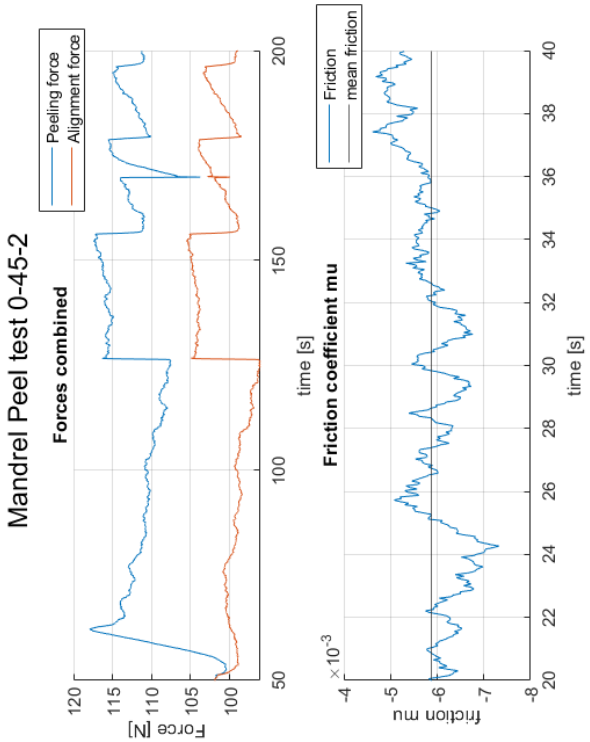

(c) Measured forces and friction 0-45-2

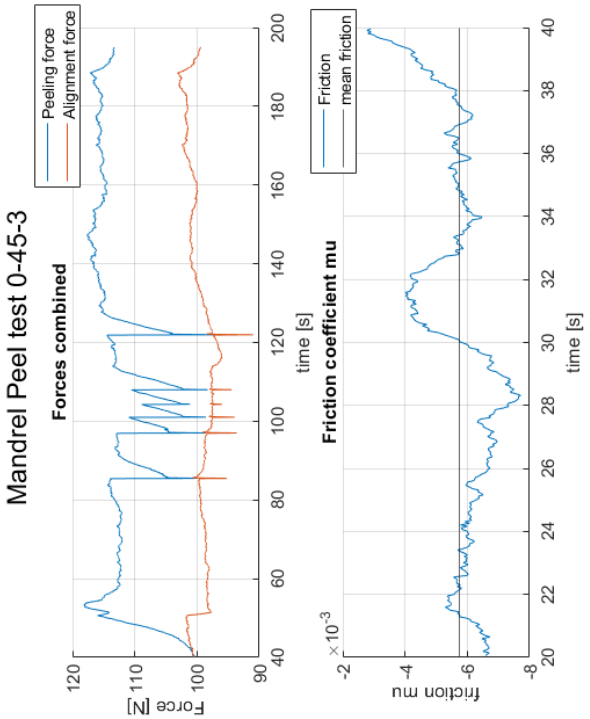

(d) Measured forces and friction 0-45-3

Figure F.3: Measured forces and friction 0-30 and 0-45 specimen

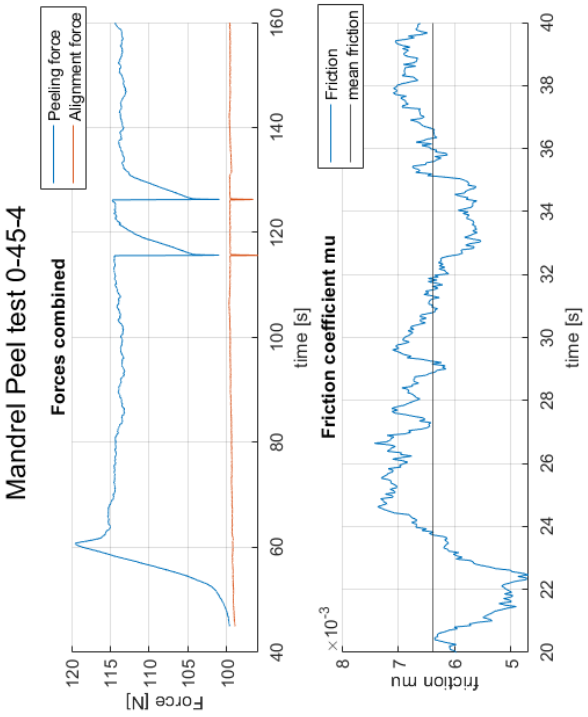

(a) Measured forces and friction 0-45-4

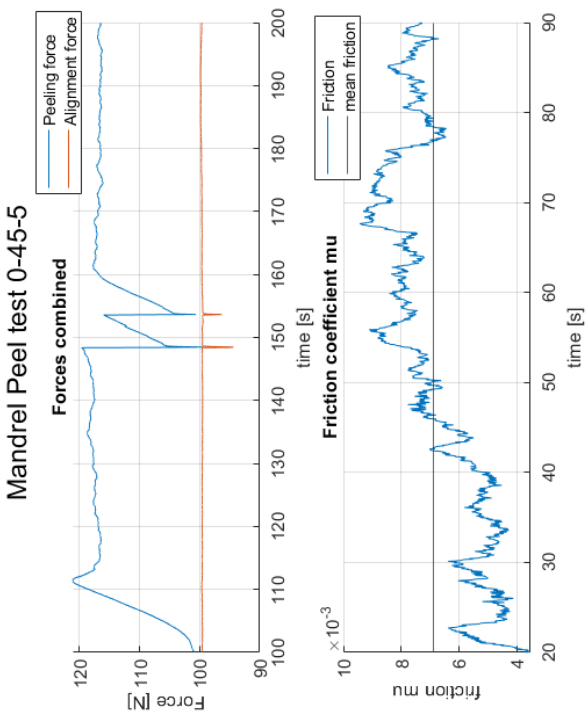

(b) Measured forces and friction 0-45-5

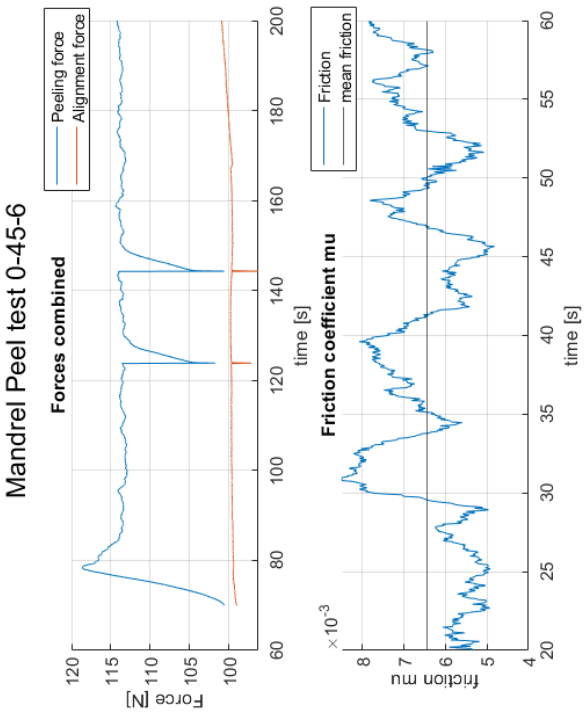

(c) Measured forces and friction 0-45-6

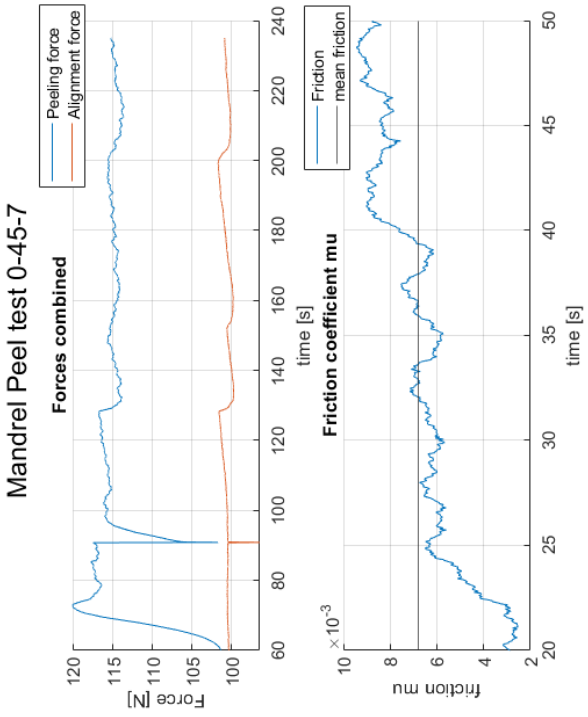

(d) Measured forces and friction 0-45-7

Figure F.4: Measured forces and friction 0-45 specimen

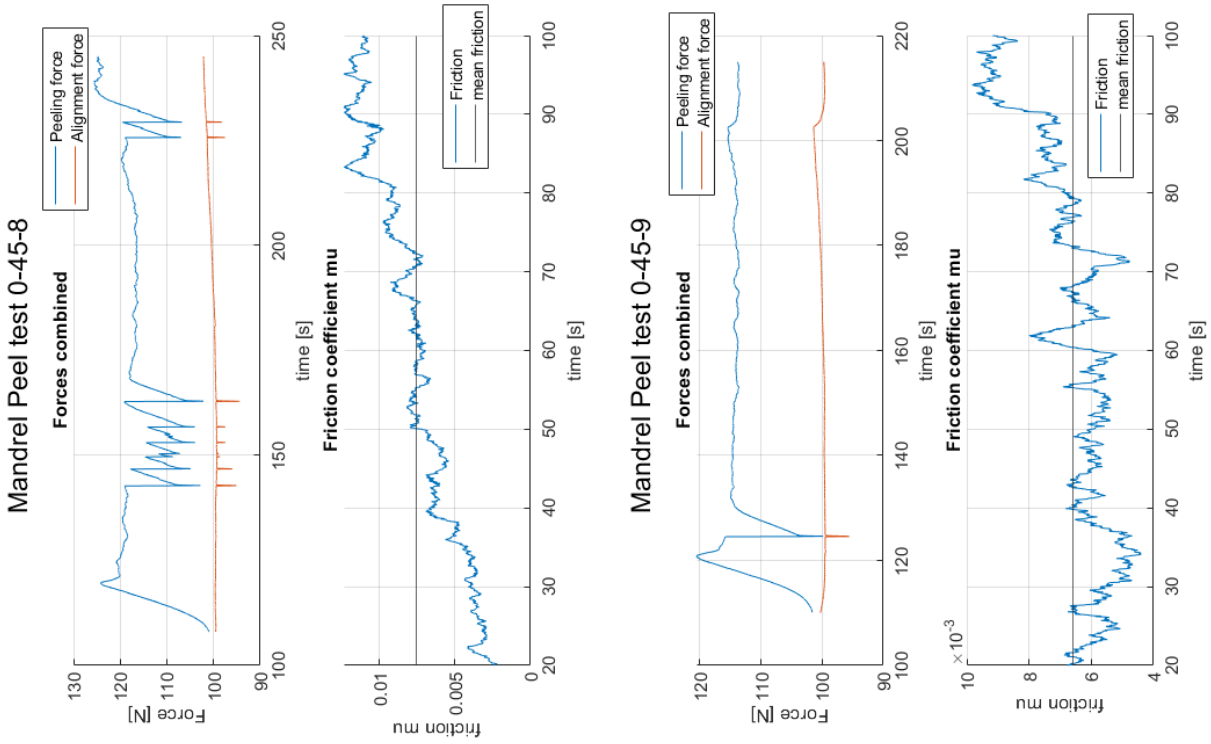

(a) Measured forces and friction 0-45-8

(b) Measured forces and friction 0-45-9

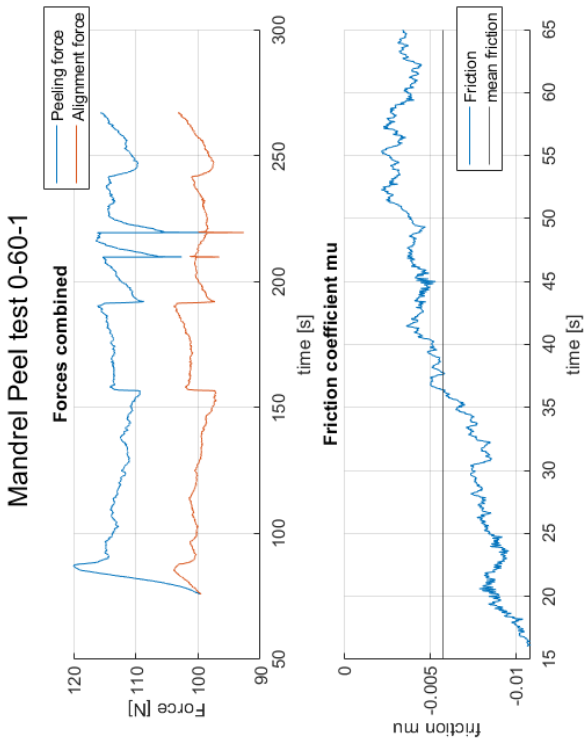

(c) Measured forces and friction 0-60-1

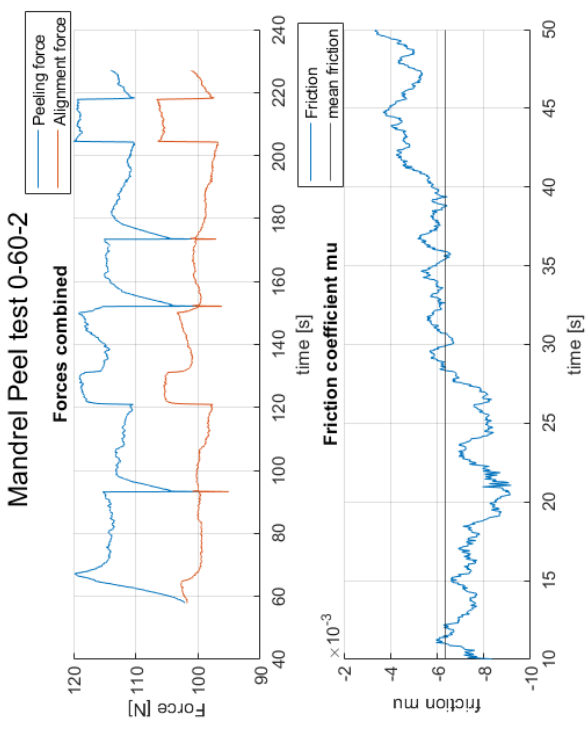

(d) Measured forces and friction 0-60-2

Figure F.5: Measured forces and friction 0-45 and 0-60 specimen

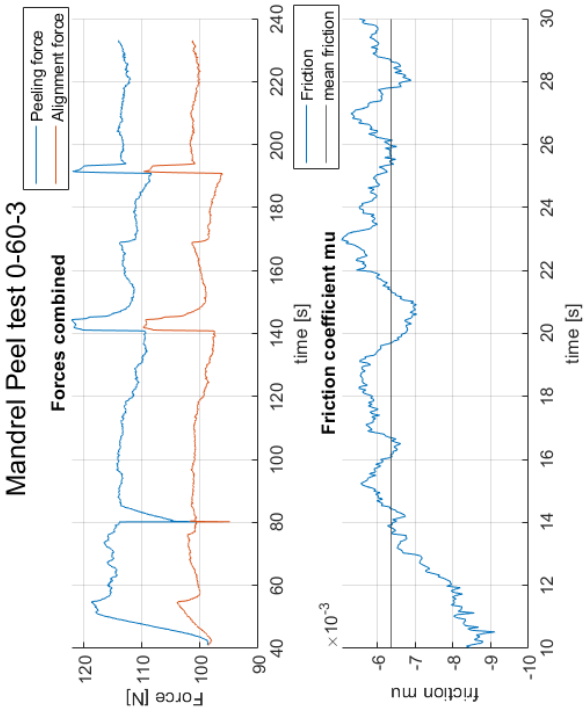

(a) Measured forces and friction 0-60-3

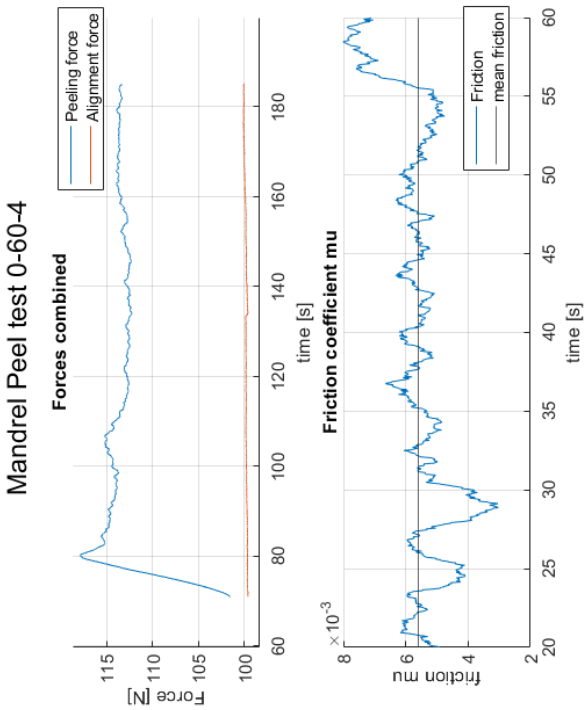

(b) Measured forces and friction 0-60-4

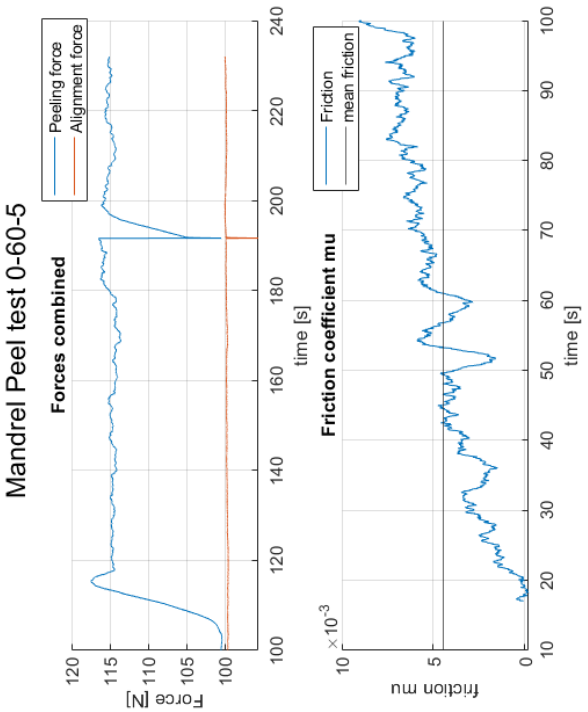

(c) Measured forces and friction 0-60-5

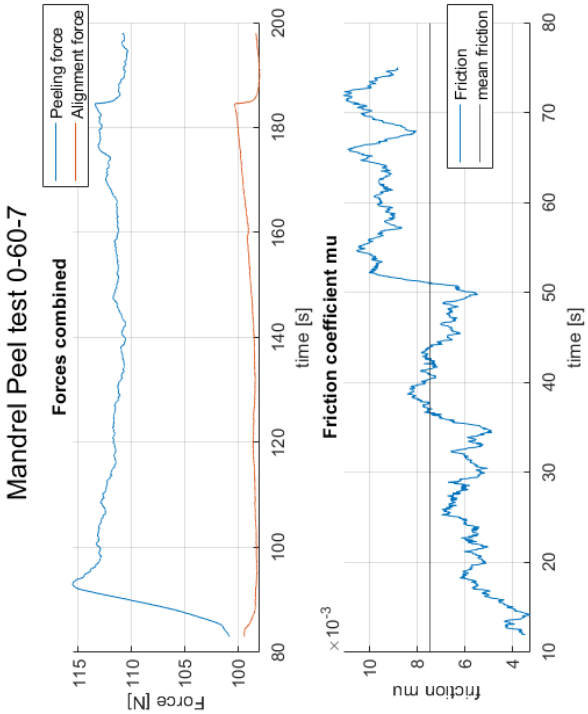

(d) Measured forces and friction 0-60-7

Figure F.6: Measured forces and friction 0-60 specimen

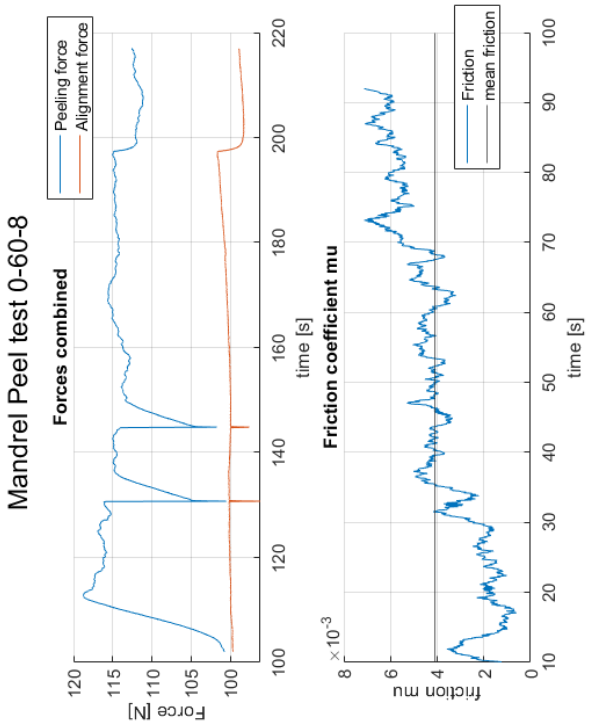

(a) Measured forces and friction 0-60-8

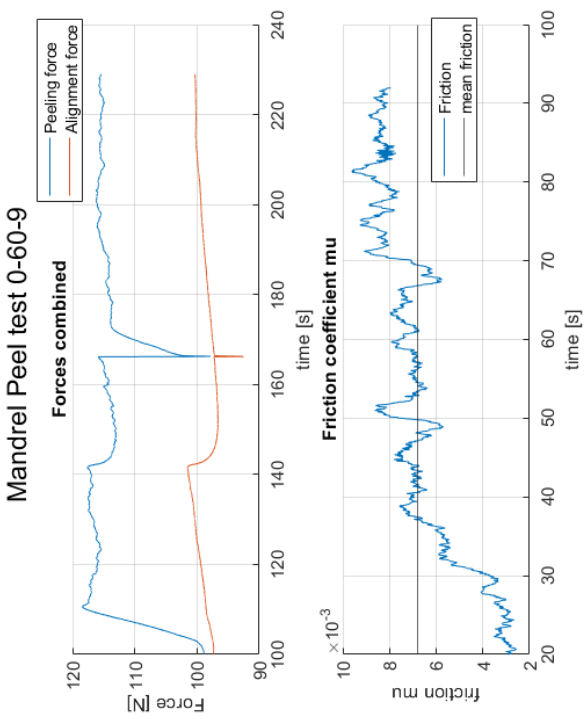

(b) Measured forces and friction 0-60-9

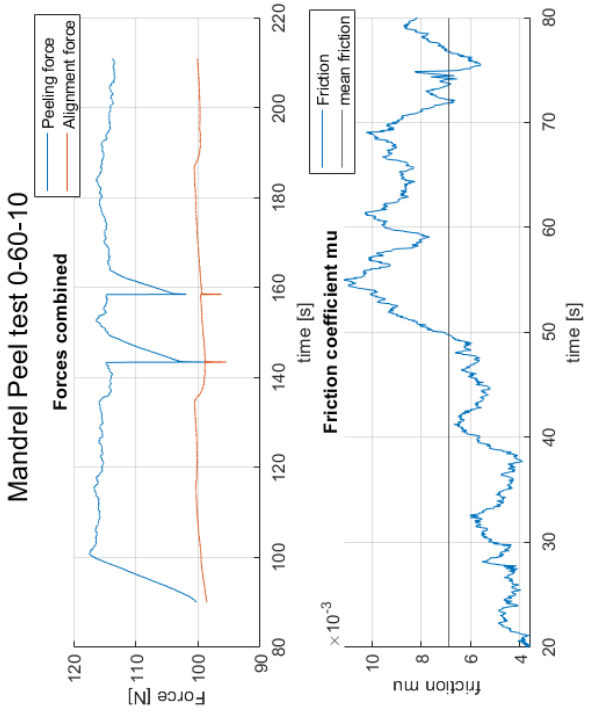

(c) Measured forces and friction 0-60-10

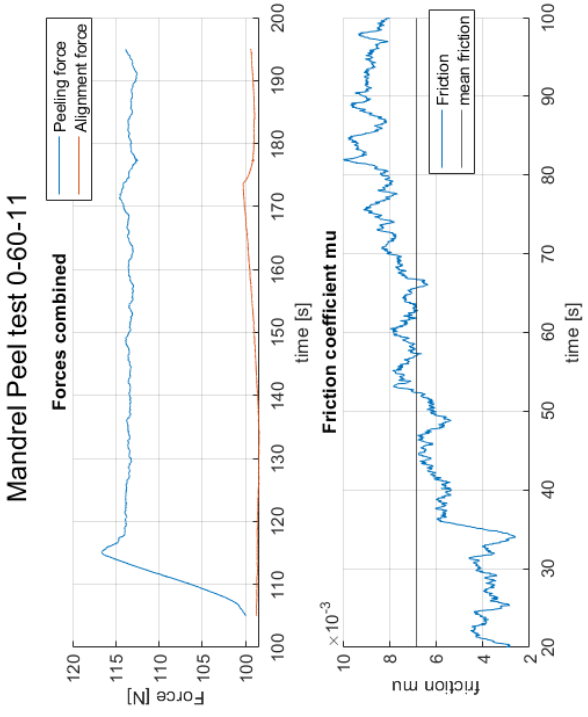

(d) Measured forces and friction 0-60-11

Figure F.7: Measured forces and friction 0-60 specimen

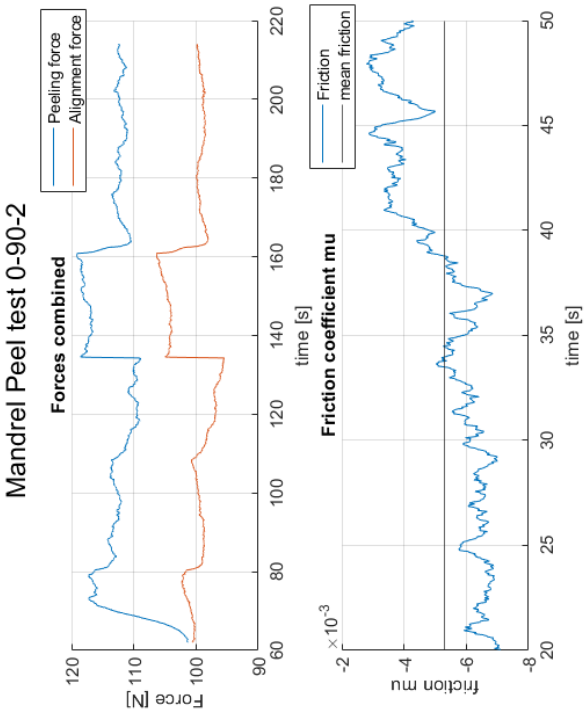

(a) Measured forces and friction 0-90-2

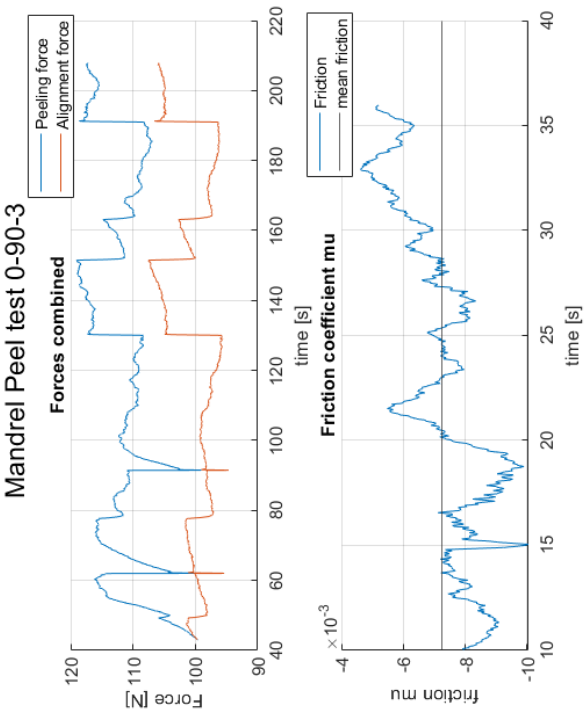

(b) Measured forces and friction 0-90-3

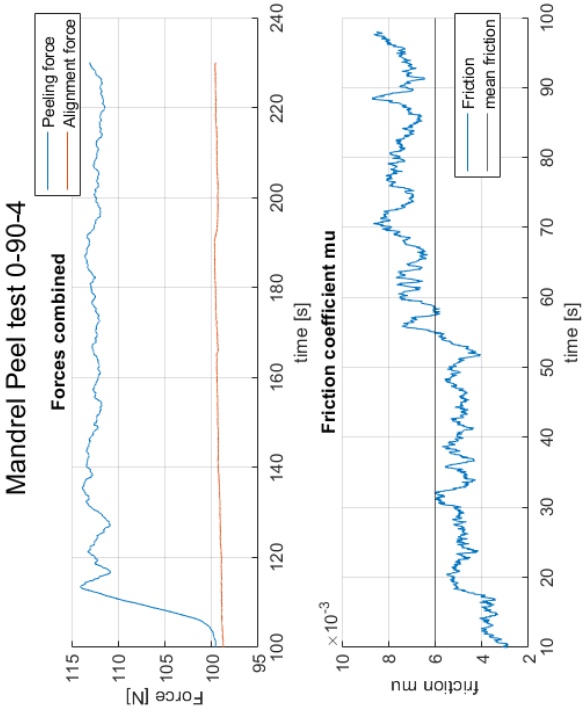

(c) Measured forces and friction 0-90-4

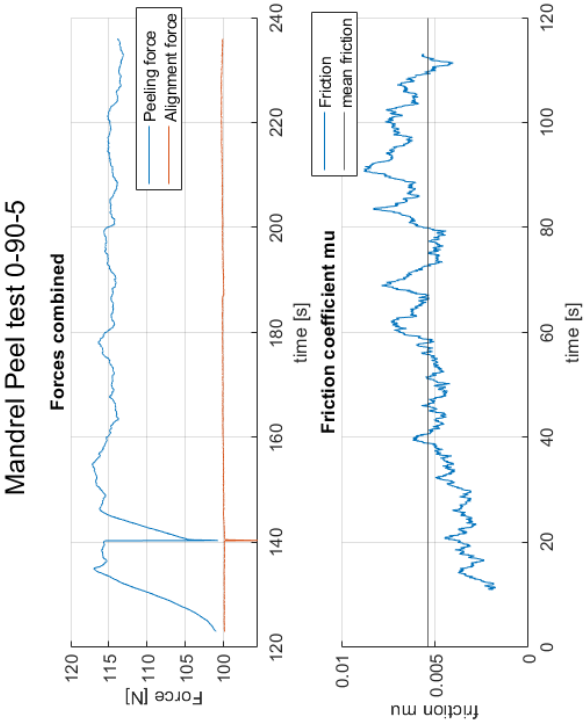

(d) Measured forces and friction 0-90-5

Figure F.8: Measured forces and friction 0-90 specimen

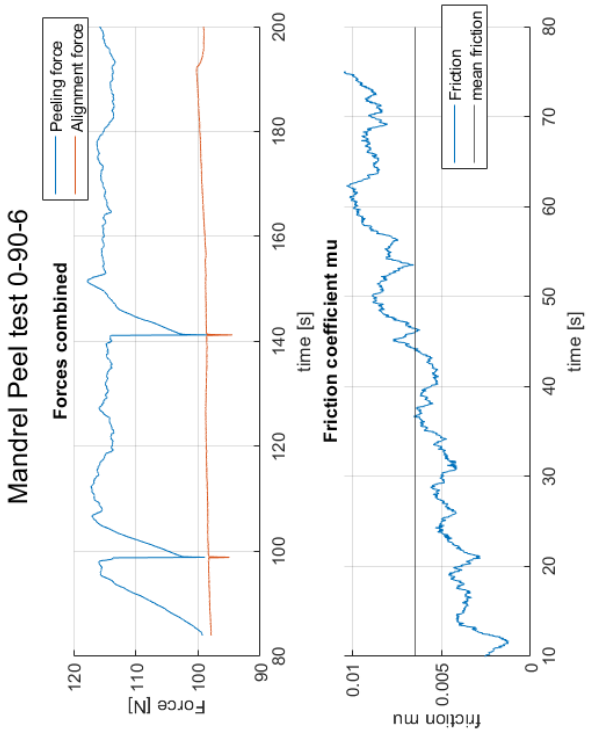

(a) Measured forces and friction 0-90-6

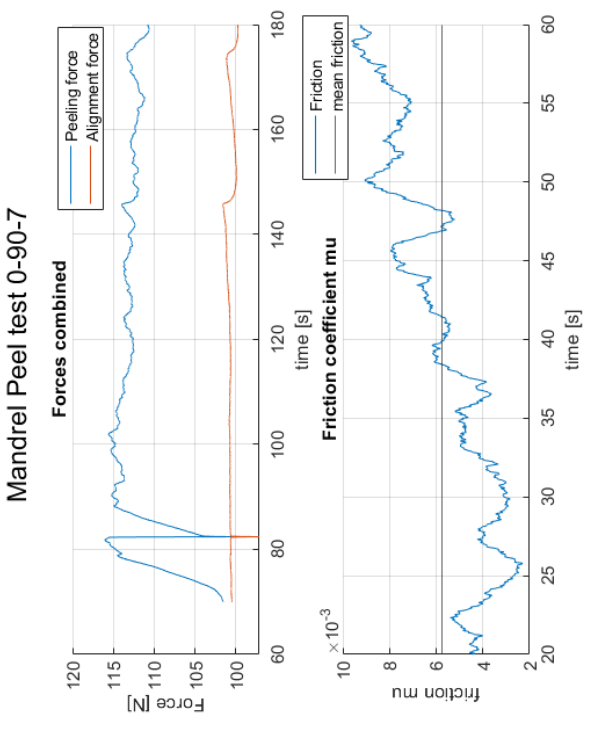

(b) Measured forces and friction 0-90-7

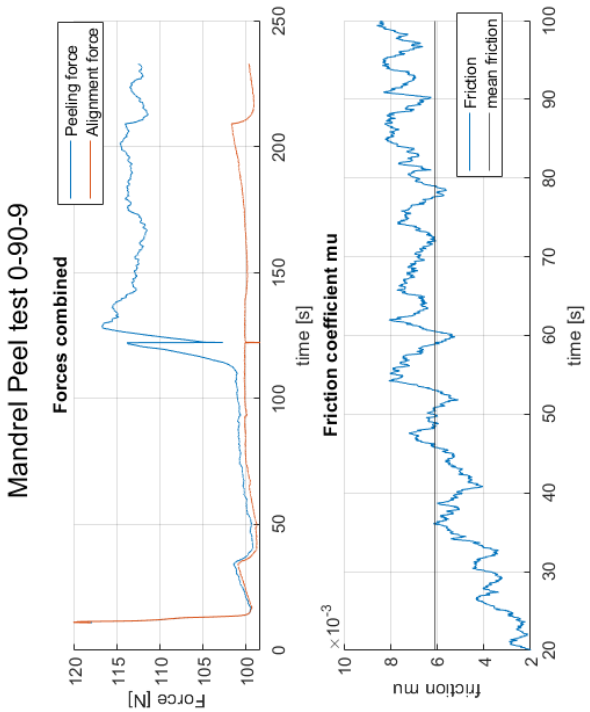

(c) Measured forces and friction 0-90-9

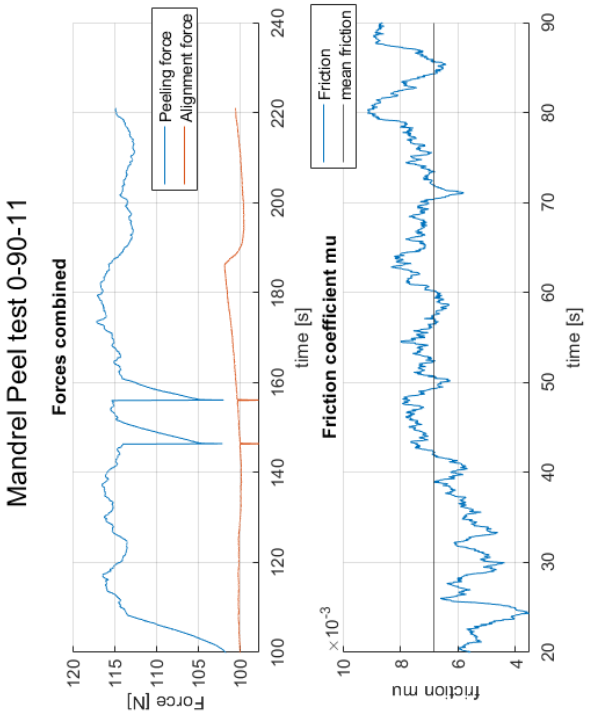

(d) Measured forces and friction 0-90-11

Figure F.9: Measured forces and friction 0-90 specimen